MULTIVARIABLE FLIGHT CONTROL DESIGN WITH PARAMETER UNCERTAINTY FOR THE AFTI/F-16

THESIS

AFIT/GE/ENG/89M-1 Brian J. Pawlowski
Capt USAF

DEPARTMENT OF THE AIR FORCE
AIR UNIVERSITY
AIR FORCE INSTITUTE OF TECHNOLOGY

Wright-Patterson Air Force Base, Ohio

AFIT/GE/ENG/89M-1

MULTIVARIABLE FLIGHT CONTROL DESIGN WITH PARAMETER UNCERTAINTY FOR THE AFTI/F-16

THESIS

AFIT/GE/ENG/89M-1 Brian J. Pawlowski
Capt USAF

AFIT/GE/ENG/89M-1

MULTIVARIABLE FLIGHT CONTROL DESIGN WITH PARAMETER UNCERTAINTY FOR THE AFTI/F-16

THESIS

Presented to the Faculty of the School of Engineering

of the Air Force Institute of Technology

Air University

in Partial Fulfillment of the

Requirements for the Degree of

Master of Science

by

Brian J. Pawlowski
Capt USAF

Graduate Electrical Engineering

March 1989

Preface

This thesis research develops a preliminary design for a pitch-pointing maneuver flight controller for the AFTI/F-16 vehicle. The design method uses the Quantitative Feedback Theory techniques developed by Dr. Isaac Horowitz of the University of California, Davis, California. I wish to express my appreciation to Dr. Isaac Horowitz and to Dr. Constantine H. Houpis, my thesis advisor, for their guidance and encouragement during this research effort which was primarily accomplished in 1983. I wish to also thank Capt. David Potts, Rtd., and the Control Techniques Group, Flight Control Division of the Flight Dynamics Laboratory for sponsoring this research.

The thesis uses the identical AFTI/F-16 aircraft model developed by A. Finley Barfield to provide the reader a point of comparison between the application and results of various control system design methods. I would like to thank Mr. Barfield for his assistance and suggestions during the definition of this study.

This thesis effort, along with the parallel efforts of Capt. Robert Betzold and Lt. Jon Walke, are the first applications of Dr. Horowitz's design techniques applied by students of the Air Force Institute of Technology. I give my sincere thanks to Bob and Jon for the mutual support we shared throughout our research efforts.

Finally, I give my love and appreciation to my wife, Jane, for her patience and understanding during this effort.

Capt. Brian J. Pawlowski

Contents

Contents

List of Figures

List of Figures

List of Figures

List of Tables

Abstract

Quantitative Feedback Theory (QFT) techniques are used in the design of a multivariable control law for the AFTI/F-16. The techniques were developed by Professor Isaac Horowitz, University of California, Davis, California. The flight control problem involves a multiple input - multiple output (MIMO) plant requiring regulation and control in the presence of parameter uncertainty and disturbances. Based on frequency response fundamentals, the technique uses feedback to achieve closed-loop system response within performance tolerances despite plant uncertainty. The range of uncertainty and the output performance specifications are quantitative parameters in the design process. The MIMO control problem is restructured into a set of two input - single output (multiple input - single output (MISO)) problems where one input is a command input to the system and the other is a disturbance input to be attenuated. The control laws for the MISO problems taken together form the solution of the MIMO problem.

To obtain a point of comparison between various design techniques, the identical aircraft model previously developed by Mr. A. Finley Barfield is used in this study. The state space form of the model is converted to the transfer function relationships between the plant input and output variables. A single design is performed over the range of flight conditions investigated.

The approach used along with evaluations of the final control laws is presented. Recommendations for further study and discussion of the results obtained are provided.

MULTIVARIABLE FLIGHT CONTROL DESIGN WITH PARAMETER UNCERTAINTY FOR THE AFTI/F-16

I. Introduction

Background

Recent advances in high performance aircraft design have increased the complexity of the flight control problem. Improvements in the short period and dutch roll damping characteristics of an aircraft have been achieved by augmenting limited authority controllers designed using existing control theory. It has also been utilized in the design of autopilots and automatic landing systems.

Current emphasis in aircraft design incorporates control characteristics early in the design process to improve aircraft performance. The aerodynamic design is no longer limited by the requirement of providing stability and natural damping. Improved maneuverability can be achieved at the expense of static stability. Thus, the control system must provide complete artificial stability as well as acceptable performance characteristics.

The development of digital fly-by-wire control systems on advanced high performance aircraft gives the pilot control over aircraft motion variables. Rather than governing control surface deflection, the stick input is used to command a desired change in rate or acceleration. The pilot's control stick provides the desired command input to the full authority fly-by-wire control system. The system determines the necessary signals to deflect the control surfaces in a manner which will obtain the response desired. The designer is able to develop a system allowing the pilot to command the aircraft response most beneficial to a given situation. If necessary, individual controllers can be designed to provide improved performance for specific mission phases.

Strong requirements are placed on a full authority fly-by-wire system to ensure

reliability, durability, and safety. The flight control system must operate after a number of failures. This requirement may result in the use of redundant channels within the flight control system to permit failure detection and isolation. The importance of system reliability is readily apparent when considering aircraft designs where artificial stability is provided by the flight control system. System failure can result in aircraft loss due to the high authority and fast response of fly-by-wire systems.

The advent of Direct Force capabilities allows entirely new maneuvers to be performed by an aircraft. These Control Configured Vehicle (CCV) capabilities are obtained through the use of multiple control surfaces coupled with the flight control system. Figure I-1 portrays the development of direct force modes using multiple control surfaces for the AFTI/F-16. The term direct force relates to forces which are uncoupled or disassociated from the aircraft's rotation. A detailed description of the six new control modes derived from the use of direct forces is given by Mr. A. Finley Barfield in Reference 2.

The CCV maneuvering capabilities along with the advances in aircraft design have complicated the flight control design problem. The plant to be controlled consists of multiple inputs and outputs. Conventional control methods have provided successful multivariable designs. Unfortunately, the difficulty and time required to apply the methods has increased. Many iterations of the design procedures are necessary to fulfill the various design requirements as each feedback loop is closed.

A number of multivariable control theories have developed with varied results when applied to the flight control problem. The frequency domain design methods developed by Dr. Isaac Horowitz, University of California, Davis, California, have demonstrated good results in this area. The fundamentals of Dr. Horowitz's design theory used in this thesis are presented in Chapters II and III. For a more detailed theoretical description of the techniques, see References 5, 8, 9, 12 and 16.

The feasibility of various modern control techniques is of primary interest to the Air Force Institute of Technology and the Air Force Flight Dynamics Laboratory, Wright-

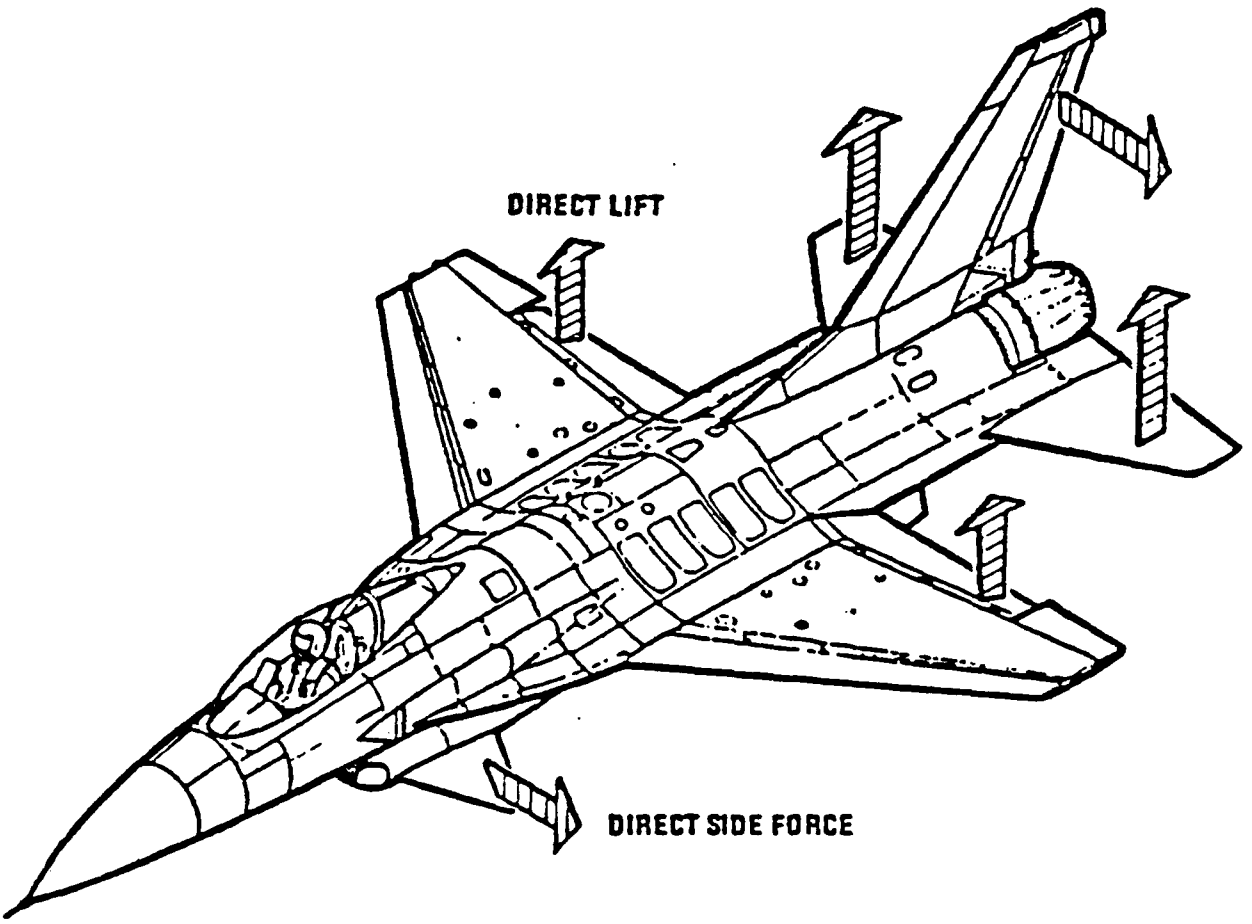

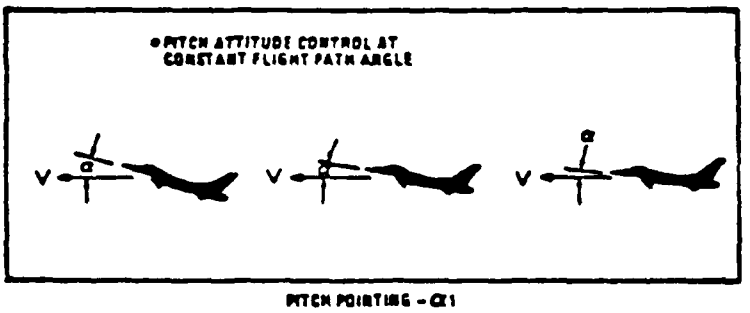

PITCH POINTING - CX1

Fig. I-1. Direct Force Development Using Multiple Surfaces

Patterson Air Force Base, Ohio. The research of this thesis effort uses the identical aircraft model, assumptions, and design requirements used in the research by Mr. Barfield (Ref 2). The goal is to provide a basis of comparison between the methods of Dr. Isaac Horowitz, as applied in this thesis, and that of Dr. Brian Porter applied in the thesis by Mr. Barfield.

Research Objective and Scope

The objective of this thesis research is to design and evaluate a flight controller, using the Quantitative Feedback Theory (QFT) technique of Dr. Isaac Horowitz (Ref 8, 9, 12 and 16), for an AFTI/F-16 aircraft. The design focuses on obtaining a controller for the longitudinal CCV maneuver of pitch pointing. The evaluation examines controller robustness, control surface deflection, and bandwidth considerations on the loop transmission and compensator functions acquired.

The design is performed for several flight conditions in the flight envelope. The flight conditions considered are listed below.

1. 0.6 Mach; 30,000 Feet
2. 0.9 Mach; 20,000 Feet
3. 1.6 Mach; 30,000 Feet

The flight condition at 0.2 Mach; Sea Level investigated by Mr. Barfield is not included in this report since air-to-air combat is being emphasized. Also, the plant transfer functions describing this condition are non-minimum phase (have right-half-plane zeros). Analysis of this case requires using the Optimum Blending Method or the Singular G Method of Dr. Horowitz which was investigated by Lt. Jon Walke (Ref 15) and is beyond the scope of this report.

A controller is considered robust when the system performance is satisfactory at flight conditions other than the condition for which it was specifically designed. Robustness is evaluated by using the controller design, based on a nominal plant, for a pitch pointing maneuver. In practice, a nominal plant is chosen which exhibits similar frequency domain

characteristics as the actual plant over the range of flight conditions. The controller obtained is then used for simulation of pitch pointing at each flight condition considered.

To reemphasize, the scope of this thesis effort uses the identical aircraft model, assumptions, and design requirements used in the research by Mr. Barfield (Ref 2). The design requirements are adjusted and relaxed slightly to be appropriate for the limited scope of this study. The goal is to provide a basis of comparison between the methods of Dr. Isaac Horowitz and Dr. Brian Porter.

Assumptions

The following basic assumptions are made to simplify the design complexity to the level of a preliminary design. Refer to Reference 2 for a thorough description and justification of each.

- The aircraft is a rigid body and mass is held constant.
- Thrust is not changing.
- The earth's surface is an inertial reference frame.
- The atmosphere is assumed fixed with respect to the earth.
- The equations of motion can be decoupled into a longitudinal and a lateral-directional set of equations.
- Linearization about an operating condition is acceptable for point designs.
- Aerodynamics are fixed for Mach and altitude.

General Approach

The basic approach for this research effort is to acquire proficiency with the QFT method of Dr. Horowitz (Ref 5, 8, 9, 12 and 16) and apply it to the design of a multivariable flight control system for the AFTI/F-16 aircraft. Due to the interest in CCV control modes for improving combat performance, a controller is developed to provide pitch pointing over the range of flight conditions considered. Pitch rate and normal

acceleration are chosen as command outputs. The control inputs to the plant are flaperon and elevator surface positions. The state space representation of the full equations of motion, including actuator and sensor models, is converted to transfer function relationships between the plant input and output variables. Plant uncertainty arises as parameters vary with airspeed and altitude.

The QFT method, based on frequency domain fundamentals, uses feedback to achieve a closed-loop response within performance tolerances despite plant uncertainty. The range of uncertainty and the output performance specifications are quantitative parameters in the design process. The QFT method restructures the multiple input - multiple output (MIMO) uncertainty problem into a set of equivalent two input - single output (multiple input - single output (MISO)) uncertainty problems where one input is a command input to the system and the other a disturbance input to be attenuated. The control laws of the set of MISO problems taken together form the solution of the MIMO problem.

Design Requirements

A set of general design requirements is established to guide the research. A discussion of each requirement is given in Reference 2.

- The design will provide control and stability augmentation.
- Responses are to be fast and well behaved.
- Surface position and rate limits must not be exceeded.
- The outputs of the system will be aircraft rates and accelerations.
- Feedbacks can be reliably obtained with existing sensors.
- Conventional and specific CCV maneuver capabilities are available.

The general guidelines listed above were those used by Mr. Barfield. The additional requirement of minimizing loop transmission and compensator bandwidth is desirable to avoid unwanted effects from structural interaction, typically represented as noise.

To reduce the scope of this study, only the CCV maneuver of pitch pointing is addressed. The control surface position and rate responses are presented in the results. The responses are compared to the aircraft position and rate limits. However, no attempt is made to incorporate these limits in the design process. Such limits can be included as design parameters using a secondary approach described by Dr. Horowitz in Reference 14.

Sequence of Presentation

The presentation of this research effort is organized as follows. Chapters II and III briefly describe the Quantitative Feedback Theory developed by Dr. Isaac Horowitz of the University of California, Davis, California. The fundamentals required to solve the single loop uncertainty problem are given in Chapter II. These fundamentals are used in the multiple input - multiple output design procedure described in Chapter III. These two chapters were written in cooperation with Capt. Robert Betzold (Ref 3). A description of the aircraft chosen for the thesis is provided in Chapter IV, along with the state space model used to derive the plant transfer function matrix. The application of the design technique is presented in Chapter V. Representative results obtained at intermediate points in the design process are given. The final results are presented in Chapter VI. Conclusions and recommendations for further study are stated in Chapter VII.

II. Multiple Input - Single Output Design Theory

Introduction

Chapters II and III present an overview of the Quantitative Feedback Theory (QFT) technique used in the design of multiple input - multiple output (MIMO) flight control systems for this thesis. Examples are presented to aid in the understanding of the material. The technique is valid for the general n-by-n case. However, for simplicity, the examples below are either single loop or two-by-two systems. See References 9 and 16 in the bibliography for a discussion of the three-by-three case and extrapolation to the general case.

The flight control problem involves a multiple input - multiple output plant requiring regulation and control due to parameter uncertainty and disturbances. The mathematical equations describing the motion of an aircraft are highly non-linear. For design purposes, these equations are linearized about a point in the flight envelope, or flight condition. *Uncertainty arises as the linearized coefficients vary with airspeed and altitude.*

The QFT technique developed by Dr. Isaac Horowitz uses feedback to achieve a closed-loop system response within performance tolerances despite plant uncertainty. The range of plant uncertainty and the output performance specifications are quantitative parameters in the design process (Ref 9:81). The fundamentals of the design method are presented in the discussion of the two input - single output design problem of Chapter II. The multiple input - multiple output design procedure is described in Chapter III, using the fundamentals developed in Chapter II.

Problem Definition

The general multiple input - single output (MISO) problem involves a plant transfer function, P, with uncertain parameters (gain, poles, and zeros) known only to be members of finite sets. The design specifications dictate the desired response of the plant to inputs and/or disturbances. The problem is to obtain a contr .er forcing the plant output to satisfy

performance tolerances over the range of plant uncertainty.

The basic MISO control loop structure is shown in Figure II-1.

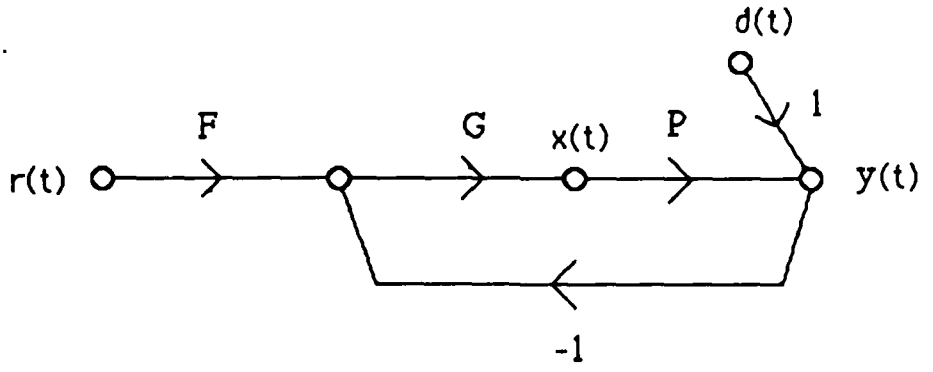

Fig. II-1. Two Degree-of-Freedom MISO Feedback Structure

In the figure, r(t) is the command input to the system and d(t) is a disturbance input to be attenuated. P is the plant transfer function whose characteristics are not precisely known. The compensator, G, and the prefilter, F, are designed to force the system output, y(t), to be a member of a set of acceptable responses despite the uncertainty in P and the disturbance input, d(t). The plant input signal, x(t), is identified since it is generally of interest due to physical or practical constraints. The signals r(t) and y(t) are assumed measurable quantities and the latter is available for feedback. Access to both signals allows the use of the two degree-of-freedom structure of Figure II-1 and provides the designer with two independent compensator elements, F and G (Ref 10:13). It is also assumed r(t), y(t), and (for now) the plant, P, where $y(t) = Px(t)$, are all Laplace transformable functions (Ref 10:8).

There are four transfer functions of interest from Figure II-1. The overall system transfer functions T_R and T_D are the control ratios of the output y(t) to the inputs r(t) and d(t) respectively, i.e.,

$$T_R = \frac{Y}{R} = \frac{FGP}{1 + GP} \tag{II-1}$$

$$T_D = \frac{Y}{D} = \frac{1}{1 + GP} \tag{II-2}$$

The loop transmission L is defined as L = GP for the system in Figure II-1. The control ratios in terms of L are written as follows:

$$T_R = \frac{Y}{R} = \frac{FL}{1 + L} \tag{II-3}$$

$$T_D = \frac{Y}{D} = \frac{1}{1 + L} \tag{II-4}$$

The transfer functions describing the plant input x(t) to the command and disturbance inputs are shown below.

$$I_R .= \frac{X}{R} = \frac{FG}{1 + GP} = \frac{FG}{1 + L} \tag{II-5}$$

$$I_D = \frac{X}{D} = \frac{-G}{1 + GP} = \frac{-G}{1 + L} \tag{II-6}$$

The design specifications may impose constraints on any or all of the above transfer functions, but for the purpose of this example, only the transfer functions T_R and T_D are considered.

Design Specifications

The design specifications, or closed-loop system response tolerances, describe the upper and lower limits for acceptable output response to a desired input or disturbance. Any output response between the two bounds is assumed acceptable. The response specifications must be determined prior to applying the design method. Typically, tracking response specifications are given in the time domain, such as the figures of merit M_p, t_s, t_p, and K_m (Ref 5) based upon a step forcing function, or as a region bounded by T_U and T_L as shown in Figure II-2.

Response to a step input is a good initial test of system response. Bounds T_U and T_L of the figure are the acceptable upper and lower limits, respectively, of a system's tracking performance to a step input. Desired system response to a step disturbance generally

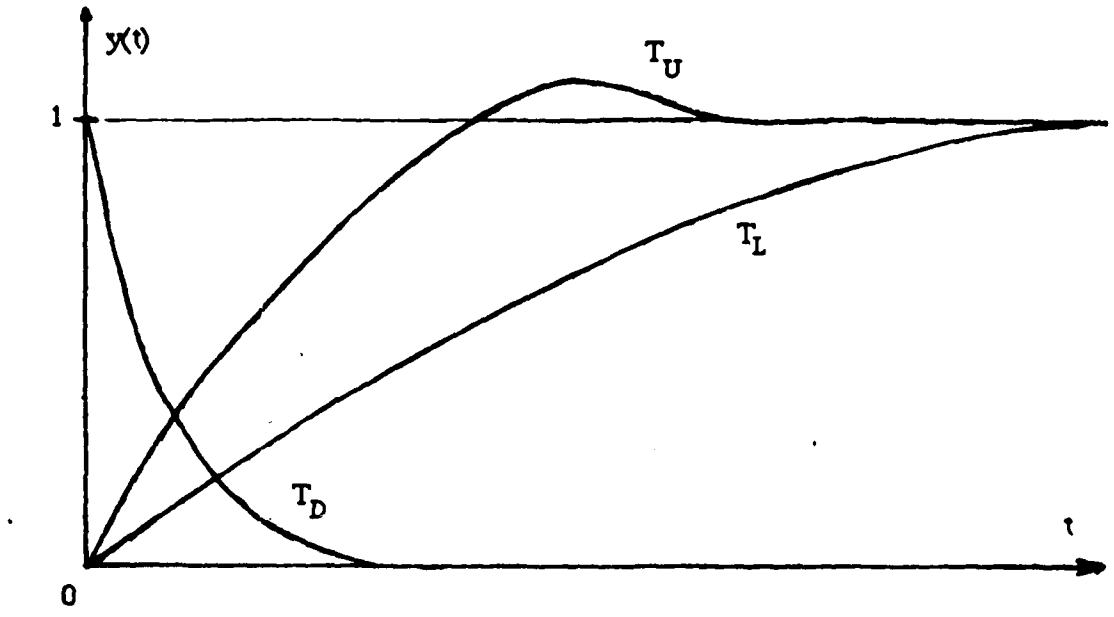

Fig. II-2. Time Domain Step Response Specifications

requires maintaining the output below a given value, thus only an upper bound is necessary as shown by the curve T_D in Figure II-2. Additional similar bounds are needed if other inputs are to be considered.

The design technique is a frequency domain approach, therefore the time domain specifications must be translated to bounds in the frequency domain. The desired control ratios, $T_{MR} = [Y/R]_{MR}$ and $T_{MD} = [Y/D]_{MD}$, are modeled to satisfy the performance specifications using the pole-zero placement method as described in Reference 5, Sections 12.2 and 12.8. For response to a step input, a third order model with one zero is suggested.

$$T_M(s) = \frac{A(s - z_1)}{(s - p_1)(s - p_2)(s - p_3)} = \frac{A(s - z_1)}{(s^2 + 2\zeta\omega_n s + (\omega_n)^2)(s - p_3)} \qquad \text{(II-7)}$$

The pole-zero pattern corresponding to Equation (II-7) is shown in Figure II-3. The locations of the roots are adjusted until the step response of the modeled control ratio matches a bound.

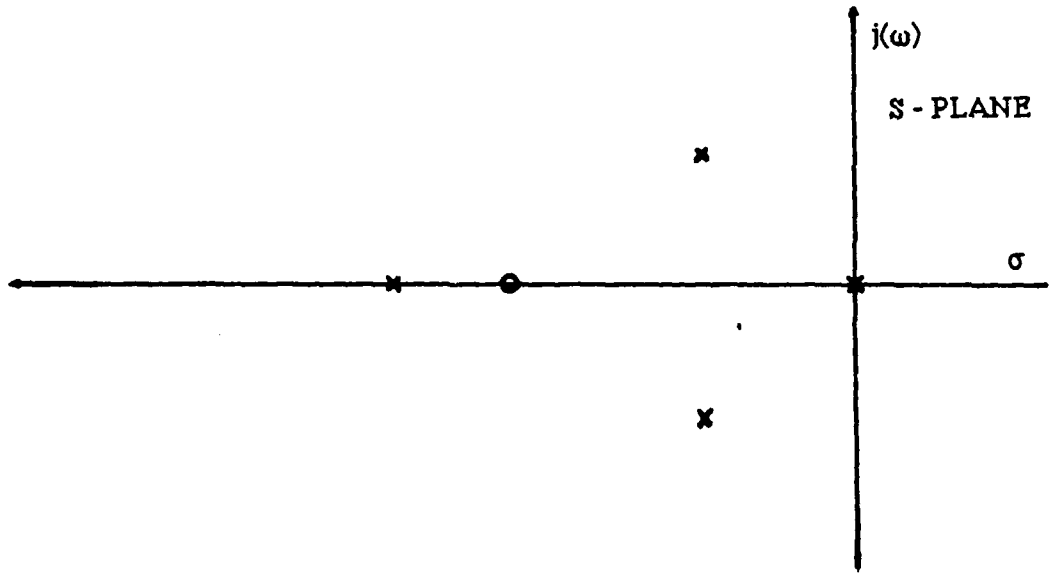

Fig. II-3. Third-Order Control Ratio Pole-Zero Pattern

The frequency domain characteristics of the problem are considered during the response modeling process. It is desired to keep the magnitude difference (as a function of frequency) between the upper and lower bound models of $|T_{MR}(j\omega)|$ as large as possible over the entire frequency range. Choosing a lower bound model with a greater pole-to-zero ratio than the upper bound model ensures the magnitude difference continually increases and approaches infinity in the limit as ω approaches infinity.

Errors made during the modeling process manifest themselves in one of two ways. First, if the lower acceptable response model is not truly acceptable, the system may not meet the design specifications over the assumed range of uncertainty in P. And second, if the entire range of allowable outputs is not considered, overdesign may arise with respect to the variation in T. As a result, the bandwidth of the compensation can be larger than necessary, increasing the cost of the compensator (Ref 10:5).

Once control ratios are obtained for each time response bound, a Log-magnitude plot of the frequency response (Bode plot) for each $T_M(j\omega)$ is made on the same graph as shown in Figure II-4. These plots are a frequency domain representation of the design specifications on T_R and T_D. The frequency domain specifications are used to obtain bounds on the loop transmission $L(j\omega)$. The largest value of ω_h, obtained in the manner

shown in Figure II-4, is used as the initial upper frequency bound for obtaining plant templates (to be discussed later).

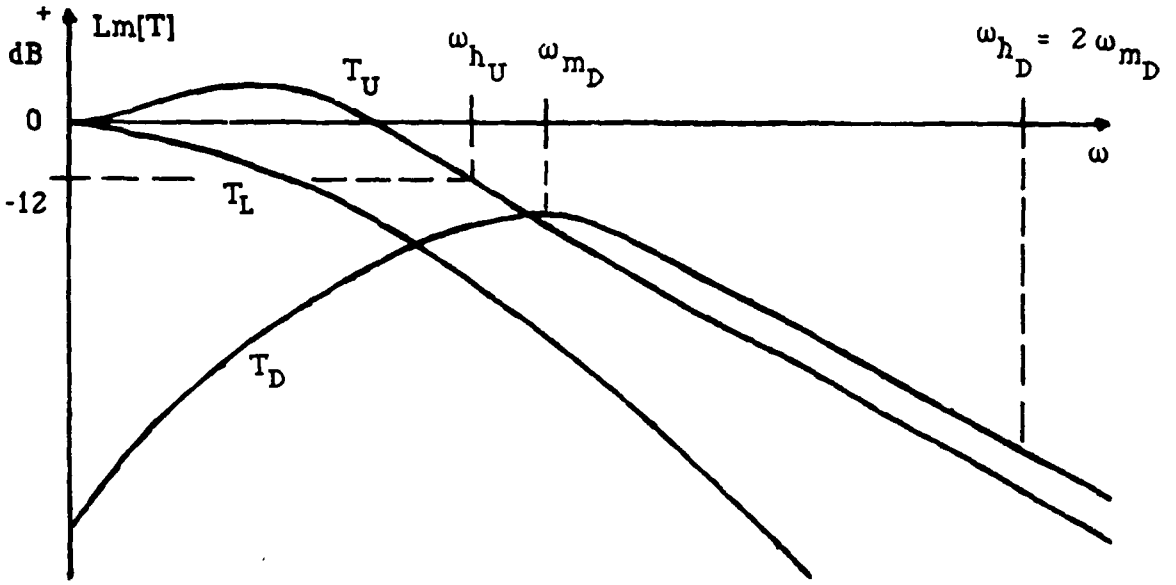

Fig. II-4. Frequency Domain Specifications

Nichols Chart

The primary tool used in the design of the compensator elements G and F is the Nichols chart, shown in Figure II-5. If the open loop transmission of a unity feedback system (L = GP, assuming F = 1 for now, in Figure II-1) is plotted using the horizontal and vertical scales on the chart, then at any given frequency, the magnitude and phase angle of $T_R = L/(1 + L)$ can be read directly from the curved scales. Conversely, any point corresponding to the magnitude and angle of T_R on the curved scales provides a point corresponding to the magnitude and angle of L on the horizontal and vertical scales (Ref 5:332-334). This correspondence between L and T_R on the Nichols chart is very important.

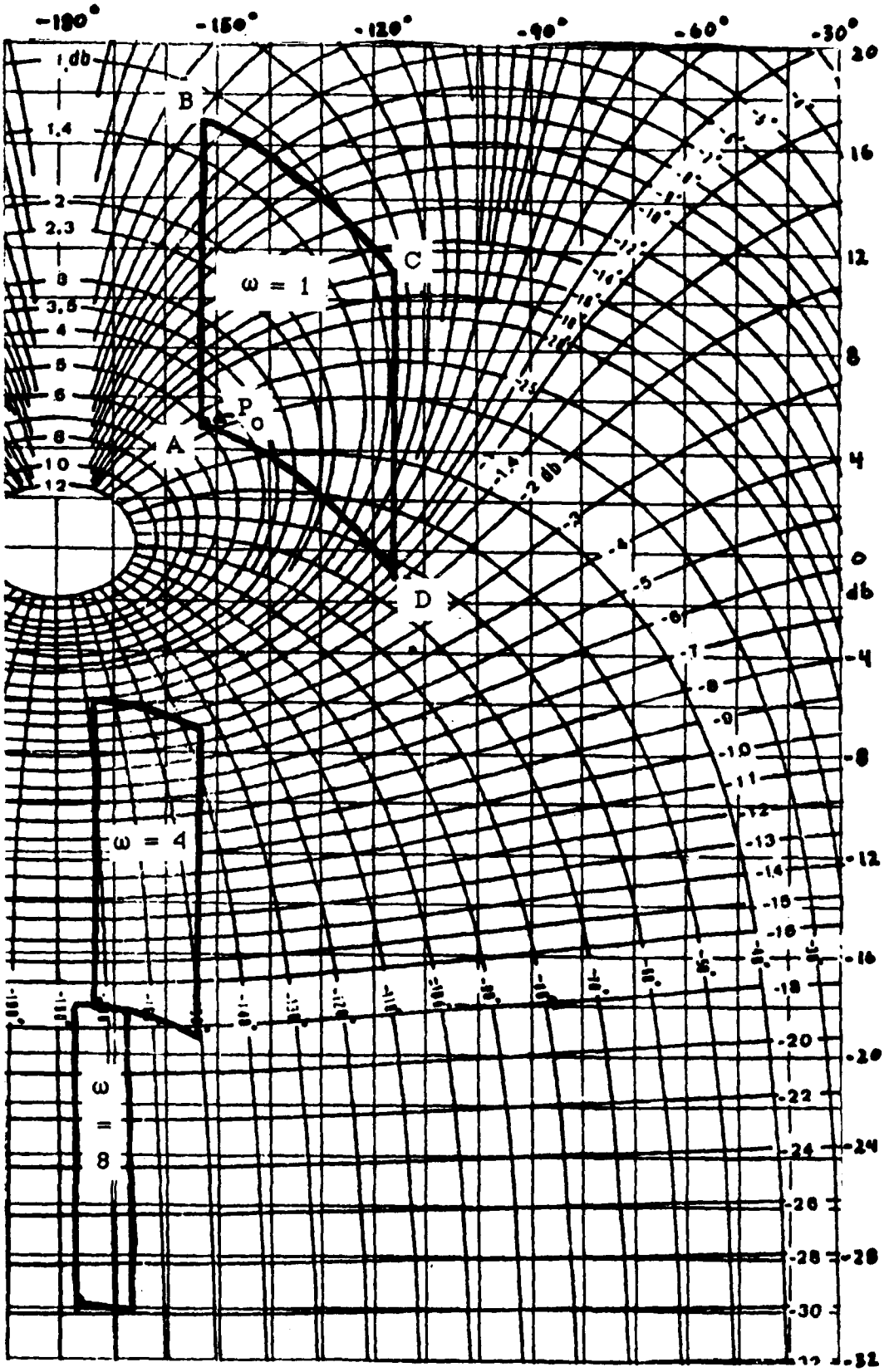

Fig. II-5. Nichols Chart with Plant Templates

Likewise, the Nichols chart can be used for the disturbance response problem. Recall from Equation (II-4), the control ratio relating the output to the disturbance input is given by $T_D = 1/(1 + L)$. Using the transformation, $L = 1/m$ (Ref 1:152-155), the control ratio becomes $T_D = m/(1 + m)$, which is suitable for the Nichols chart. One could design the inverse of the loop transmission m directly on the Nichols chart, but it is much easier to realize that by turning the Nichols chart upside down, reflecting the vertical angle lines of L about the -180 degree line (i.e. -190° becomes -170°, -210° becomes -150°, etc.), and reversing the signs on all magnitude lines, the chart can be used directly to design L itself. The horizontal and vertical lines still correspond to the magnitude and angle of L, and the curbed magnitude lines correspond to the magnitude of (1 + L) (Ref 1:155). For design purposes, only the magnitude of (1 + L) is required. Therefore, the curved angle lines on the chart can be ignored. In practice, the transformation $L = 1/m$ is merely implied by turning the Nichols chart upside down and modifying the scales as described above. The dummy variable m need not be considered further.

Plant Templates

A plant template is a plot on the Nichols chart of the range of uncertainty in the plant P at a given frequency (Ref 8:290). Consider the example $P(s) = K/s(s+a)$ where the gain K is described by: $2 < K < 8$, and the location of the second pole is given by: $0.5 < a < 2.0$. An infinite number of possible P's exist due to the variation in parameters K and a; however each parameter is a member of a set with finite boundaries. Likewise, the magnitude and phase angle of all possible P's lie within finite boundaries when plotted at a given frequency. The plant template is obtained by plotting $Lm[P(j\omega)]$ vs. $Ang[P(j\omega)]$ for all possible $P(j\omega)$'s at a given frequency on the Nichols chart. Note, only the boundaries of the template need be calculated. The plant transfer functions at the boundaries are found by holding one parameter constant at a boundary value, i.e. set $K = 2$, and vary a in increments from 0.5 to 2.0 to obtain a set of plant transfer functions. The frequency

response at $\omega_i = 1$ for the P's obtained in this manner provide a set of points from A, (K = 2, a = 0.5), to D, (K = 2, a = 2), on the Nichols chart as shown in Figure II-5. The process is continued until the complete template is formed. For example, for a = 0.5, vary K from 2 to 8 to obtain the line from A, (a = 0.5, K = 2), to B, (a = 0.5, K = 8). Templates are needed for a number of frequencies taken at regular intervals, such as every octave, up to the largest ω_h value. A set of templates is shown in the figure to demonstrate the change in size and location of the range of uncertainty in P for different frequencies.

Nominal Plant

To facilitate the shaping of the loop transmission, the designer needs a reference or nominal plant transfer function. A nominal plant P_0 is chosen by the designer to be used in the definition and shaping of the nominal loop transmission $L_0 = GP_0$. There are no rules or constraints governing the selection of P_0. The nominal plant is not required to be from the set of possible P's, but selecting P_0 to lie at a recognizable point on the plant templates is usually convenient. For convenience in the example, P_0 was selected to lie at the lower left corner of the templates. This allows the bounds on L_0, described below, to be drawn as close to the center of the Nichols chart as possible. Once the nominal plant is chosen, the value of P_0 is marked on each template, as shown in Figure II-5. For the example, the plant described by $P_0 = 2/(s + 0.5)$ is selected as the nominal plant.

Derivation of Bounds on L(jω)

The system response y(t) is uniquely determined by the transfer function T(s). Likewise, T(s), for a stable, minimum phase system (no right-half-plane poles or zeros), is completely specified by the magnitude of the frequency response $|T(j\omega)|$ as described in References 8 and 10. The bounds on $|T(j\omega)|$ are known by determining the frequency domain specifications as described previously. The specifications for the $|T(j\omega)|$ are translated to bounds $B(j\omega)$ on $L(j\omega)$ using the correspondence between T_R (T_D) and L on

the Nichols chart.

Given the design specifications for $T_R(j\omega)$, the frequency response of the output can vary from the value on the bound T_U to the value on the bound T_L at a given frequency (see Figure II-4). For the given example, at the frequency $\omega_i = 1$, assume $|T_R(jl)|$ can vary from 0.7 dB to -0.8 dB. The allowable relative variation $\delta_R(jl)$ is 0.7 dB - (-0.8) dB or 1.5 dB. In general, the allowable relative variation in $|T_R(j\omega)|$ at a given frequency is expressed as:

$$\delta_R(j\omega_i) = Lm[T_U(j\omega_i)] - Lm[T_L(j\omega_i)] \qquad \text{(II-8)}$$

where $T_U(j\omega)$ and $T_L(j\omega)$ are the frequency domain bounds on $T_R(j\omega)$.

The uncertainty in the plant P is related to an uncertainty in the control ratio as follows. Recall from Figure II-1 and Equation (II-3), $T_R = FL/(1+L)$ where $L = GP$. It is assumed that the compensators F and G can be constructed with negligible uncertainty. Then, the uncertainty in P results in an uncertainty in the loop transmission, i.e.,

$$\Delta Lm[P(j\omega_i)] = \Delta Lm[L(j\omega_i)] \qquad \text{(II-9)}$$

since $Lm[L] = Lm[GP] \approx Lm[G] + Lm[P]$ and the uncertainty in G, $\Delta Lm[G]$, is assumed negligible. Likewise, the uncertainty in P is related to an uncertainty in the control ratio via Equations (II-3) and (II-9), i.e.,

$$\Delta Lm[T(j\omega_i)] \approx \Delta Lm \frac{L(j\omega_i)}{1 + L(j\omega_i)} \qquad \text{(II-10)}$$

where $Lm[T] = Lm[FL/(1+L)] = Lm[F] + Lm[L/(1+L)]$ and the uncertainty in F, $\Delta Lm[F]$, is assumed negligible (Ref 10:15-16). The variation in P arises due to parameter uncertainty, thus the problem is to find an L satisfying the allowable relative variation requirements on the closed-loop response for the entire uncertainty range of P. The design specifications state the requirements on the closed-loop response $Y(j\omega)$ and thus $T(j\omega)$ as given by Equation (II-10). It is desired to obtain constraints on the loop transmission, $L(j\omega)$ (Ref 8:291, 10:18).

L(jω) Bounds on the Nichols Chart

The relative uncertainty in L is shown to equal to the range of uncertainty in P by Equation (II-9). As described earlier, the plant template is a plot on the Nichols chart of the range of uncertainty in P at a given frequency. From the relations: Lm[L] = Lm[P] + Lm[G] and Ang[L] = Ang[P] + Ang[G], a template may be translated (but not rotated) horizontally or vertically on the Nichols chart, where horizontal and vertical translations correspond to the angle and magnitude requirements respectively on G(jω) at a given frequency (Ref 8:290). Drawing a line on each of the templates parallel to the horizontal or vertical grid lines (see Figure II-5) of the Nichols chart is suggested to maintain correct template orientation.

With the template corresponding to $\omega_i = 1$ of Figure II-5, translate it to position 1 shown in Figure II-6. Since the template is the range of uncertainty in P and L = GP, where G is to be precisely determined, it follows that the area now covered by the template corresponds to the variation in L and T due to the uncertainty of P. Recall the correspondence between L and T on the Nichols chart. Using the curved magnitude contours, i.e. contours of constant Lm[T(jω)], read the maximum and minimum values of T covered by the template. If the difference between the maximum and minimum values is greater than the allowable variation $\delta_R(j\omega_i)$ in T at the frequency $\omega_i = 1$, (as given by Equations (II-8) and (II-10) and determined from Figure II-4), shift the template vertically as shown in Figure II-6, until the difference equals $\delta_R(j1)$ (to position 2). Conversely, if the difference is less than that allowed, move the template vertically downward until the equality is obtained. When the position of the template achieves the equality (position 2 of the example), mark the nominal point P_o of the template on the Nichols chart. The point marked corresponds to the magnitude and phase angle values of $L_o(j1)$ read from the horizontal and vertical scales of the Nichols chart, where the nominal loop transmission, $L_o(j\omega_i)$, is given by:

$$L_o(j\omega_i) = G(j\omega_i)P_o(j\omega_i) \qquad \text{(II-11)}$$

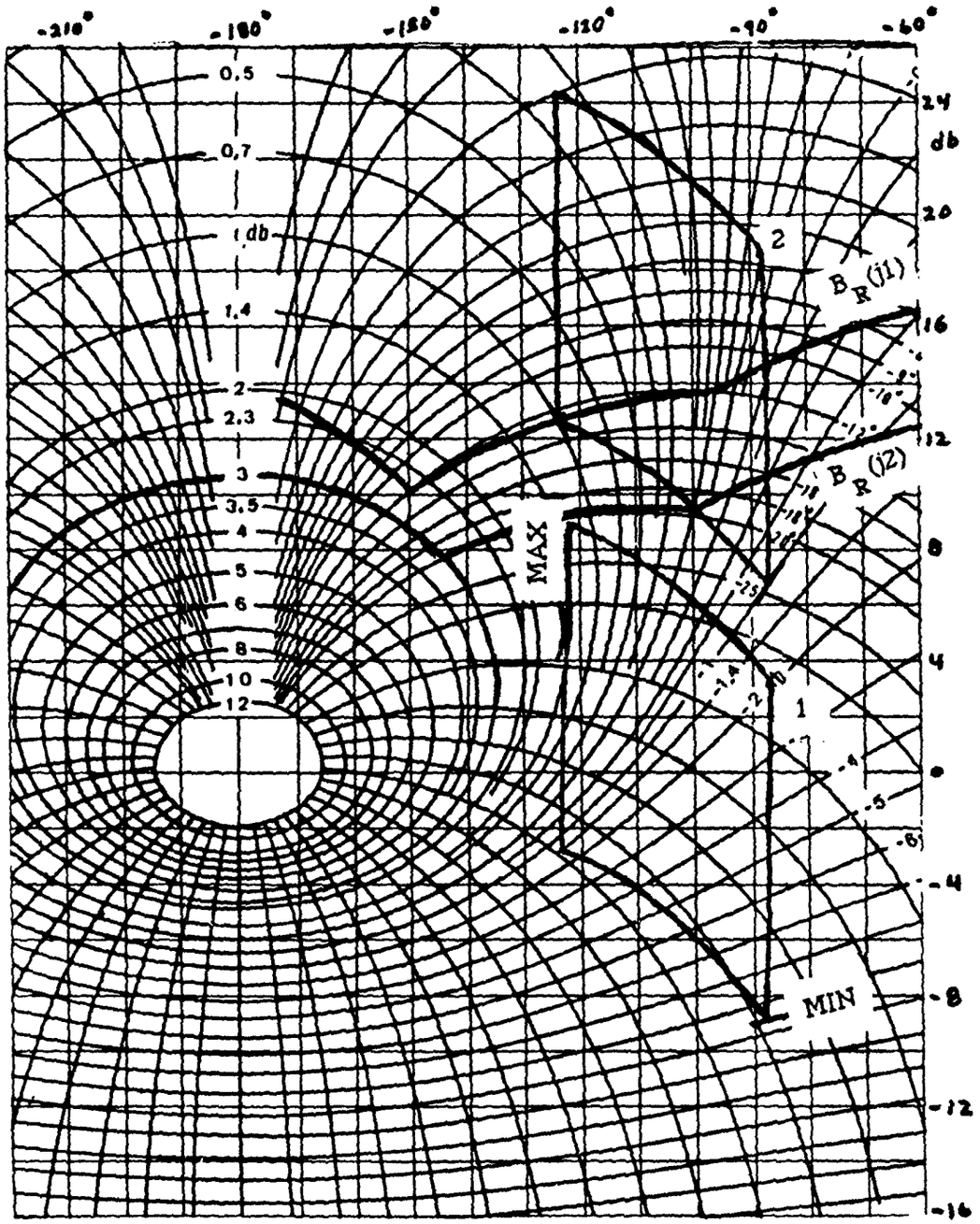

Fig. II-6. $L_o(j\omega_i)$ Bounds on the Nichols Chart

Repeat the process horizontally across the chart at different values of Ang[$L_o(j\omega)$]. The points marked on the chart form a curve $B_R(j\omega_i)$ representing the boundary of $L_o(j\omega_i)$ at the given frequency of the template. As long as $L_o(j\omega_i)$ lies above or outside the boundary $B_R(j\omega_i)$ at the frequency $\omega = \omega_i$, the variation in T due to the uncertainty in P is less than or equal to the relative change in T allowed by the design specifications at that frequency. Repeat the boundary $B_R(j\omega_i)$ derivation for various frequencies, ω_i, using the corresponding plant templates to obtain a series of bounds on $L_o(j\omega_i)$ (Ref 8:291-292).

Likewise, the step disturbance response specification (line T_D of Figure II-4) is converted to bounds on $L_o(j\omega_i)$. In order to effectively reject the disturbance, the following inequality must be satisfied:

$$\frac{1}{|\,1 + L(j\omega)\,|} \leq |\,C(j\omega)\,| \qquad \text{(II-12)}$$

where $|C(j\omega)|$ is the magnitude of the boundary, T_D, of Figure II-4. Expressing the magnitudes in decibels and rearranging terms, the inequality is written as:

$$\text{Lm}\,[1 + L(j\omega)] \geq -\text{Lm}\,[C(j\omega)] \qquad \text{(II-13)}$$

A template is placed on the inverted Nichols chart such that its lowest point rests directly on the contour of constant Lm[1 + L(jω)] equal to -Lm[C(jω)] at the frequency ω_i for which the template is drawn. The point P_o is marked on the chart and the template slid along the same contour forming a bound $B_D(j\omega_i)$ on $L_o(j\omega_i)$. Bounds are formed in this manner for all frequencies ω_i considered using the set of templates. Employing the rectangular (Lm[L]) grid, transcribe the disturbance bounds $B_D(j\omega_i)$ onto the upright Nichols chart having the command response bounds $B_R(j\omega)$ already drawn (see Figure II-7). At each frequency of interest, the lower of the two bounds is erased. The remaining bound, labeled $B_o(j\omega_i)$, places the greatest demand on $L_o(j\omega)$ at the given frequency. The point being made is the worst case bound must be used in the shaping of $L_o(j\omega)$.

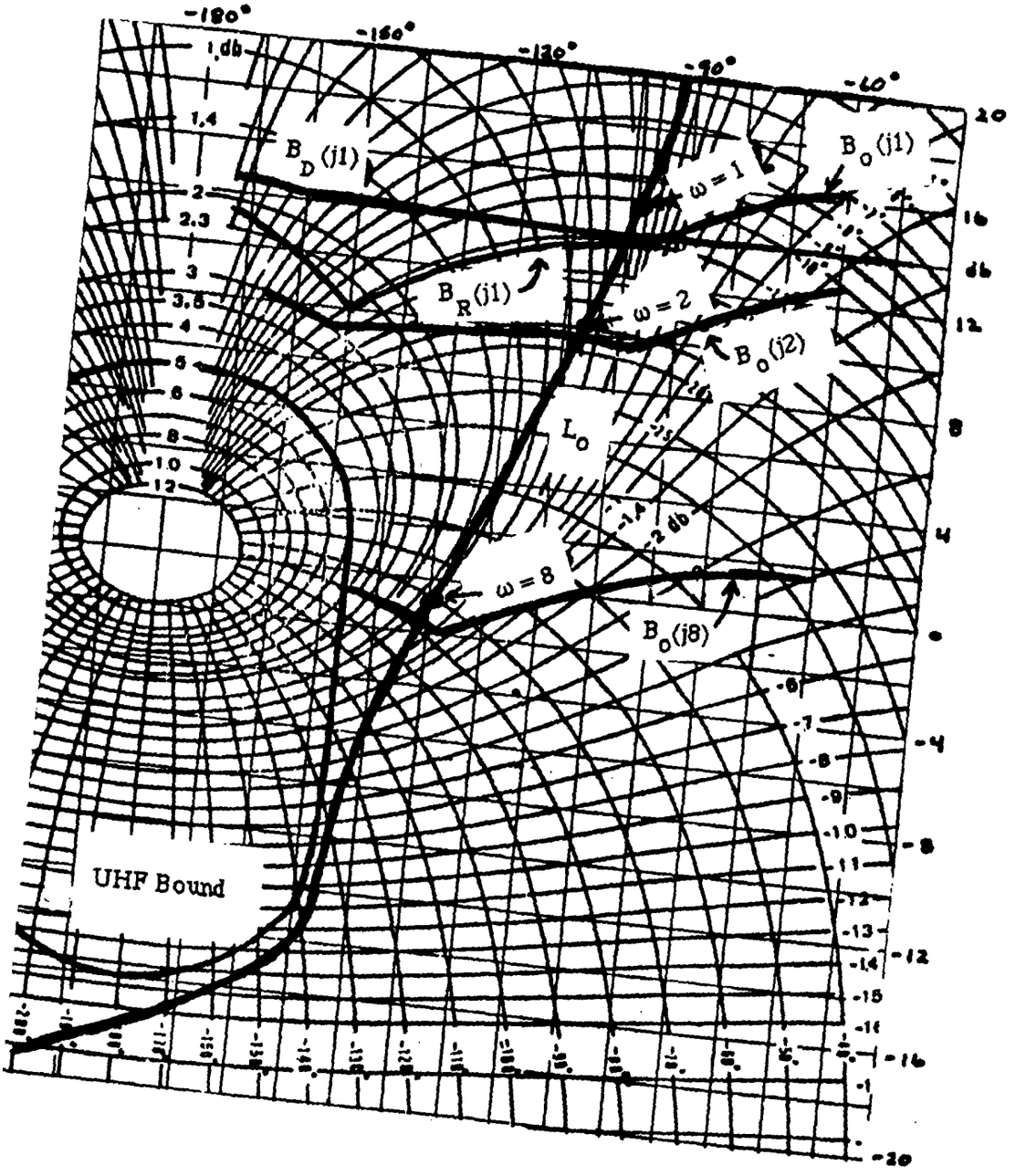

Fig. II-7. Nominal $L_o(j\omega_i)$

Universal High Frequency Bound

The universal high frequency (UHF) bound ensures the loop transmission L has positive phase and gain margins, whose values depend on the oval of constant magnitude chosen (see Figure II-7). As the frequency ω increases, the plant templates become narrower and can be considered vertical lines as ω approaches infinity. The allowable variation in T increases with frequency also. The result is the bounds of $L_0(j\omega_i)$ tend to become a narrow region about the 0 dB, -180 degree point (origin) of the Nichols chart at high frequency. To avoid placing closed-loop poles near the $j\omega$ axis resulting in oscillatory response, a UHF bound is needed on the Nichols chart. With increasing ω, the bounds on L_0 approximately follow the ovals encircling the origin. Choose one of the ovals near the origin. In Figure II-7, the contour of constant magnitude equal to 5 dB is used for this example. From the templates corresponding to high frequency, find the template with the greatest vertical displacement, Δv, in dB. Δv may be accurately determined by finding the maximum change in $Lm[P(j\omega)]$ in the limit as ω approaches infinity. Translate the lower half of the 5 dB oval down the length of the template, i.e. Δv, as shown, thus obtaininng the UHF bound (see Figure II-7) (Ref 10:20-22).

Shaping of the Nominal Loop Transmission $L_0(j\omega)$

The shaping of a nominal loop transmission conforming to the boundaries of L_0 is the most crucial step in the design process. A minimum bandwidth design has the value of L_0 on its corresponding bound at each frequency. In practical designs, the goal is to have the value of L_0 occurring above the corresponding bound, but as close as possible to keep the bandwidth to a minimum. Figure II-7 shows a practical design for L_0. Note, any right-half-plane (rhp) poles and/or zeros occurring in P_0 must be included in L_0 to avoid any attempt to cancel them with zeros and/or poles of G. Although not required, using the poles and zeros of P_0 as a starting point in the design of L_0 is suggested, avoiding any implicit cancellation of roots in determining G. Figure II-8 provides an algorithm which

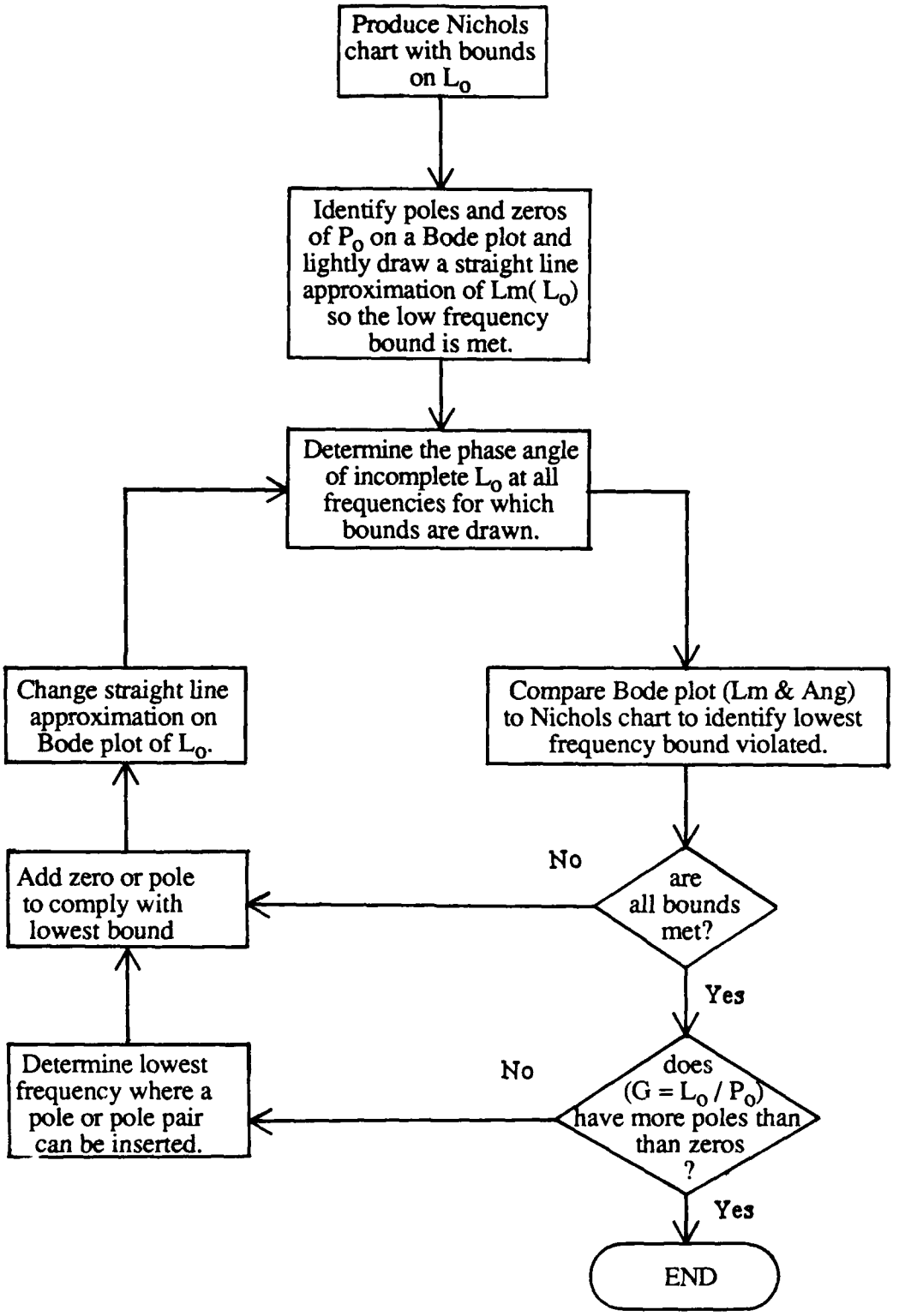

Fig. II-8. Algorithm for Loop Transmission Shaping

may be helpful in shaping L_o. For additional discussion concerning loop transmission shaping along with specific examples, see Appendix A.

Solving for the Compensator G

The compensator G is obtained from the relation: $G = L_o/P_o$. If the L_o found above does not contain the zeros and poles of P_o, then the compensator G must cancel them. Note, cancellation occurs only for purposes of design using the nominal plant transfer function.

Provided the nominal loop transmission $L_o(j\omega)$ is shaped properly, i.e. meets requirement of being on or above the bound $B_o(j\omega_i)$, at each corresponding frequency, the variation in T resulting from the uncertainty in P is guaranteed to be less than or equal to the allowable relative change in T obtained from the design specifications (Ref 8:291). The design of the prefilter F is the final step in the design process.

Design of the Prefilter F

Design of a proper $L_o(j\omega)$ only guarantees the variation in $|T(j\omega)|$ is less than or equal to that allowed. The purpose of the prefilter is to position $Lm[T(j\omega)]$ within the frequency domain specifications. For the example given above, the magnitude of the frequency response must lie within the bounds shown in Figure II-4 and redrawn in Figure II-9. One method to determine bounds on the prefilter F is as follows. Place the nominal point of the $\omega_i = 1$ template on the Nichols chart where the $L_o(jl)$ point occurs. Record the maximum and minimum value of $Lm[T(jl)]$, 1.2 and 1.0 in the example, obtained from the curved magnitude contours. Compare the values found above to the maximum and minimum values allowed by the frequency domain specifications of Figure II-4 at $\omega_i = 1$, (0.7 dB and -0.8 dB). Determine the range in dB $Lm[T(j\omega)]$ must be raised or lowered to fit within the bounds of the specifications. For example, at $\omega_i = 1$, the actual $Lm[T(j1)]$ must be within the bounds as given by: $(Lm[T_U] = 0.7\ dB) > Lm[T(j1)] > (Lm[T_L] = -0.8\ dB)$.

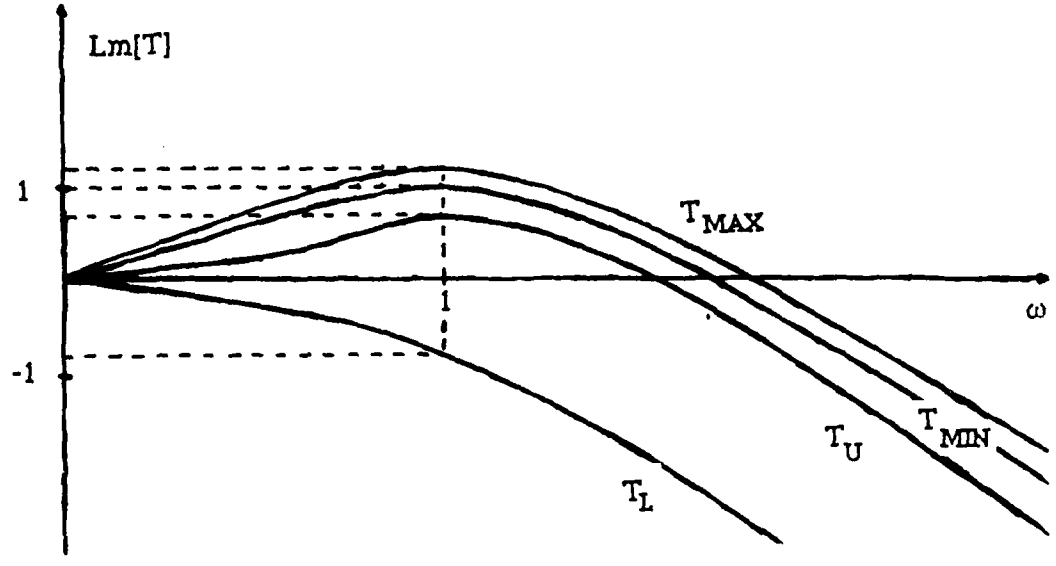

Fig. II-9. Requirements on the Prefilter F

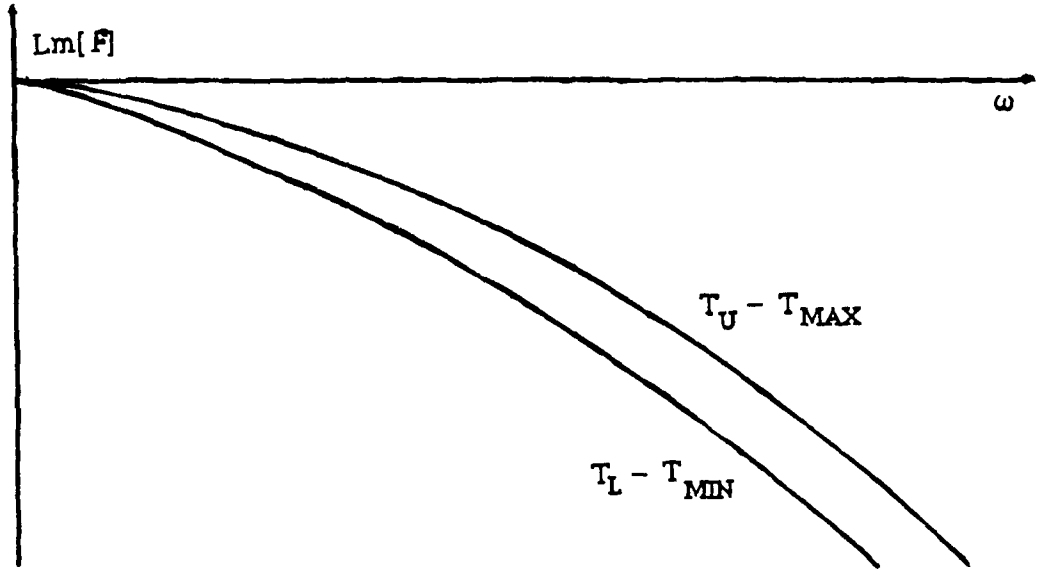

Fig. II-10. Frequency Bounds on the Prefilter F

But, from the plot of $L_o(j1)$, the actual range of Lm[T(j1)] is: 1.2 dB > Lm[T(j1)] > 1.0 dB. To lower Lm[T(j1)] from the actual range to the desired range, the prefilter, Lm[F(jω)], required at $\omega_i = 1$ is: (0.7 dB - 1.2 dB) > Lm[F(j1)] > (-0.8 dB - 1.0 dB), or -0.5 dB > Lm[F(j1)] > -1.8 dB (see Figure II-9). The process is repeated for each frequency corresponding to the templates used in the design of $L_o(j\omega)$. Therefore in Figure II-9, the difference between the T_U and T_{max} curves and the difference between the T_L and T_{min} curves indicate the requirements for F(jω) as a function of frequency.

Bounds on F, (Lm[T_U] - Lm[T_{max}]) > Lm[F] > (Lm[T_L] - Lm[T_{min}]), are plotted as a function of frequency as shown in Figure II-10. Using a straight line approximation, determine a transfer function F(s) whose magnitude lies within these bounds. The transfer function obtained in this manner is the prefilter F (Ref 8:301).

The single loop design is complete with the design of F. The system response is guaranteed to remain within the bounds of the design specifications, provided the uncertainty in P stays within the range assumed prior to the design process (Ref 8:288).

Summary

This chapter presents an overview of the MISO design technique of Dr. Horowitz for minimum phase systems with uncertain plants. The technique is based entirely in the frequency domain and makes considerable use of Nichols and Bode plots. Graphical methods can be used for much of the design process.

Design specifications are translated into the frequency domain and constitute limits or boundaries on the frequency response of the system control ratio and the loop transmission. The two compensator elements G and F are synthesized to control the system response to inputs and disturbances.

III. Multiple Input - Multiple Output Design Theory

Introduction

The design approach for each loop of the multiple input - multiple output system is identical to that for the MISO system described in Chapter II. But first, the MIMO system is separated into a set of MISO systems. The set taken as a whole is equivalent to the actual MIMO model.

In general, an n x n MIMO system can be represented in matrix notation as $\mathbf{y} = \mathbf{Pu}$, where **y** is the vector of plant outputs, **u** is the vector of plant inputs, and **P** is the plant transfer function matrix relating **u** to **y**. The **P** matrix is formed from either the linear differential equations describing the system or directly from the system state space representation.

Dr. Horowitz has shown, by the use of fixed point theory, the inverse of the **P** matrix, defined as **Q'**, contains elements which are the reciprocals of n^2 single loop transfer functions equivalent to the original MIMO plant. The MIMO problem is then broken into n loop designs and n^2 prefilter/disturbance problems which are handled as described in Chapter II. The solution of the MISO problems taken as a whole is guaranteed to solve the original MIMO problem (Ref 11:677, 12 and 16).

The MIMO Plant

The MIMO plant is represented by the diagram of Figure III-1. The n x 1 input vector **u** produces an n x 1 output vector **y**. The relationship between **y** and **u** is described by the n x n plant matrix **P** which is known only to be an element of a set of possible **P**'s. It is assumed the range of uncertainty in **P** can be determined, probably in the form of empirical data relating **u** to **y**. Note the input and output vectors are assumed to be the same dimension. Although this may appear to be a restrictive assumption, it can be shown only n outputs can be independently controlled with n inputs (Ref 7:530-536).

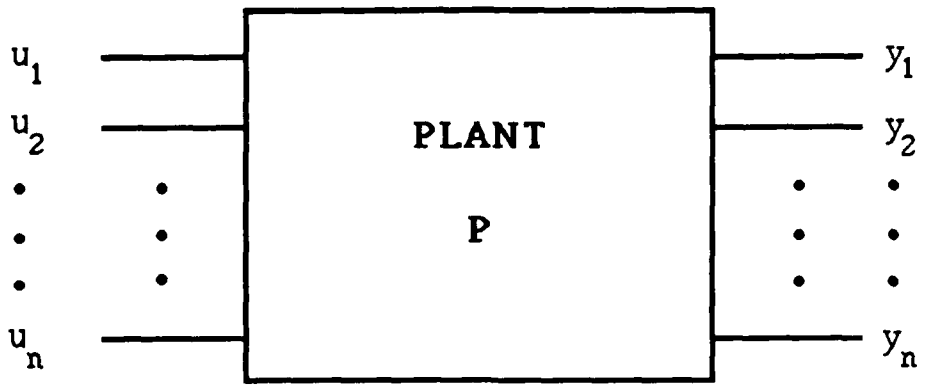

Fig. III-1. General n x n MIMO Plant

Thus if the existing model defines an unequal number of inputs and outputs, the first step is to modify the model to make the dimensions of the input and output vectors equal.

The plant matrix **P** can be derived directly from the set of coupled, linear, time-invariant differential equations describing the behavior of the plant in response to its inputs. For example, consider a general plant model of the form shown below.

$$\begin{aligned} [(a)y_1 + (bs^2 + cs)y_2] &= [(f)\,u_1 + (g)u_2] \\ [(ds)y_1 + (e)y_2] &= [(h)u_1 + (i)u_2] \end{aligned} \tag{III-1}$$

The variables (a) through (i) are constant coefficients, the y's are the outputs, and the u's are the inputs to the plant. The system described by Equation (III-1) can be represented in matrix notation as given below.

$$\begin{bmatrix} a & bs2 + cs \\ ds & e \end{bmatrix} \mathbf{y} = \begin{bmatrix} f & g \\ h & i \end{bmatrix} \mathbf{u} \tag{III-2}$$

Define the matrix multiplying the output vector **y** as **M** and the matrix multiplying the input vector **u** as **N**. The system is now described by the equation:

$$\mathbf{My} = \mathbf{Nu} \tag{III-3}$$

The plant matrix required is defined by:

$$\mathbf{y} = \mathbf{Pu} \tag{III-4}$$

Thus, the plant transfer function matrix is found from the equation:

$$\mathbf{P} = \mathbf{M}^{-1}\mathbf{N} \tag{III-5}$$

The standard state space representation for a system is described by the equation (Ref 5:93):

$$\begin{aligned} \dot{\mathbf{x}} &= \mathbf{Ax} + \mathbf{Bu} \\ \mathbf{y} &= \mathbf{Cx} \end{aligned} \tag{III-6}$$

The block diagram for this system is shown in Figure III-2.

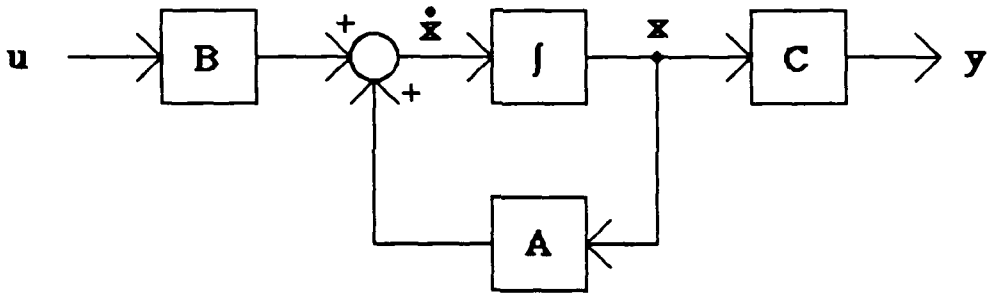

Fig. III-2. Standard State Space Diagram

Although any number of states may be represented, it is again assumed the input and output vectors, **u** and **y** respectively, are of equal dimension. Assuming the system is linearized and the matrices, **A**, **B**, and **C**, are time invariant, the plant transfer function matrix **P** is obtained from the equation:

$$\mathbf{P} = \mathbf{C}[s\mathbf{I} - \mathbf{A}]^{-1}\mathbf{B} \tag{III-7}$$

The plant matrix is a representative member of a set of possible plant matrices due to the uncertainty in the plant parameters. In practice, a finite set of **P** matrices is formed representing the plant under varying conditions.

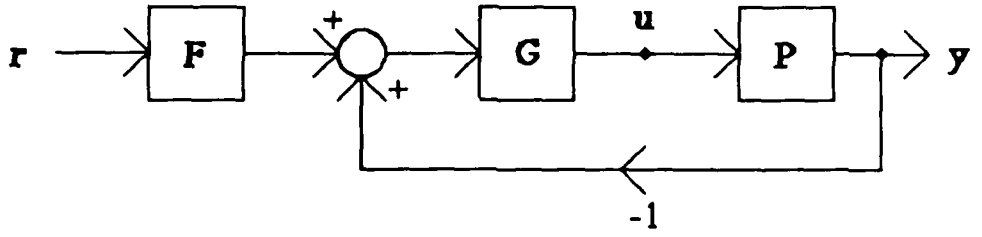

Fig. III-3. Two Degree-of-Freedom MIMO Feedback Structure

MIMO Compensation

The compensation scheme for the MIMO system is similar to the MISO system of Chapter II. The basic MIMO control structure is shown in Figure III-3 where **P** is the plant matrix with uncertain parameters, **G** is a diagonal compensator matrix, and **F** is a diagonal compensator matrix, and **F** is a prefilter matrix. Designs involving a nondiagonal **G** matrix (Ref 13:14) are not considered in this thesis. The functions **G** and **F** are identical to those of G and F of the MISO system of Chapter II. Figure III-4 shows a detailed breakdown of the two-by-two MIMO structure with a diagonal **G** matrix where:

$$\mathbf{G} = \begin{bmatrix} g_1 & 0 \\ 0 & g_2 \end{bmatrix} \quad \mathbf{F} = \begin{bmatrix} f_{11} & f_{12} \\ f_{21} & f_{22} \end{bmatrix} \quad \mathbf{P} = \begin{bmatrix} p_{11} & p_{12} \\ p_{21} & p_{22} \end{bmatrix}$$

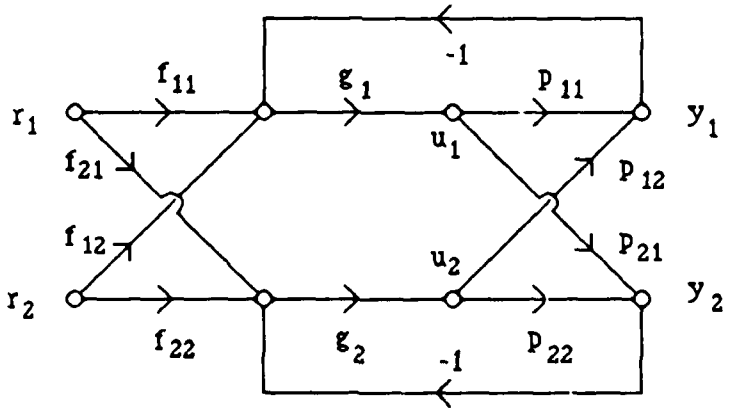

Fig. III-4. Two-by-Two MIMO Feedback Structure

Constraints on the Plant Matrix

The set of **P** matrices is tested to ensure two critical conditions are met (Ref 9:86-90):

1. **P** must not be singular for any possible combination of plant parameters, i.e. $\mathbf{P}^{-1}$ must exist.
2. As $s \longrightarrow \infty$, $|p_{11}p_{22}| > |p_{12}p_{21}|$ for all possible plants. This is a requirement for the two-by-two case. For explanation of the constraint inequality for three-by-three and higher cases, see Reference 9.

The first condition is absolutely necessary to ensure controllability of the plant. The inverse of **P** produces the effective transfer functions used in the design. If condition 2 is not satisfied, it may be possible to change the ordering of the input or output vector which changes the ordering of the **P** matrix elements.

Effective MISO Loops

The following procedure is used to obtain the set of MISO systems equivalent to the MIMO system. The matrix, $\mathbf{Q}' = \mathbf{P}^{-1}$ is defined having elements, q_{ij}'. the n^2 effective transfer functions needed are given by: $q_{ij} = 1/q_{ij}'$. Reference 9 contains the derivation and proof of this equivalence. The n x n MIMO system is now treated as n^2 MISO problems. Figure III-5 shows the four effective MISO loops resulting from the two-by-two MIMO system (Ref 11:682).

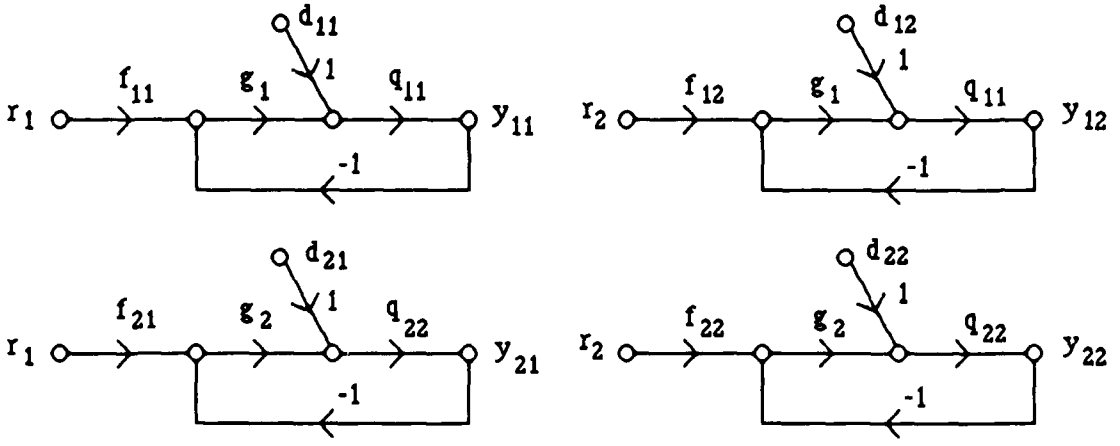

Fig. III-5. Effective MISO Loops

Each loop in Figure III-5 is handled as an individual MISO design problem in accordance with the procedures presented in Chapter II. The f's and g's are the compensator elements F and G described previously. The disturbances, d_{ij}, represent the interaction between the various loops. Each d_{ij} is obtained from the relationship below.

$$-d_{ij} = \sum_{k} \frac{b_{kj}}{|q_{ik}|}, \quad k \neq i \tag{III-8}$$

The term, b_{kj}, in Equation (III-8) is the modeled transfer function of the upper response bound, (T_U or T_D in Figure II-4), for the respective input/output relationship. The bounds are obtained from the design specifications (Ref 11:681-684 and 16). Note the first digit of the subscript of b_{kj} refers to the output variable and the second digit refers to the input variable. The bound, b_{kj}, is a function of the response requirements on the output, y_k, due to the input, r_j.

A recent improvement (the Improved Method) in the design technique involves modification of the q's on the second and subsequent loops based on the g's already designed. This reduces the inherent overdesign in the early part of the design process. During the final loop, the exact equation representing the loop and the interactions of the other loops are used (Ref 11:977). The use of the improved method is demonstrated in the description of the design performed for this thesis (see Chapter V).

Basically Non-Interacting (BNIC) Loops

When the response of an output, y_k, due to an input, r_j, is ideally zero, the y_{kj} loop is called a basically non-interacting (BNIC) loop(Ref 11:697). Due to loop interaction and plant uncertainty, the ideal response is not achievable. Therefore, the performance specifications describe maximum allowable responses and the loop is handled exclusively as a disturbance rejection problem.

Summary

This chapter describes the multiple input - multiple output plant and the plant transfer function matrix **P** describing it. Guidelines are presented for obtaining the plant matrix which relates the output vector to the input vector.

The division of the MIMO system into an equivalent set of MISO systems is given via the inverse of the **P** matrix. The MISO problems are solved in accordance with MISO design theory presented in Chapter II. The solution of the MISO problems guarantees the solution of the MIMO problem.

IV. The AFTI/F-16 Aircraft

Introduction

This chapter presents a brief description of the AFTI/F-16 aircraft and the basic differences between it and the standard production F-16 fighter aircraft. The state space model used to obtain the plant transfer function matrix is given along with a definition of the input and output variables used in the controller design. See reference 2 for the detailed derivation of the state space model describing the AFTI/F-16.

Aircraft Description

The AFTI is a highly modified F-16 aircraft. Two prototype aircraft have been built to flight test the integration of advanced technology characteristics and determine the benefits obtainable over conventional fighter aircraft. The characteristics include three digital flight control computers for triple redundancy and a flight control system designed to perform specific mission phases. The three computers operate independently to calculate the flight control laws. A redundancy management system uses comparison monitoring of the three computers and internal self-test features to detect failed system components and provide a two/fail operate capability. Thus, the system can continue operation after two similar failures. Eight separate control modes are implemented in the flight control computers with extensive gain scheduling to achieve unprecedented performance over the mission phases.

The AFTI differs from a conventional F-16 both internally and externally. The primary external modifications to date are the addition of twin vertical canards mounted under the engine inlet and a dorsal fairing between the cockpit and the vertical tail. The vertical canards provide for the development of direct sideforces. The dorsal fairing houses avionics and instrumentation needed in the flight test effort.

Internally, a completely new flight control system is used in the AFTI while retaining

the original F-16 sensors. Longitudinal and lateral accelerometers measure body accelerations at the pilot's station. Body rotational rates are sensed using rate gyros located very close to the aircraft's center of gravity. Angle of attack is also sensed by two fuselage side-mounted cones and a hemispherical differential pressure probe extending from one side of the aircraft. The F-16 uses quadruple redundancy in its flight control system. Thus, four identical accelerometers are employed on each axis as well as sets of four identical rate gyros each to sense roll, pitch, and yaw rates about the respective axes. The AFTI uses only three accelerometers per axis to provide the same fail/operate capability as the F-16. The signals obtained from the fourth are used by the flight test instrumentation.

The AFTI/F-16 aircraft is displayed in Figure IV-1. The solid black regions in the figure denote the control surfaces used for the development of the state space model (Ref 2). Since the longitudinal mode of pitch pointing is being investigated in this study, the surfaces of interest are the horizontal tail and the trailing edge flaperons. For longitudinal maneuvers, the horizontal tail surfaces operate symmetrically as elevators. Likewise, the flaperons on the trailing edge of each wing operate symmetrically as flaps. The sign convention used is also shown in the figure.

Longitudinally, without a control system, the aircraft is statically unstable at subsonic flight conditions as demonstrated in Figure IV-2. By design, the center of gravity (CG) is located behind the aerodynamic center (AC). Typically the difference between the CG and AC is measured in percent of the mean aerodynamic chord (MAC). As shown in the figure, the aircraft is approximately three percent unstable in the subsonic region and only neutrally stable in the transonic region. At supersonic speeds, the aircraft is statically stable, but less stable than most conventional aircraft. Designing the CG to be located behind the AC, i.e. an unstable design, negates the need for the elevator to continuously develop a down load in trimmed flight. The tail is used to add lift to the aircraft. This design feature reduces drag and allows the aircraft to obtain higher load factors. Thus, faster turn rates and longer operational range can be achieved.

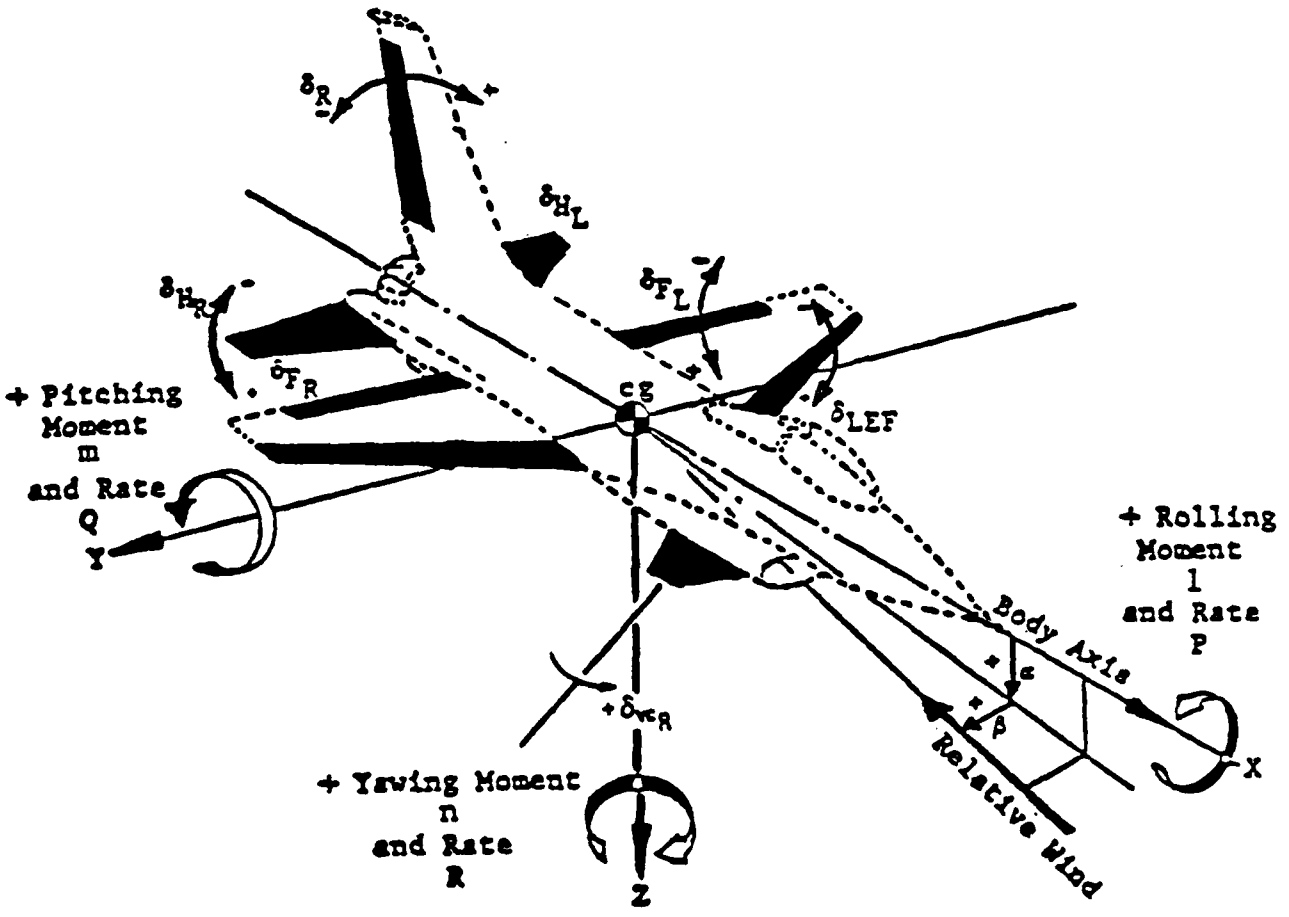

Fig. IV-1. AFTI/F-16 Control Surface Location

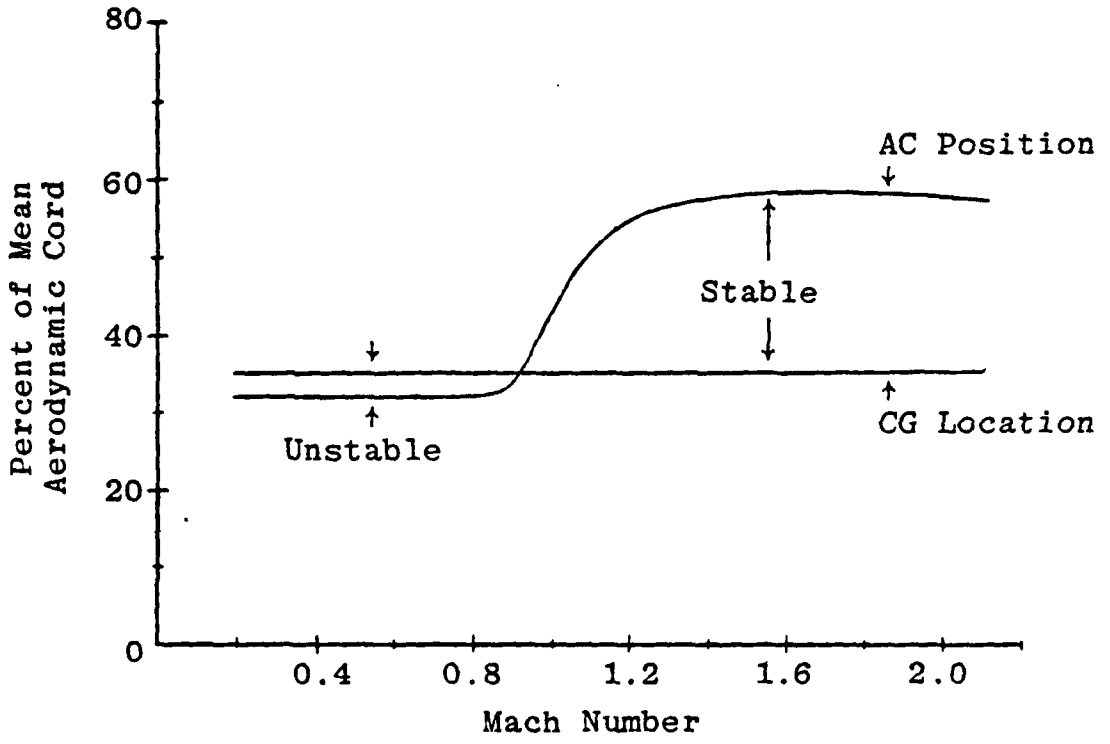

Fig. IV-2. Longitudinal Static Stability Plot

The unaugmented transfer functions describing the aircraft dynamics at the three flight conditions considered in this thesis are given in Appendix C. Investigating Cases 1 and 2, at subsonic flight conditions the short period roots are real and one is unstable. The flight control system must provide longitudinal stability as well as the performance desired.

Definition of the State Space Model

The linear state space model used to represent the unaugmented aircraft dynamics was developed by Mr. Barfield. The state equations are written in the form:

$$\dot{\mathbf{x}} = \mathbf{A}\mathbf{x} + \mathbf{B}\mathbf{u} \qquad \text{(IV-1)}$$

$$\mathbf{y} = \mathbf{C}\mathbf{x} \qquad \text{(IV-2)}$$

where the longitudinal axis state vector is given by:

$$x = \begin{bmatrix} \alpha \\ \theta \\ u \\ A_{nps} + k_1\delta_e + k_2\delta_f \\ q \\ \delta_e \\ \delta_f \end{bmatrix} \qquad \text{(IV-3)}$$

The state vector elements are defined in Table IV-1 below along with the corresponding units of each element. Note the state vector element $A_{nps} + k_1\delta_e + k_2\delta_f$ is the longitudinal acceleration at the pilot's station augmented with the contributions from control surface deflections. The state vector element resulted in this form during transformations by Mr. Barfield on the system state space representation in order to achieve a **B** matrix in zero-$\mathbf{B}_2$ form (Ref 2:52). This form was desired to permit easier computation of transmission zeros in Mr. Barfield's design effort. The $k_1\delta_e$ and $k_2\delta_f$ terms are subsequently removed by Equation (IV-2) to yield A_{nps} and q as output variables by accounting for the deflection terms in the **C** matrix (see Appendix B). Reference 2 provides a complete description of the state space model developed by Mr. Barfield to represent the AFTI/F-16.

Table IV-1. Longitudinal Axis State Vector Element Definitions

Element	Units	Definition
α	deg	angle of attack
θ	deg	pitch angle
u	ft/sec	velocity along the x-axis
A_{nps}	g	longitudinal acceleration at the pilot's station
q	deg/sec	pitch rate
δ_e	deg	elevator deflection angle
δ_f	deg	flap deflection angle

The output states chosen to be controlled are the longitudinal acceleration at the pilot's station A_{nps} and the pitch rate q. These quantities are selected as output variables because the pilot controls them in flying the aircraft. The pilot feels (and desires to command) angular rates and accelerations at the position where he is physically attached to the aircraft. A_{nps} is available for feedback via flight control accelerometers located at the pilot's station. Likewise, body rotational rates can be measured and fed back from sensors near the aircraft CG (Ref 2). The output state vector **y** is defined in Equation (IV-4).

Longitudinal motion of the aircraft is controlled through deflection of the elevator and flap control surfaces. Elevator and flap actuator models for these control surfaces are included in the state space model. Thus, δ_{ecmd} and δ_{fcmd} are the respective command inputs to the elevator and flap actuator models (Ref 2). The inputs to the state space model are given by the vector **u** below.

$$\mathbf{y} = \begin{bmatrix} A_{nps} \\ q \end{bmatrix} \qquad \mathbf{u} = \begin{bmatrix} \delta_{ecmd} \\ \delta_{fcmd} \end{bmatrix} \tag{IV-4}$$

The state space model components for matrices **A**, **B**, and **C** and the constants k_1 and k_2 of Equation (IV-3) are provided in Appendix B for the three flight conditions considered in this thesis.

Summary

This chapter provides a brief description of the AFTI/F-16 aircraft and the state space model used to represent the unaugmented dynamics of the aircraft. The state space model developed by Mr. Barfield is converted into plant transfer functions required for the application of the design method as described in Chapter V.

V. Application of the Design Technique

Introduction

The application of the improved Quantitative Feedback Theory (QFT) technique (Ref 12) of Dr. Isaac Horowitz is described in this chapter. The technique is applied to a model of the AFTI/F-16 longitudinal aircraft dynamics developed by Mr. Barfield (Ref 2). A flight controller design for the longitudinal maneuver of pitch pointing is obtained.

The following presentation is the step-by-step approach recommended to apply the design technique. Each procedure used to design the flight controller is given.

Definition of the MIMO Plant

The general form of the multiple input - multiple output plant is shown in Figure III-1. The longitudinal aircraft dynamics of the AFTI/F-16 are modeled by a two input - two output plant. The plant output vector **y** and the plant input vector **u** are obtained from the state space model defined in Chapter IV. The vector elements are given by Equation (IV-4) and repeated below for convenience.

$$\mathbf{y} = \begin{bmatrix} A_{nps} \\ q \end{bmatrix} \qquad \mathbf{u} = \begin{bmatrix} \delta_{ecmd} \\ \delta_{fcmd} \end{bmatrix} \tag{V-1}$$

Deriving the Plant Transfer Function Matrix

The method of Dr. Horowitz is a frequency domain approach requiring the plant to be described as a transfer function matrix. The state space representation of the plant developed by Mr. Barfield must be translated into a set of transfer functions relating the input and output variables. The transfer function matrix is obtained from the state space model using Equation (III-7) repeated below for convenience.

$$\mathbf{P} = \mathbf{C}[s\mathbf{I} - \mathbf{A}]^{-1}\mathbf{B} \tag{V-2}$$

For the two input - two output plant of this study, the **P** matrix obtained from Equation

(V-2) is a two-by-two matrix. The input/output relationship is given in matrix form by:

$$\mathbf{y} = \mathbf{P}\,\mathbf{u} \tag{V-3}$$

In terms of the various matrix elements, this relationship is written as:

$$\begin{bmatrix} A_{nps} \\ q \end{bmatrix} = \begin{bmatrix} p_{11} & p_{12} \\ p_{21} & p_{22} \end{bmatrix} \cdot \begin{bmatrix} \delta_{ecmd} \\ \delta_{fcmd} \end{bmatrix} \tag{V-4}$$

where:

$$p_{11} = \frac{[\ A_{nps}\ ]}{[\ \delta_{ecmd}\ ]} \qquad p_{12} = \frac{[\ A_{nps}\ ]}{[\ \delta_{fcmd}\ ]}$$

$$p_{21} = \frac{[\ q\ ]}{[\ \delta_{ecmd}\ ]} \qquad p_{22} = \frac{[\ q\ ]}{[\ \delta_{fcmd}\ ]} \tag{V-5}$$

The plant transfer function matrix **P** is obtained for each flight condition using a computer program. As stated in Chapter III, each plant matrix is a member of a set of possible plant matrices due to the uncertainty in plant parameters. Plant uncertainty is demonstrated by the variation in gain, poles, and zeros of the transfer functions from flight condition to flight condition. The **P** matrix elements obtained from the state space data (Appendix B) for the three flight conditions considered are given in Appendix C.

MIMO Compensation Structure

The compensation scheme for the MIMO system uses a two degree-of-freedom unity feedback structure. This control structure is used by the technique when only the plant output and system command input quantities are known. The control structure is shown in Figure III-3 for the general case. The designer is provided two design degrees-of-freedom in that the two separate compensation matrices **F** and **G** may be designed. The compensator **G** guarantees the variation in the closed-loop system (due to plant uncertainty) remains less than or equal to the variation allowed by the closed-loop response tolerances.

The prefilter **F** positions the closed-loop frequency response within the bounds of the frequency domain specifications (Chapter II). Measurement of the plant output quantities y and the system command input quantities **r** allows the use of this structure. For the two-by-two plant being considered, the control structure is shown in Figure V-1.

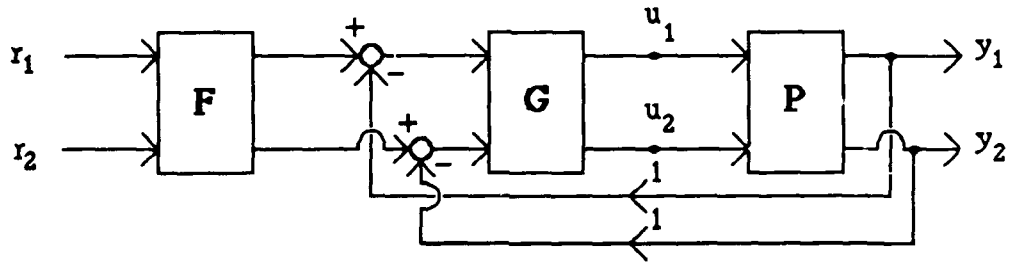

Fig. V-1. MIMO Compensation Structure for a 2 x 2 Plant

For a two-by-two MIMO plant, the general system diagram is given in Figure III-4 in terms of the individual matrix elements. The structure shown in Figure III-4 is reduced to that of Figure V-2 based on the following design considerations. The design technique is used to obtain a longitudinal pitch pointing controller. In the pitch pointing maneuver, the aircraft pitch rate is to track the pilot's pitch rate command input while maintaining longitudinal acceleration at a negligible value.

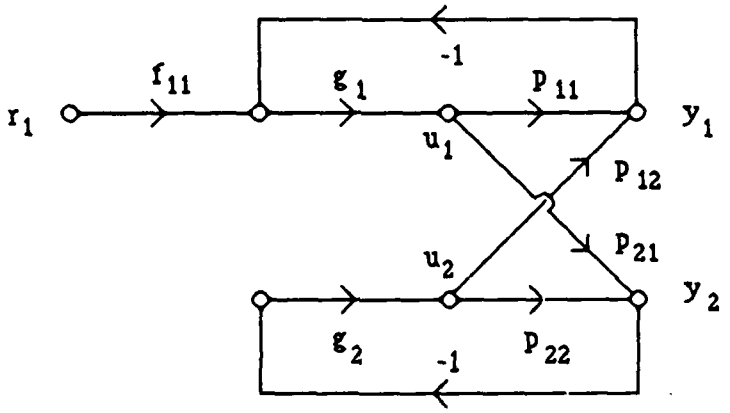

Fig. V-2. Simplified 2 x 2 MIMO System Diagram

The first reduction of the system from the most general case is to use a diagonal G matrix. The assumption is made that the output q is controlled by the input δ_{ecmd} while the output A_{nps} is determined by the input δ_{fcmd} in order to diagonalize the **G** matrix. Investigating the aircraft dynamics (Ref 2), the assumption is reasonable though not entirely accurate. A controller design incorporating both control surfaces to control individual plant outputs can be obtained by using the corresponding diagonal and off-diagonal G matrix elements. Using a diagonal **G** is not a restriction of the technique, but simplifies the design effort for a preliminary design.

The second simplification is to assume there is only one command input to the system. Recall for the pitch pointing maneuver, the pilot commands a rate in pitch with no desired change in acceleration. Let the pilot's pitch rate command be defined as the r_1 input and the acceleration command as the r_2 input. Since the change in acceleration is desired to equal to zero, then r_2 is set equal to zero and may be ignored for the remainder of this study.

The final reduction of the system control structure is made on the **F** matrix. The matrix elements f_{12} and f_{22} are set equal to zero since the input to the elements r_2 is zero. The prefilter element f_{21} is also set equal to zero because no interaction is assumed between the acceleration loop and the pitch rate command input. The acceleration output y_2 is ideally zero for a command input in pitch rate. Therefore, the acceleration loop is BNIC with respect to the pitch rate command input. Incorporating these simplifications into the diagram of Figure III-4 results in the diagram of Figure V-2.

Equivalent MISO Problem Set

The Quantitative Feedback Theory technique transforms the MIMO design problem into an equivalent set of MISO design problems. The theoretical development of the technique requires the plant transfer function matrix **P** to meet two constraints for the 2 x 2 case (Ref 9). The equivalent MISO set of transfer functions describing the plant are

obtained from the inverse of the plant transfer function matrix, $\mathbf{P}^{-1}$. The solution of the MISO problems taken as a whole is guaranteed to solve the MIMO problem (Ref 11,12).

Test Plant Transfer Function Matrix Against Constraints. The 2 x 2 plant matrix, **P**, obtained at each flight condition is tested against the two constraints given in Chapter III. In Appendix C, the plant transfer function matrices and the results of the constraint tests are given for each case. To illustrate this operation, the **P** matrix elements and the test results are presented below for the second case.

Case 2: 0.9 Mach; 20,000 Feet

$$p_{11}(s) = \frac{-2.128(s + 0.012228)(s - 0.001170)(s + 1.3144 \pm j13.07744)}{(s + 0.0075694 \pm j0.0540)(s - 0.96451)(s + 3.2234)(s + 20)}$$

$$p_{12}(s) = \frac{1.4992(s + 0.0122185)(s - 0.00113786)(s - 8.48425)(s + 8.4714)}{(s + 0.0075694 \pm j0.0540)(s - 0.96451)(s + 3.2234)(s + 20)} \qquad \text{(V-6)}$$

$$p_{21}(s) = \frac{-481.2(s)(s + 0.012642)(s + 1.510776)}{(s + 0.0075694 \pm j0.0540)(s - 0.96451)(s + 3.2234)(s + 20)}$$

$$p_{22}(s) = \frac{-129.46(s)(s + 0.012548)(s + 1.64587)}{(s + 0.0075694 \pm j0.0540)(s - 0.96451)(s + 3.2234)(s + 20)}$$

The constraint test results are:

1. **P** is non-singular.
2. As $s \longrightarrow \infty$, $|p_{11}p_{22}| > |p_{12}p_{21}|$ becomes: $275.5 > 721.4$

   Constraint 2 is not met.

Investigating the results shown in Appendix C, constraint 2 is not met for all three cases. The constraints on the **P** matrix must be met to apply the QFT technique (see Chapter III). Rearranging the output vector allows the constraints to be met. Having met the constraints, the MIMO system can be broken into a set of equivalent MISO systems.

Rearrange the Output Vector to Meet the Constraints. As shown in Appendix C, constraint 2 is not met for all three flight conditions. By rearranging the output vector as shown in Equation (V-8), this constraint is met. The modified relationship between the input and output variables is expressed as:

$$\begin{bmatrix} q \\ A_{nps} \end{bmatrix} = \begin{bmatrix} p_{11} & p_{12} \\ p_{21} & p_{22} \end{bmatrix} \bullet \begin{bmatrix} \delta_{ecmd} \\ \delta_{fcmd} \end{bmatrix} \tag{V-7}$$

where the output vector, **y**, is redefined as:

$$\mathbf{y} = \begin{bmatrix} q \\ A_{nps} \end{bmatrix} \tag{V-8}$$

and the **P** matrix elements are given by:

$$p_{11} = \frac{[\ q\ ]}{[\ \delta_{ecmd}\ ]} \qquad p_{12} = \frac{[\ q\ ]}{[\ \delta_{fcmd}\ ]}$$

$$p_{21} = \frac{[\ A_{nps}\ ]}{[\ \delta_{ecmd}\ ]} \qquad p_{22} = \frac{[\ A_{nps}\ ]}{[\ \delta_{fcmd}\ ]} \tag{V-9}$$

The effect on the **P** matrix elements p_{ij} due to rearranging the output vector is easily realized by the following operation. Simply change the p_{ij} subscripts from the old set to the new set as shown in Table V-1. The transfer function parameter values, i.e. gain, poles and zeros, remain unchanged through the transformation.

Table V-1. Plant Transfer Function Subscript Change

Subscript Value

OLD	⟶	NEW
11		21
12		22
21		11
22		12

The transfer functions resulting from the output vector modification are given in Appendix D for each flight condition. The revised set of transfer functions are retested against the plant matrix constraints. The results for Case 2 are given below.

Case 2: 0.9 Mach; 20,000 Feet

$$
\begin{aligned}
p_{11}(s) &= \frac{-481.2(s)(s + 0.012642)(s + 1.510776)}{(s + 0.0075694 \pm j0.0540)(s - 0.96451)(s + 3.2234)(s + 20)} \\
p_{12}(s) &= \frac{-129.46(s)(s + 0.012548)(s + 1.64587)}{(s + 0.0075694 \pm j0.0540)(s - 0.96451)(s + 3.2234)(s + 20)} \\
p_{21}(s) &= \frac{-2.128(s + 0.012228)(s - 0.001170)(s + 1.3144 \pm j13.07744)}{(s + 0.0075694 \pm j0.0540)(s - 0.96451)(s + 3.2234)(s + 20)} \\
p_{22}(s) &= \frac{1.4992(s + 0.0122185)(s - 0.00113786)(s - 8.48425)(s + 8.4714)}{(s + 0.0075694 \pm j0.0540)(s - 0.96451)(s + 3.2234)(s + 20)}
\end{aligned}
\qquad \text{(V-10)}
$$

The constraint test results are:

1. **P** is non-singular.
2. As $s \longrightarrow \infty$, $|p_{11}p_{22}| > |p_{12}p_{21}|$ becomes: $721.4 > 275.5$

The constraints are met.

Appendix D demonstrates the constraints are met at all flight conditions after modifying the plant output vector. Having met the constraints, the inverse of the plant matrix is used to break the MIMO design problem into an equivalent set of MISO design problems.

Equivalent MISO Design Problems. The technique transforms the MIMO system into an equivalent set of MISO systems as explained in Chapter III are derived in reference 9. The set of MISO plant transfer functions are obtained from the inverse of the MIMO plant transfer function matrix. Recall from Chapter III, the matrix $\mathbf{Q}' = \mathbf{P}^{-1}$ is defined having elements q_{ij}'. The reciprocals of the q_{ij}' elements are the transfer functions required, i.e. $q_{ij} = 1/q_{ij}'$. The set of q_{ij} transfer functions are given in matrix form by the matrix **Q**.

$$\mathbf{Q} = \begin{bmatrix} q_{11} & q_{12} \\ q_{21} & q_{22} \end{bmatrix} \tag{V-11}$$

where:

$$q_{ij} = \frac{\det [\mathbf{P}]}{\mathrm{Adj}[p_{ij}]} \tag{V-12}$$

Note the **Q** matrix elements are the reciprocals of the $\mathbf{P}^{-1}$ matrix elements. A computer program is used to obtain the q_{ij} transfer functions at each flight condition. The sets of these functions are listed in Appendix E for all three cases. The functions for the second case are given below to illustrate the results.

Case 2: 0.9 Mach; 20,000 Feet

$$q_{11}(s) = \frac{2.07171(s + 0.0027369)(s + 0.0121827)}{(s + 0.0126422)(s + 1.510776)(s + 20)}$$

$$q_{12}(s) = \frac{-468.47082(s)(s + 0.0027369)(s + 0.0121827)}{(s-0.00117)(s + 0.012228)(s + 1.31436 \pm j13.077)(s + 20)}$$

$$q_{21}(s) = \frac{-7.700494(s + 0.0027369)(s + 0.0121827)}{(s + 0.0125478)(s + 1.64587)(s + 20)} \tag{V-13}$$

$$q_{22}(s) = \frac{-664.9586(s)(s + 0.0027369)(s + 0.121827)}{(s - 0.0011379)(s + 0.012219)(s - 8.48425)(s + 8.4714)(s + 20)}$$

The 2 x 2 MIMO control problem is treated as four equivalent MISO control problems where the MISO plant transfer functions are given by the **Q** matrix elements. The four equivalent MISO loops are shown in Figure III-5. Recall from the particular design considerations described earlier in the chapter, the 2 x 2 MIMO system is simplified as shown in Figure V-2. The simplification reduces the four loop design problems of Figure III-5 to the two shown in Figure V-3.

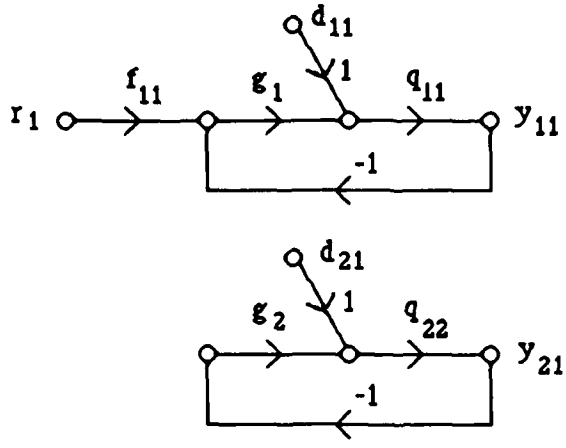

Fig. V-3. Two Equivalent MISO Loops

In Figure V-3, the pitch rate loop output is y_{11}, which is the pitch rate output y_1 due to the pitch rate command input r_1. The acceleration loop output is y_{21}, which is the acceleration output y_2 due to the command input r_1. The interactions between the pitch rate and acceleration loops are represented as disturbance inputs. The inputs d_{11} and d_{21} are obtained using Equation (III-8).

$$-d_{11} = \frac{b_{21}}{q_{12}} \qquad -d_{21} = \frac{b_{11}}{q_{21}} \tag{V-14}$$

The numerator terms b_{11} and b_{21} are the respective upper bound transfer functions for the pitch rate and acceleration loops (see Design Specifications below). Note the acceleration (lower) loop of Figure V-3 is a BNIC loop. Thus, it is treated as a disturbance attenuation problem.

Improved Design Technique. An improved MIMO synthesis technique developed by Dr. Horowitz (Ref 12) provides several advantages over the previous method. The original MIMO design method, based on fixed point theory (Ref 9), replaces the uncertain n x n MIMO system by n^2 uncertain MISO systems whose solutions are guaranteed to solve the

original MIMO problem. However, some overdesign is inherent in this method. An improved technique retains the MISO equivalence approach, but does not require fixed point theory for its derivation. The addition of constraints on the MIMO plant (Chapter III) allows the design method to achieve arbitrarily small sensitivity over an arbitrarily large frequency bandwidth. Also, the overdesign inherent in the original method is reduced (Ref 12:977-978).

Applying the new technique, the loop chosen to be designed first is completed using the original method (Ref 9). The second loop is designed after the first loop is finalized. The design of the final loop is based on the exact equation of the closed-loop transfer function found by applying Mason's Rule (Ref 5) to the system shown in Figure V-2. A new effective single loop plant, q_{11}*, is obtained which is a function of the first loop designed and the interaction between loops (Ref 13:102-103).

$$q_{11}(s)^* = \frac{q_{11}(s)}{1 + \dfrac{-\gamma(s)}{1 + l_2(s)}} \tag{V-15}$$

where:

$$\gamma(s) = \frac{q_{11}(s)q_{22}(s)}{q_{12}(s)q_{21}(s)} \qquad \text{and} \qquad l_2(s) = g_2(s)q_{22}(s) \tag{V-16}$$

The disturbance input to the final loop is no longer a function of the uncertainty (upper bound) of the first loop, thus reducing the overdesign of the original method. The final loop disturbance input is a function of the off-diagonal prefilter matrix elements (Ref 12:979) which equal zero in this study. Therefore, the disturbance input to the final loop is zero.

The acceleration loop is chosen as the first loop to be designed since it is strictly a disturbance attenuation problem. The pitch rate loop is then designed afterwards. Choosing the pitch rate loop to be designed first requires solving a disturbance attenuation problem and a tracking problem simultaneously. Thus, by initially designing the

acceleration loop, some reduction of the design effort is achieved. Applying the improved MIMO synthesis technique results in the modified set of equivalent SISO and MISO loops, respectively, shown in Figure V-4 where the new effective MISO plant transfer function for the pitch rate loop is given by Equation (V-15).

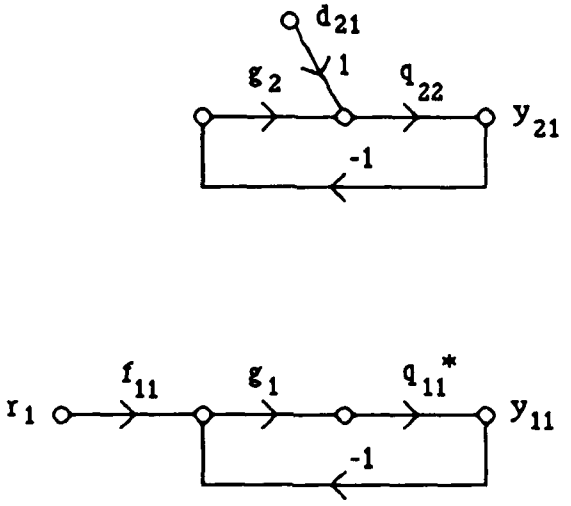

Fig. V-4. Equivalent SISO and MISO Loops of the Improved Technique

Refer to references 12 and 13 in the bibliography for a detailed explanation of the improved synthesis technique and an example of its application. The remainder of this chapter illustrates the application of the new method to the problem considered in this study.

Design Specifications

The purpose of determining output performance tolerances and the technique used to obtain them is given in Chapter II. Recall the design specifications are quantitative parameters in the design process. Thus, closed-loop system response tolerances must be determined prior to the design phase. The design specifications describe the upper and lower limits of acceptable output response to a desired input or disturbance. Note, typically system response to a step disturbance requires the output to remain below a given value, therefore only an upper bound on the output is necessary.

The function of a pitch pointing controller is to track a command input in pitch rate while maintaining longitudinal acceleration at a negligible value. Specifications on the pitch rate output y_{11} and the acceleration output y_{21} are needed to define the limits of acceptable system response. The type of system forcing function is also specified since system response is a function of the input used.

A step input is chosen as the desired pitch rate command input r_1. A good initial test of system response is provided by a step input since it combines both an abrupt change in magnitude as well as a constant (non-varying) value. Another advantage of using a step input is most standard response specifications (Ref 5) are based on a step forcing function. In general, a system having acceptable step response performs well with other input types.

The pitch rate step response bounds are shown in Figure V-5. The curves are sketched after investigating the simulations shown in reference 2 and determining reasonable response bounds in terms of aircraft rate and position limits, aircraft maximum capabilities, and desirability for combat applications (i.e. fast response with minimum overshoot). The upper bound b_{11} is drawn to permit a rise time of 0.9 seconds and a maximum overshoot of 1.5 percent. The lower bound a_{11} allows a first order response with a maximum settling time of 4.6 seconds. Any smooth and well behaved response lying within the bounds is acceptable.

The optimal acceleration step response equals zero. However, this optimum response is not physically realizable. Maintaining the acceleration below a negligible value is a viable solution. The maximum value chosen, 0.15 g, is shown by the dashed line in Figure V-6. The representative upper bound b_{21} provides for an initial transient in acceleration and settles to a small value, well below 0.15 g. Any acceleration step response having the general shape of b_{21} and whose peak magnitude is less than 0.15 g is acceptable. Since the acceleration loop is treated as a disturbance attenuation problem, a lower bound on the acceleration step response is not necessary.

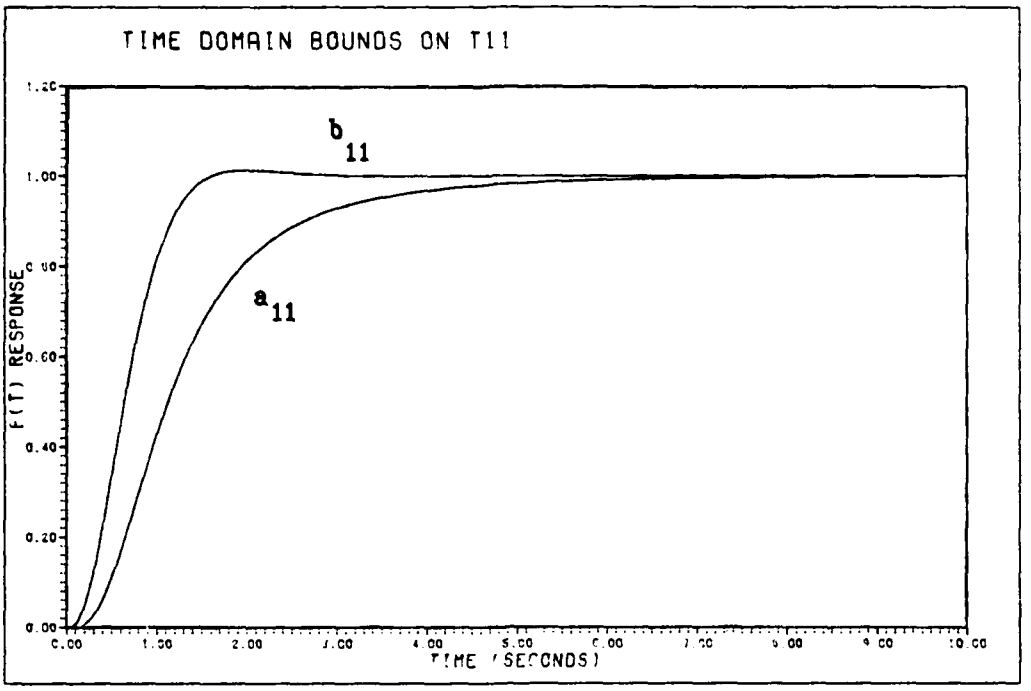

Fig. V-5. Pitch Rate Time Response Specifications

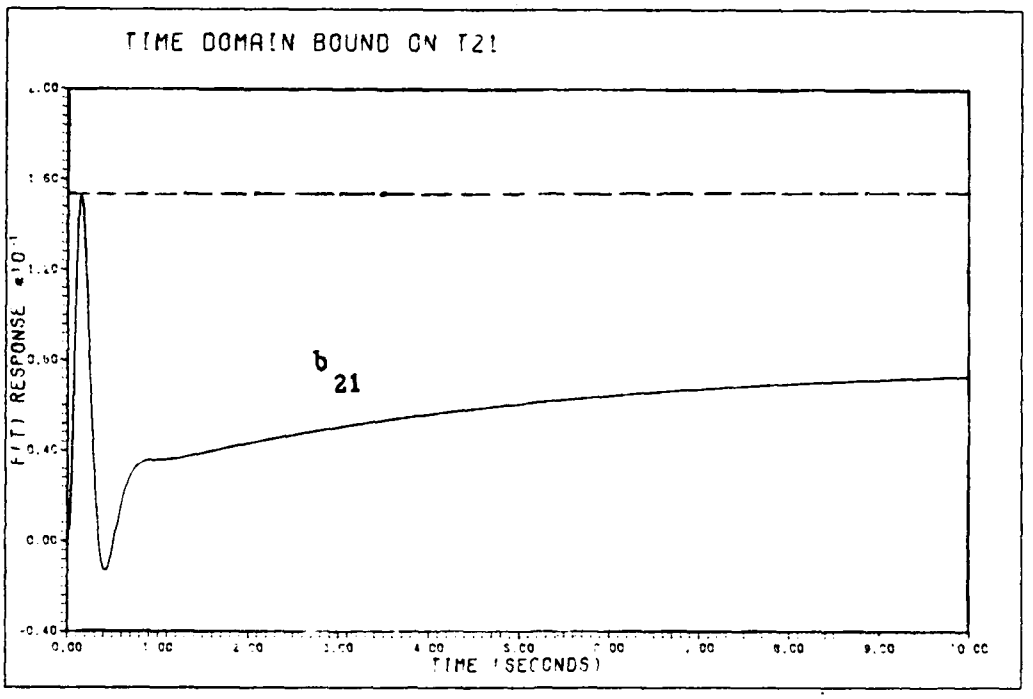

Fig. V-6. Acceleration Time Response Specifications

The bound curves are defined using the following notation. Lower bounds are specified by a_{ij} where the (ij) subscripts correspond to the loop output variable with the same subscripts. The upper bounds are given by b_{ij} with the same subscript correspondence. For example, the bound b_{21} *is the upper acceleration step response bound* related to the acceleration loop output y_{21}. The bounds a_{11}, b_{11}, and b_{21} are equivalent to the bounds T_l, T_u, and T_d respectively, as discussed in Chapter II.

Control ratios are modeled for each output response bound using the method presented in Chapter II. A control ratio pole-zero pattern is adjusted until its time domain step response matches a bound curve. The control ratios obtained for the step response bounds are given by Equations (V-17), (V-18), (V-19).

$$a_{11}(s) = \frac{221.7(s + 0.75)}{(s + 0.6417)(s + 1.558)(s + 5.40)(s + 5.50)(s + 5.60)} \qquad \text{(V-17)}$$

$$b_{11}(s) = \frac{60.26(s + 2.70)}{(s + 2.5 \pm j1.5)(s + 4.350)(s + 4.40)} \qquad \text{(V-18)}$$

$$b_{21}(s) = \frac{438(s + 2)(s + 2.1)(s + 2.15)(s + 2.5)(s + 5.73)(s + 5.65)}{(s + 0.225)(s + 8.8)(s + 8.85)(s + 8.9)(s + 8.95)(s + 9)(s + 12)(s + 15)(s + 18)} \qquad \text{(V-19)}$$

The Bode magnitude plot for each bound control ratio is shown in Figure V-7. These plots are the frequency domain bounds on the closed-loop pitch rate and acceleration frequency responses. The MISO closed-loop transfer functions are specified by t_{ij}, where the (i) subscript refers to the i'th system output and (j) refers to the j'th system input. Thus, the closed-loop transfer function for the pitch rate loop is t_{11} and the acceleration loop is t_{21}. The design specifications require the frequency response of t_{11} and t_{21} to remain within the corresponding frequency domain bounds of Figure V-7 for the frequency range of interest.

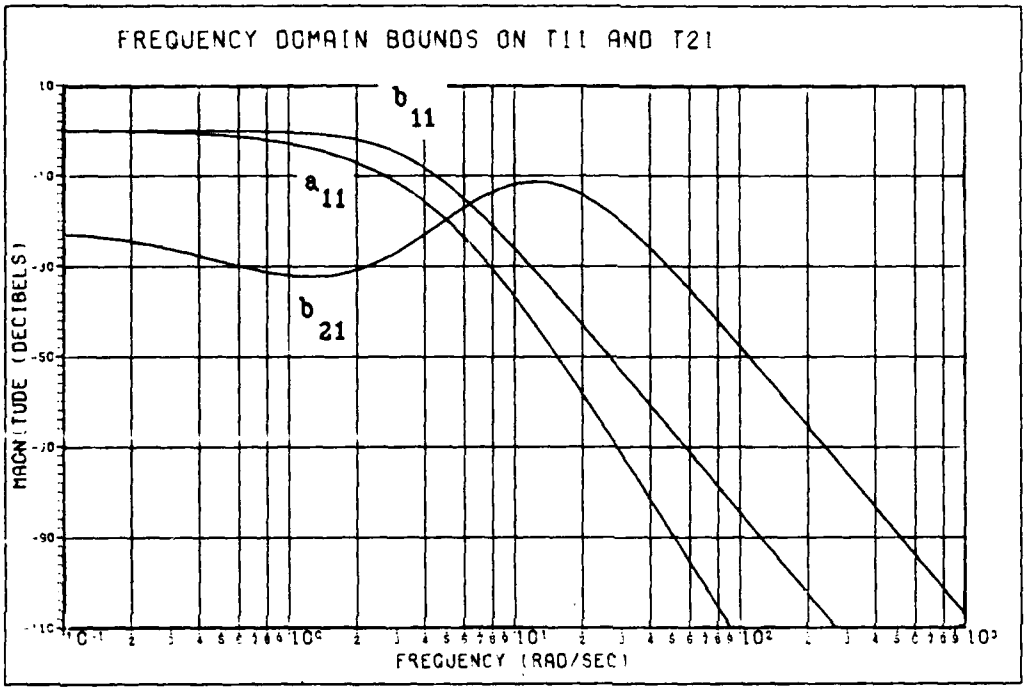

Fig. V-7. Pitch Rate and Acceleration Frequency Domain Specifications

Disturbance Attenuation Compensator Design - Acceleration Loop

The procedure used to design the acceleration loop compensator g_2 is presented in this section, following the general guidelines of Chapter II. As stated earlier, the acceleration loop is a BNIC loop and is treated as a disturbance attenuation problem. The acceleration loop is shown in Figure V-8.

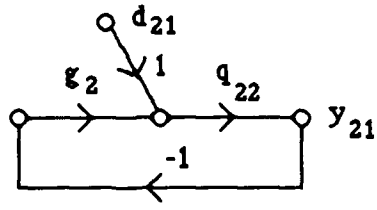

Fig. V-8. Acceleration Loop

The objective is to design $g_2(s)$ such that the closed-loop transfer function $t_{21}(s)$ has no right half plane poles and satisfies the performance tolerances $b_{21}(j\omega)$ on $t_{21}(j\omega)$. The closed-loop transfer function of the acceleration loop is given by Equation (V-20).

$$t_{21}(s) = \frac{y_{21}(s)}{d_{21}(s)} = \frac{q_{22}(s)}{1 + g_2(s)q_{22}(s)} = \frac{q_{22}(s)}{1 + l_2(s)} \qquad \text{(V-20)}$$

where the loop transmission is expresses as:

$$l_2(s) = g_2(s)q_{22}(s) \qquad \text{(V-21)}$$

and the disturbance input is:

$$-d_{21}(s) = \frac{b_{11}(s)}{|q_{21}(s)|} \qquad \text{(V-22)}$$

The equivalent SISO plant transfer function for the acceleration loop is q_{22}. A nominal plant is chosen as a reference to facilitate the definition and shaping of the nominal loop transmission l_{20}. In this study, the nominal q_{220} is chosen having similar frequency domain characteristics as the actual q_{22} transfer functions (see Figure F-4, Appendix F). The nominal transfer function is given by Equation (V-23).

$$q_{220}(s) = \frac{-158.0(s)(s + 0.001)(s + 0.02)}{(s - 0.0009)(s + 0.025)(s + 4.0)(s - 4.1)(s + 20)} \qquad \text{(V-23)}$$

The nominal plant transfer function is used to determine the compensator g_2 from the nominal loop transmission l_{20} shaped on the Nichols chart. The nominal loop transmission

is defined by Equation (V-24).

$$l_{20}(s) = g_2(s)q_{220}(s) \tag{V-24}$$

The output response must remain below the design specification in order to meet the acceleration performance tolerances and is obtained from Equation (V-20).

$$y_{21}(j\omega) = t_{21}(j\omega)d_{21}(j\omega) \tag{V-25}$$

The output specification is expressed in the frequency domain by the inequality below.

$$|y_{21}(j\omega)| \leq |b_{21}(j\omega)| \tag{V-26}$$

Inserting Equations (V-20), (V-22) and (V-25) into Equation (V-26), then:

$$\frac{|q_{22}(j\omega)|\,|d_{21}(j\omega)|}{|1 + g_2(j\omega)q_{22}(j\omega)|} = \frac{|q_{22}(j\omega)|\,|b_{11}(j\omega)|}{|1 + g_2(j\omega)q_{22}(j\omega)|\,|q_{21}(j\omega)|} \leq |b_{21}(j\omega)| \tag{V-27}$$

After rearranging terms, Equation (V-27) is written as:

$$\frac{1}{|1 + g_2(j\omega)q_{22}(j\omega)|} \leq \frac{|b_{21}(j\omega)|\,|q_{21}(j\omega)|}{|b_{11}(j\omega)|\,|q_{22}(j\omega)|} \tag{V-28}$$

Inverting both sides of Equation (V-28), the inequality of Equation (V-29) is obtained.

$$|1 + g_2(j\omega)q_{22}(j\omega)| \geq \frac{|b_{11}(j\omega)|\,|q_{22}(j\omega)|}{|b_{21}(j\omega)|\,|q_{21}(j\omega)|} \tag{V-29}$$

Equation (V-29) establishes the constraint on $[1 + l_2(j\omega)]$ (recall Equation (V-21)). The maximum constraint on $l_2(j\omega)$ over the range of flight conditions is needed to obtain the bounds $B_{20}(j\omega_i)$ for shaping the nominal loop transmission $l_{20}(j\omega)$.

The Nichols chart is the primary tool used to perform the design. The chart is turned upside down and the scales modified according to the procedure described in Chapter II for the disturbance attenuation problem. The rectangular grid corresponds to the magnitude and phase of $l_2(j\omega)$ while the curved grid corresponds to the magnitude and phase of $[1 + l_2(j\omega)]$. The constraint on $l_2(j\omega)$ is achieved from Equation (V-29) and the correspondence between $l_2(j\omega)$ and $[1 + l_2(j\omega)]$ on the inverted Nichols chart.

The usual approach employed to draw bounds on $l_{20}(j\omega)$ requires plant templates. However, due to their small size, plant templates are impractical to use at various design

frequencies of interest. The bounds can be obtained numerically following the procedure outlined below and described in further detail in Appendix H and Chapter V of reference 3. The design frequencies used are listed in Table V-2.

Table V-2. Acceleration Loop Design Frequencies (Radians/Second)

0.01	2.0	17.0
0.04	4.0	20.0
0.1	5.0	50.0
0.2	8.0	100.0
0.4	10.0	200.0
0.5	12.0	500.0
0.8	14.0	1000.0

The quotient on the right side of Equation (V-29) consists of known elements. The quotient is evaluated at each design frequency, $\omega = \omega_i$, of Table V-2 for each flight condition. The result is a Log-magnitude value expressed in dB. Using the curved grid on the inverted Nichols chart, the magnitude curve corresponding to a given quotient is located. Taking points along the curve at small increments, the magnitude and angle values for the bound $B_{2k}(j\omega_i)$ on $l_{2k}(j\omega)$ are read from the rectangular grid on the inverted chart. This is accomplished for all design frequencies at each flight condition k. The resulting constraint on the acceleration loop transmission for a given flight condition is given by Equation (V-30).

$$l_{2k}(j\omega) \geq B_{2k}(j\omega_i) \tag{V-30}$$

However, the maximum constraint over the range of flight conditions is needed to obtain the bounds on the nominal loop transmission $l_{20}(j\omega)$. Using the relationship of Equation (V-21) and the known equivalent plant $q_{22k}(j\omega)$ (Appendix E), the constraint on the loop transmission can be converted to a constraint on the compensator $g_{2k}(j\omega_i)$.

$$g_{2k}(j\omega_i) \geq \frac{B_{2k}(j\omega_i)}{q_{22k}(j\omega_i)} = B_{g2k}(j\omega_i) \tag{V-31}$$

Note, $B_{2k}(j\omega_i)$ is known only at specific points read from the Nichols chart, it is not a function. Evaluating Equation (V-31) to determine the bound $B_{g2k}(j\omega_i)$ on $g_{2k}(j\omega_i)$ is a point by point process where: $Lm[B_{g2k}(j\omega_i)]Ang[B_{g2k}(j\omega_i)] = Lm[B_{2k}(j\omega_i)]Ang[B_{2k}(j\omega_i)] - Lm[q_{22k}(j\omega_i)]Ang[q_{22k}(j\omega_i)]$. A math spreadsheet program is used to simplify the labor involved in obtaining the bound $B_{g2k}(j\omega_i)$ for each flight condition. Its use is demonstrated in the example of Appendix H for $\omega_i = 8$.

Investigating the magnitude values of the three $B_{g2k}(j\omega_i)$ bounds (obtained from the three flight conditions) at a given angle, the maximum magnitude value is selected for that angle value. This selection process is repeated at each angle considered. The set of maximum magnitude values selected for the set of angle values is the maximum bound $B_{g20}(j\omega_i)$ on $g_2(j\omega_i)$. The maximum constraint $B_{g20}(j\omega_i)$ on $g_2(j\omega_i)$ is converted to the maximum constraint $B_{20}(j\omega_i)$ on the nominal loop transmission $l_{20}(j\omega)$ by multiplying $q_{220}(j\omega_i)$ through Equation (V-31). In equation form:

$$g_2(j\omega_i)q_{220}(j\omega_i) \geq B_{20}(j\omega_i) = B_{g20}(j\omega_i)q_{220}(j\omega_i) \qquad \text{(V-32)}$$

From the equality of Equation (V-24), the left side of Equation (V-32) can be expressed in terms of the nominal loop transmission, i.e.:

$$l_{20}(j\omega) \geq B_{20}(j\omega_i) \qquad \text{(V-33)}$$

The bound $B_{20}(j\omega_i)$ places the greatest demand on the nominal loop transmission $l_{20}(j\omega)$ at a given design frequency, $\omega = \omega_i$. Again, obtaining $B_{20}(j\omega_i)$ from Equation (V-32) is a point by point process where $B_{20}(j\omega_i)$ is found by: $Lm[B_{20}(j\omega_i)]Ang[B_{20}(j\omega_i)] = Lm[B_{g20}(j\omega_i)]Ang[B_{g20}(j\omega_i)] + Lm[q_{220}(j\omega_i)]Ang[q_{220}(j\omega_i)]$. This process is demonstrated for $\omega_i = 8$ in Table H-4 of Appendix H using the spreadsheet program. Thus, Equations (V-32) and (V-33) define the maximum constraint on $l_2(j\omega)$ over the range of flight conditions necessary to obtain the bounds $B_{20}(j\omega_i)$ for shaping the nominal loop transmission $l_{20}(j\omega)$.

The points corresponding to the $B_{20}(j\omega_i)$ magnitude and angle values obtained at each design frequency ω_i are plotted on the inverted Nichols chart as shown in Figure V-9.

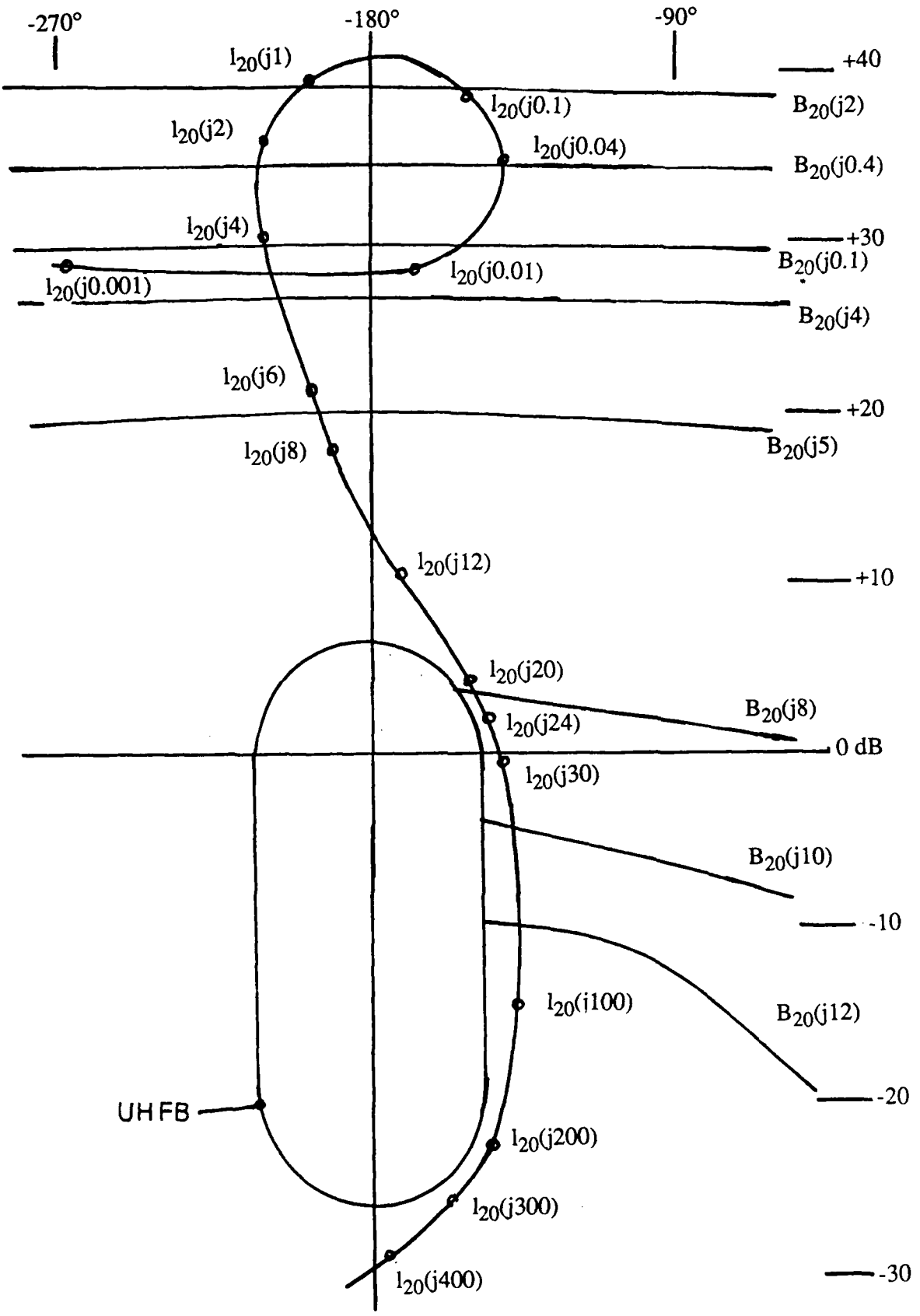

Fig. V-9. Acceleration Loop Transmission Shaping Problem

The nominal $l_{20}(j\omega)$ shaped to meet the bounds is also shown in the figure. The Universal High Frequency Bound (UHFB) chosen is the -5 dB oval on the inverted Nichols chart.

A tradeoff exists between meeting the design specifications and reducing the loop bandwidth via lowering the loop transmission below a bound at a given frequency. Recall that the acceleration response obtained is acceptable as long as it remains below 0.15 g. The bounds at $\omega_i = 2$ and $\omega_i = 4$ dominate the shaping problem. In order to reduce loop bandwidth, the $\omega_i = 2$ bound is slacked off somewhat. The optimum amount the loop transmission may fall below the bound and still meet the design specifications requires repeating the entire design process for each trial and is beyond the time limitations of this research.

The nominal loop transmission obtained from Figure V-9 is given by Equation (V-34). The acceleration loop compensator $g_2(s)$ is obtained by rearranging Equation (V-24) as shown in Equation (V-36).

$$l_{20}(s) = \frac{7.65036 \times 10^{12}(s + 0.001)(s + 0.02)(s + 4.1)(s + 13)(s + 130)}{(s - 0.009)(s + 0.09)(s + 2)^2(s - 4.1)(s + 510 \pm j680)^2(s + 60)} \quad \text{(V-34)}$$

$$g_2(s) = \frac{-4.842 \times 10^{10}(s + 0.025)(s + 4)(s + 4.1)(s + 13)(s + 20)(s + 130)}{(s)(s + 2)(s + 2)(s + 0.09)(s + 60)(s + 510 \pm j680)(s + 510 \pm j680)} \quad \text{(V-35)}$$

where:

$$g_2(s) = \frac{l_{20}(s)}{q_{220}(s)} \quad \text{(V-36)}$$

Command Tracking Compensator Design - Pitch Rate Loop

The design of the pitch rate loop compensator $g_1(s)$ and the prefilter $f_{11}(s)$ are presented in this section using the improved design technique developed by Dr. Horowitz. The pitch rate response is desired to track the pilot's pitch rate command input, thus the compensation design involves a tracking problem. The objective is to design $g_1(s)$ and $f_{11}(s)$ so the closed-loop transfer function $t_{11}(s)$ has no right half plane poles and satisfies the closed-loop performance tolerances. The pitch rate loop is shown in Figure V-10.

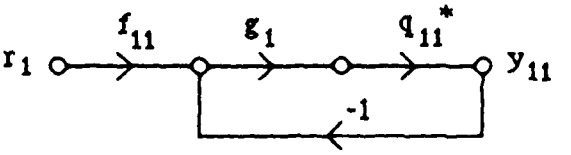

Fig. V-10. Pitch Rate Loop

The pitch rate closed-loop transfer function, given by Equation (V-37), is found by applying Mason's Rule (Ref 5:162-164) to the MIMO system diagram of Figure V-2. See Appendix J for the derivation of Equation (V-37).

$$t_{11}(s) = \frac{[f_{11}(s)][l_1(s)][1 + l_2(s)]}{[1 + l_1(s)][1 + l_2(s)] - \gamma(s)} \tag{V-37}$$

where:

$$l_i(s) = g_i(s)q_{ii}(s), \text{ for } i = 1, 2 \tag{V-38}$$

and

$$\gamma(s) = \frac{q_{11}(s)q_{22}(s)}{q_{12}(s)q_{21}(s)} \tag{V-39}$$

Equation (V-37) is rewritten as an exact expression for a single loop system via the following steps. First, divide both numerator and denominator of Equation (V-37) by the quantity $[1 + l_2(s)]$, as shown in Equation (V-40).

$$t_{11}(s) = \frac{[f_{11}(s)][l_1(s)]}{[1 + l_1(s)] + \dfrac{-\gamma(s)}{1 + l_2(s)}} \tag{V-40}$$

The denominator of Equation (V-40) is regrouped by combining (1) with the quotient term. Dividing this grouped term from the numerator and denominator, Equation (V-41) is obtained where the effective loop transmission $l_1(s)^*$ is defined by Equation (V-42).

$$t_{11}(s) = \frac{f_{11}(s)l_1(s)^*}{1 + l_1(s)^*} \tag{V-41}$$

where:

$$l_1(s)^* = \frac{l_1(s)}{1 + \dfrac{-\gamma(s)}{1 + l_2(s)}} \tag{V-42}$$

Equation (V-41) is precisely the expression for the single loop system of Figure V-10. The effective loop transmission $l_1(s)^*$ can be rewritten in terms of a new effective plant $q_{11}(s)^*$, as:

$$l_1(s)^* = [g_1(s)][q_{11}(s)^*] \tag{V-43}$$

where:

$$q_{11}(s)^* = \frac{q_{11}(s)}{1 + \dfrac{-\gamma(s)}{1 + l_2(s)}} \tag{V-44}$$

Note the new effective plant $q_{11}(s)^*$ defined by Equation (V-44), is a function of the previous acceleration loop design, $l_2(s)$, of Equation (V-38) and the interaction between loops given by $\gamma(s)$ in Equation (V-39).

The MISO synthesis techniques presented in Chapter II may now be applied to the pitch rate loop tracking problem having expressed $t_{11}(s)$ as given by Equation (V-41). To facilitate the design, the $q_{11k}(s)^*$ transfer functions are obtained at each flight condition k since the quantities on the right side of Equation (V-44) are known. The $q_{11k}(s)^*$ transfer functions are listed in Appendix G along with the frequency response plot of each case. The nominal effective plant transfer function $q_{110}(s)^*$ is selected having similar frequency response characteristics as the effective $q_{11k}(s)^*$ transfer functions.

$$q_{110}(s)^* = \frac{0.6008(s+0.0007)(s+3.995)(s+4.0)(s+15.755\pm j21.995)(s+35.736)}{(s+0.8015)(s+3.856\pm j0.4836)(s+11.9893\pm j\ 20.2778)(s+20)(s+42.021)} \tag{V-45}$$

Templates are drawn on the Nichols chart by plotting the Log-magnitude and angle of the frequency response at the chosen design frequencies (Table V-3) for the three flight

conditions. Recall from Chapter II, the templates are a plot of the range of uncertainty in the effective plant $q_{11}(j\omega)^*$. The resulting templates are shown in Figure V-11. Note the nominal point on the templates lies at the bottom corner. As observed in Figure G-1 of Appendix G, the frequency response of $q_{110}(j\omega)^*$ is nearly the same as $q_{111}(j\omega)^*$ for frequencies greater than $\omega = 1$. This resulted in the nominal point being essentially the same as the $q_{111}(j\omega)^*$ point on the templates for $\omega \geq 1$ given the small template shapes.

Table V-3. Pitch Rate Loop Design Frequencies (Radians/Second)

0.2	2.0	14.0	100.0
0.4	4.0	17.0	200.0
0.5	8.0	20.0	500.0
1.0	10.0	50.0	1000.0

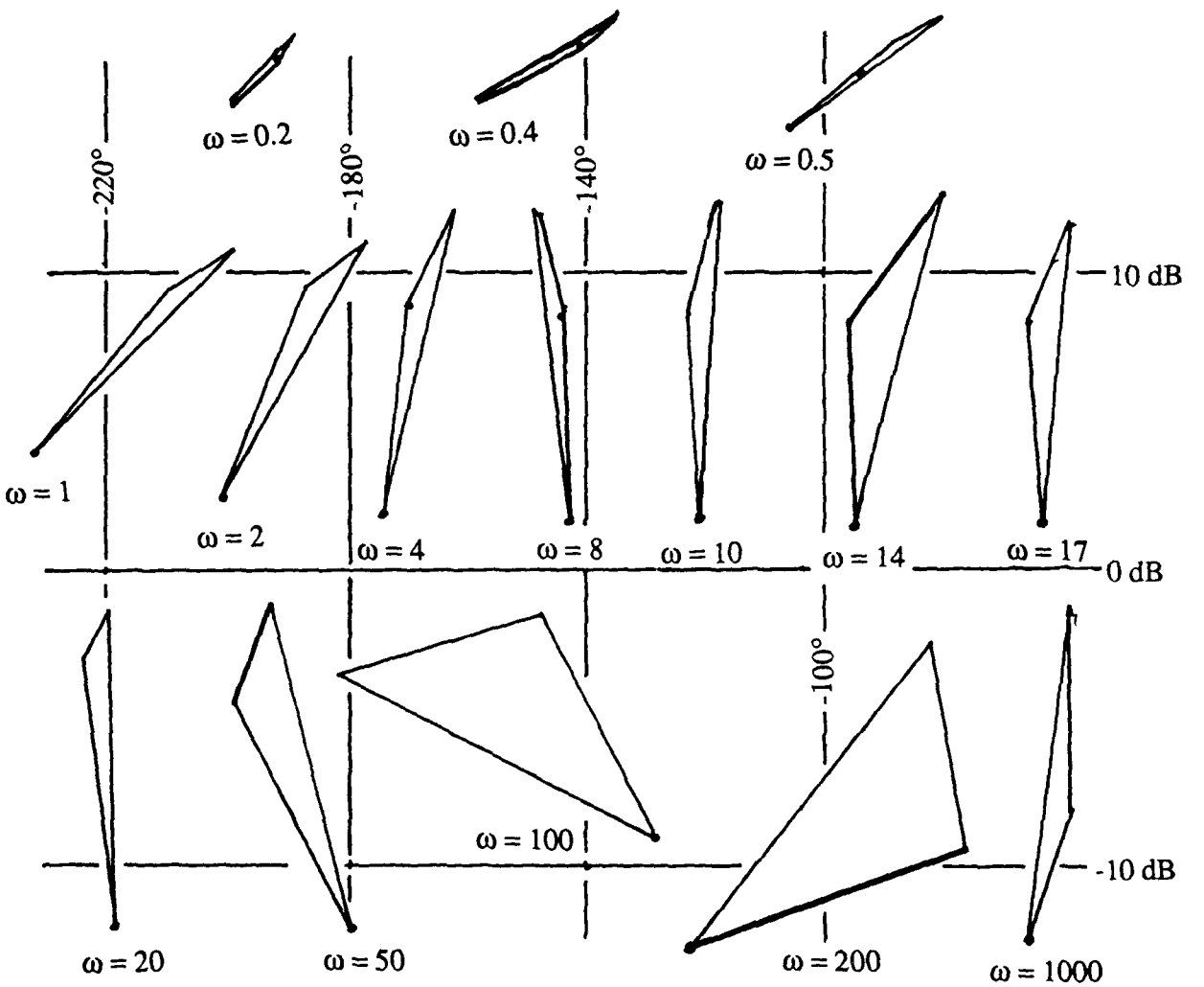

Fig. V-11. Effective Plant $q_{11}(j\omega)^*$ Templates on the Nichols Chart

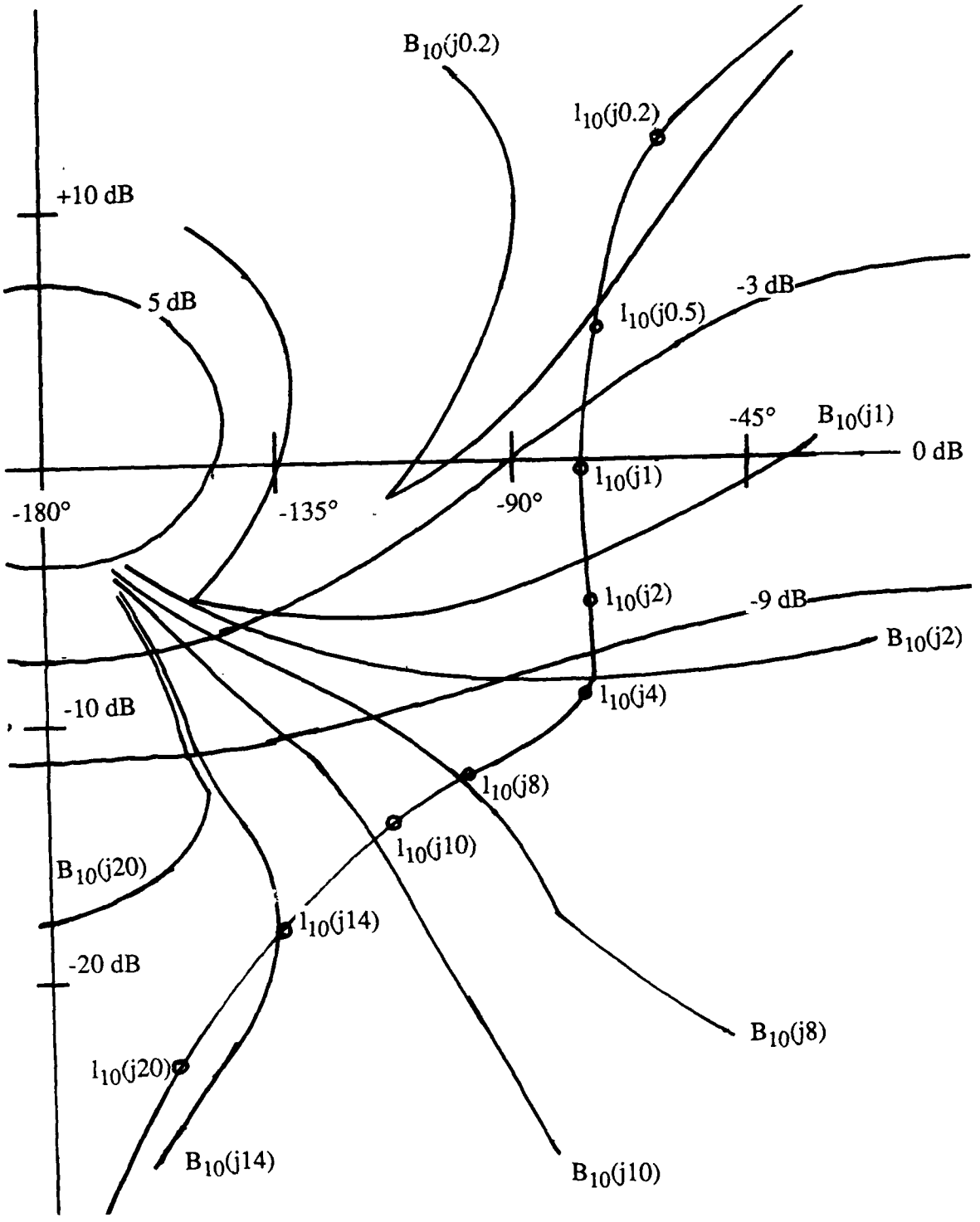

Fig. V-12. Pitch Rate Loop Transmission Shaping Problem

Bounds $B_{10}(j\omega_i)^*$ on $l_{10}(j\omega_i)^*$ are constructed on the Nichols chart using the plant templates while satisfying the closed-loop response tolerances defined by Equation (V-46). The response bound transfer functions $a_{11}(s)$ and $b_{11}(s)$ are given by Equations (V-17) and (V-18) respectively.

$$|a_{11}(j\omega_i)| \leq |t_{11}(j\omega_i)| \leq |b_{11}(j\omega_i)| \qquad \text{(V-46)}$$

Figure V-12 shows the $B_{10}(j\omega_i)^*$ bounds constructed on the Nichols chart. The nominal $l_{10}(j\omega_i)^*$ shaped to meet the bounds is also shown in the figure. The nominal loop transmission transfer function $l_{10}(s)^*$ resulting from the shaping problem is given by Equation (V-47).

$$l_{10}(s)^* = \frac{2650(s + 3.50)}{(s + 0.11)(s + 7.07 \pm j7.07)(s + 100)} \qquad \text{(V-47)}$$

From Equation (V-43), dividing $l_{10}(s)^*$ by the nominal effective plant $q_{110}(s)^*$ provides the pitch rate loop compensator $g_1(s)$:

$$g_1(s) = \frac{4410.76(s+0.802)(s+3.5)(s+3.8559\pm j0.4836)(s+11.9893\pm j20.2778)(s+20)(s+42)}{(s+0.0007)(s+0.11)(s+3.995)(s+7.07\pm j7.07)(s+15.76\pm j21.99)(s+35.74)(s+100)} \qquad \text{(V-48)}$$

The complexity of $g_1(s)$ can be reduced to that shown in Equation (V-49) by eliminating pole-zero pairs which have a non-dominant effect on the Log-magnitude of the frequency response, $Lm[g_1(j\omega)]$.

$$g_1(s) = \frac{3443.399(s + 0.802)(s + 3.856 \pm j0.484)(s + 20)}{(s + 0.007)(s + 0.11)(s + 4)(s + 7.07 \pm 7.07)(s + 100)} \qquad \text{(V-49)}$$

The final step is to design the prefilter f_{11}. Prefilter bounds are drawn on a Bode plot following the procedure described in Chapter II. A transfer function is shaped to lie within the bounds as shown in Figure V-13. The resulting prefilter design is given by Equation (V-50).

$$f_{11}(s) = \frac{0.2348(s + 10)(s + 12.4)(s +20)}{(s + 1.885 \pm j2.6475)(s + 4)(s + 12)} \qquad \text{(V-50)}$$

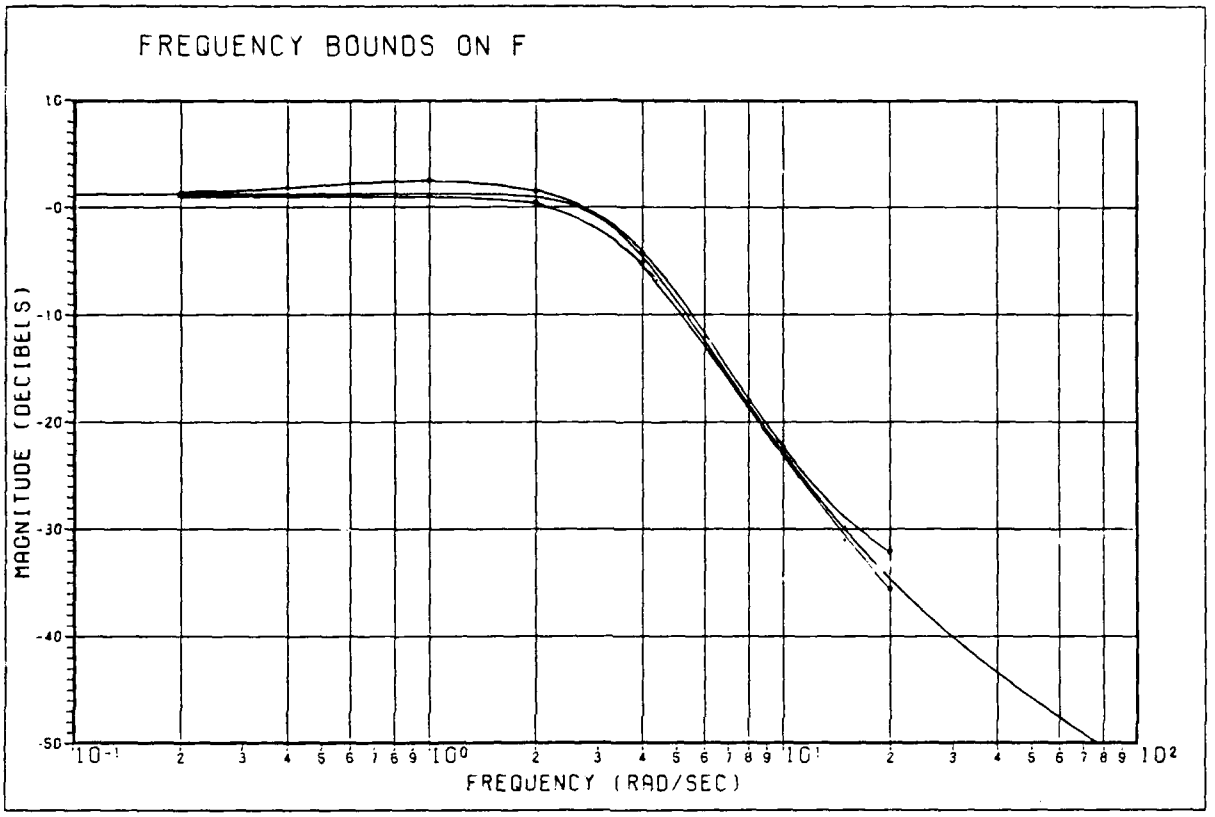

Fig. V-13. Frequency Bounds on the Prefilter, $f_{11}(j\omega)$.

Summary

This chapter presents the design steps used to solve a MIMO compensation problem. The improved QFT technique is applied to obtain a pitch pointing controller design for the AFTI/F-16 aircraft. The two-by-two MIMO design problem is broken into two equivalent MISO design problems, the solution of which guarantees the solution to the MIMO problem. The individual compensator elements found are inserted into the system diagram of Figure V-2, resulting in the pitch pointing controller.

The controller design must be verified at each flight condition. Chapter VI presents the design results and the digital simulations of the system response.

VI. Design Results and Computer Simulations

Introduction

The resulting compensators designed using the QFT technique and computer simulations of the system response are presented in this chapter. The transfer functions of the shaped loop transmissions and the corresponding **G** compensator matrix elements are given along with the prefilter **F**. The single set of compensator elements obtained is applied to the aircraft model at each flight condition. Computer simulations of the system's response are provided using the software package, TOTAL, to verify the design met the specified requirements.

Design Results

The nominal loop transmission shaped for the acceleration loop is $l_{20}(s)$. The corresponding compensator obtained is $g_2(s)$. The nominal loop transmission shaped for the pitch rate loop is $l_{10}(s)^*$ resulting with the compensator $g_1(s)$. The transfer functions for these relationships and the prefilter $f_{11}(s)$ are given below.

$$l_{20}(s) = \frac{7.65036 \times 10^{12}(s + 0.001)(s + 0.02)(s + 4.1)(s + 13)(s + 130)}{(s - 0.009)(s + 0.09)(s + 2)^2(s - 4.1)(s + 510 \pm j680)^2(s + 60)} \quad \text{(VI-1)}$$

$$g_2(s) = \frac{-4.842 \times 10^{10}(s + 0.025)(s + 4)(s + 4.1)(s + 13)(s + 20)(s + 130)}{(s)(s + 2)(s + 2)(s + 0.09)(s + 60)(s + 510 \pm j680)(s + 510 \pm j680)} \quad \text{(VI-2)}$$

$$l_{10}(s)^* = \frac{2650(s + 3.50)}{(s + 0.11)(s + 7.07 \pm j7.07)(s + 100)} \quad \text{(VI-3)}$$

$$g_1(s) = \frac{3443.399(s + 0.802)(s + 3.856 \pm j0.484)(s + 20)}{(s + 0.007)(s + 0.11)(s + 4)(s + 7.07 \pm 7.07)(s + 100)} \quad \text{(VI-4)}$$

$$f_{11}(s) = \frac{0.2348(s + 10)(s + 12.4)(S + 20)}{(s + 1.885 \pm j2.6475)(s + 4)(s + 12)} \quad \text{(VI-5)}$$

The bandwidth of the compensation in the feedback loop is important due to noise considerations. The nominal loop transmission and loop compensator bandwidths are listed in Table VI-1. For this study, the bandwidth (i.e. the phase margin frequency) of a function is defined as the frequency, in units of radians/second, where the magnitude of the frequency response of $l_{i0}(j\omega)$ is equal to one (0 dB).

Table VI-1. Loop and Compensator Bandwidths

Function	Bandwidth
$l_{10}(s)$*	0.95 r/s
$g_1(s)$	37.5 r/s
$l_{20}(s)$	36.0 r/s
$g_2(s)$	3680.0 r/s

Frequency response plots of the nominal loop transmissions and the compensators are provided on the following pages.

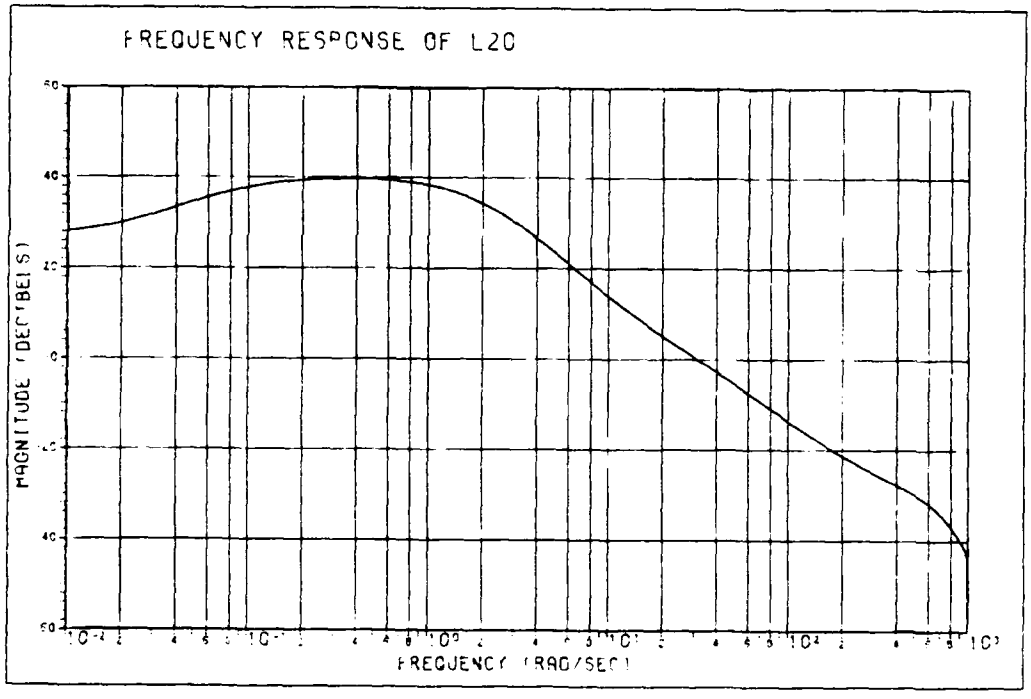

Fig. VI-1. Frequency Response of Acceleration Loop Transmission, $l_{20}(j\omega)$

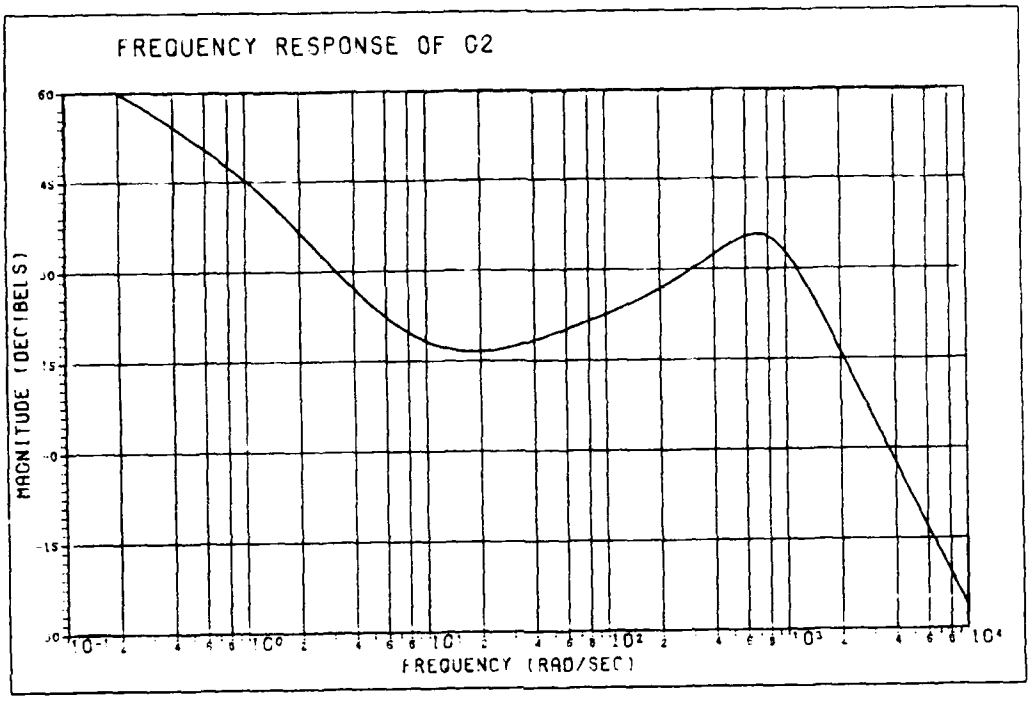

Fig. VI-2. Frequency Response of Acceleration Loop Compensator, $g_2(j\omega)$

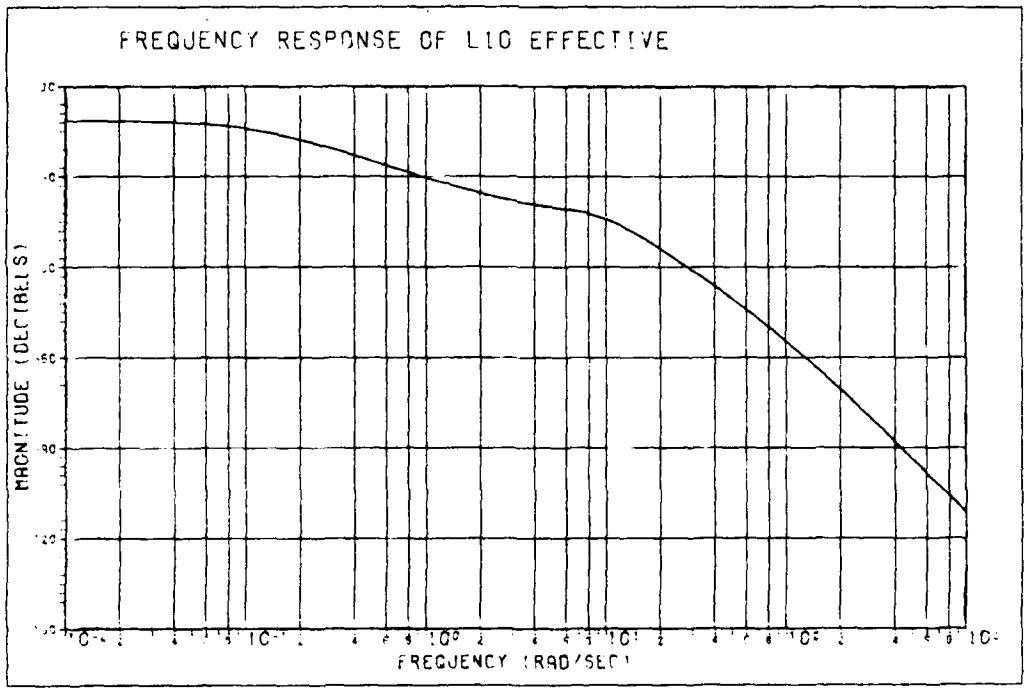

Fig. VI-3. Frequency Response of the Effective Pitch Rate LoopTransmission, $l_{10}(j\omega)$*

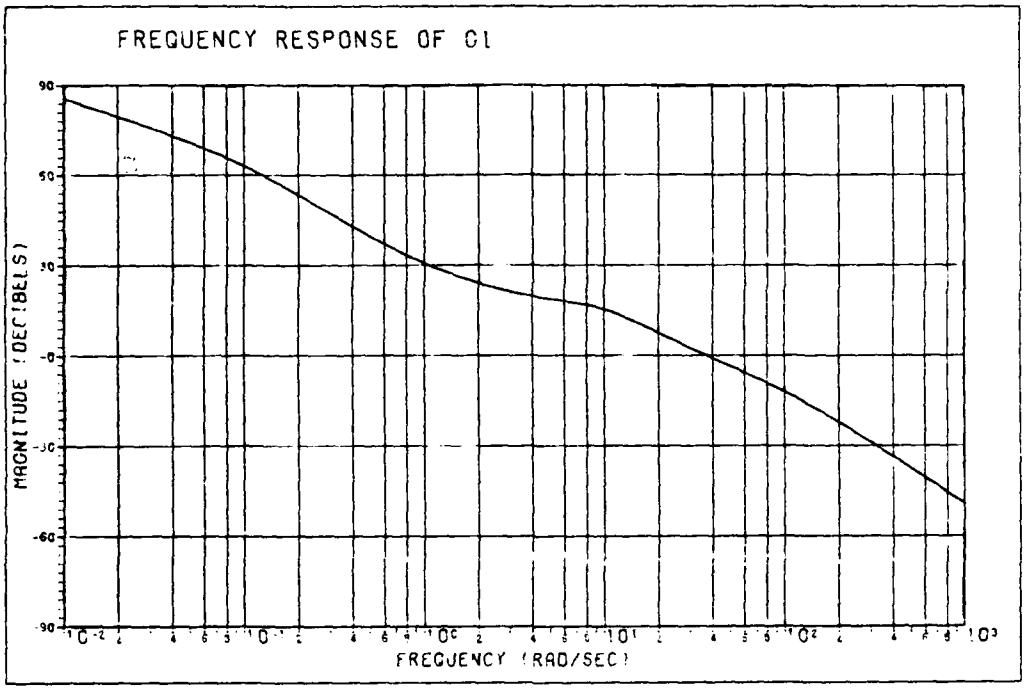

Fig. VI-4. Frequency Response of the Pitch Rate Loop Compensator, $g_1(j\omega)$

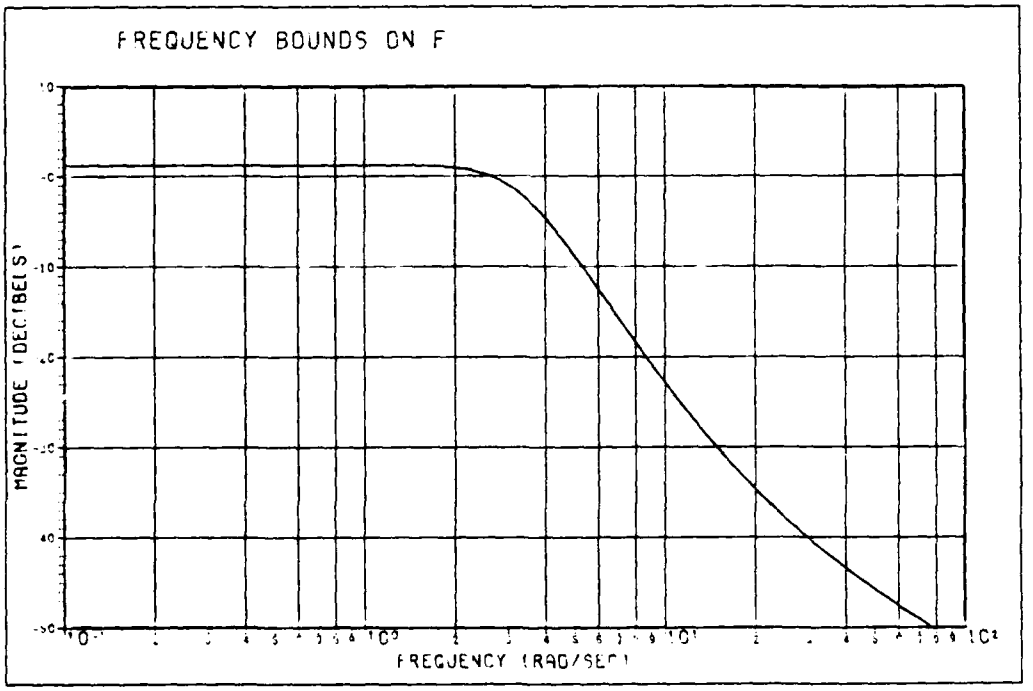

Fig. VI-5. Frequency Response of the Prefilter, $f_{11}(j\omega)$

Computer Simulation of the Controller Design

Verification of the controller design is necessary to determine if the system performance meets the desired response specifications over the range of flight conditions. To verify the design, the control laws are applied to the plant at each flight condition and the system time response is observed for a given input. To obtain the closed-loop transfer functions for the two system outputs due to the command input, the compensator elements g_1, g_2, and f_{11} are inserted into the system diagram of Figure V-2. Recall f_{21} and r_2 equal zero. Mason's Gain Rule (Ref 5:162-164) is then applied to the system. The transfer functions for the plant inputs due to the command input are found similarly. The derivation of these relationships is given in Appendix J. The closed-loop system transfer functions are constructed for each flight condition using a macro routine on the computer-aided-design package, TOTAL. Note the same compensation is used for each case.

To evaluate the pitch pointing controller design, the time responses to a 1 deg/sec step input command in pitch rate are found for each flight condition using TOTAL. In addition, a 1 deg/sec pulse input in pitch rate is applied for 2 seconds to the 0.9 Mach, 20,000 feet condition to observe a step response in pitch. Plots of the system response are presented on the following pages. A discussion of the performance results follow the figures.

System Time Response for the Pitch Pointing Maneuver

Case 1: 0.6 Mach, 30,000 Feet

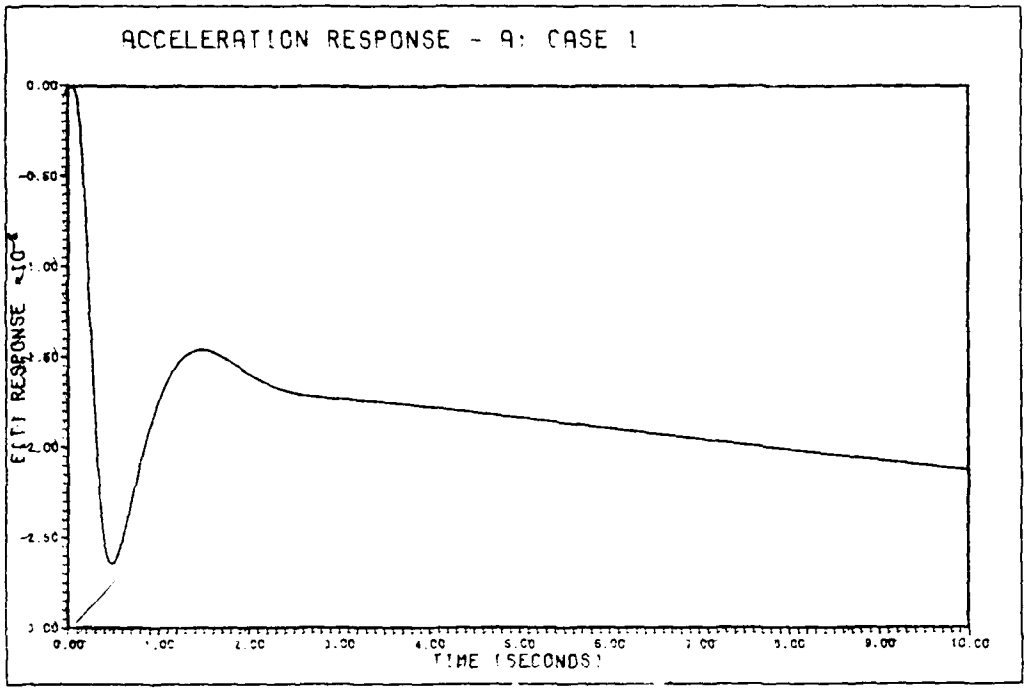

Fig. VI-6. System Response - Pitch Pointing Controller Design Acceleration Response to a 1 deg/sec Step Command in Pitch Rate

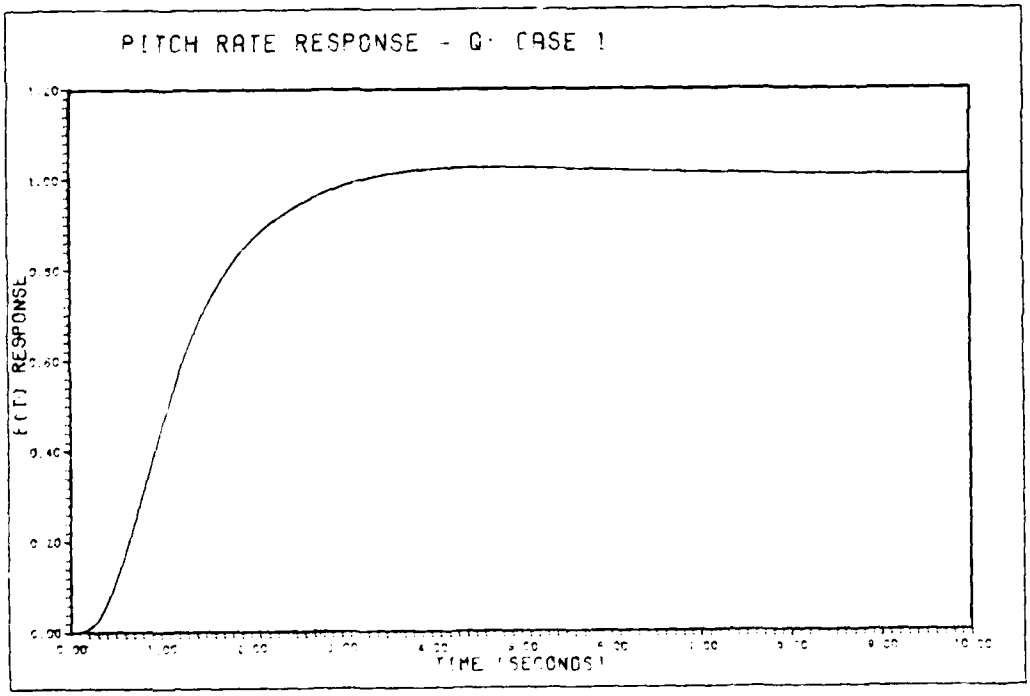

Fig. VI-7. System Response - Pitch Pointing Controller Design Pitch Rate Response to a 1 deg/sec Step Command in Pitch Rate

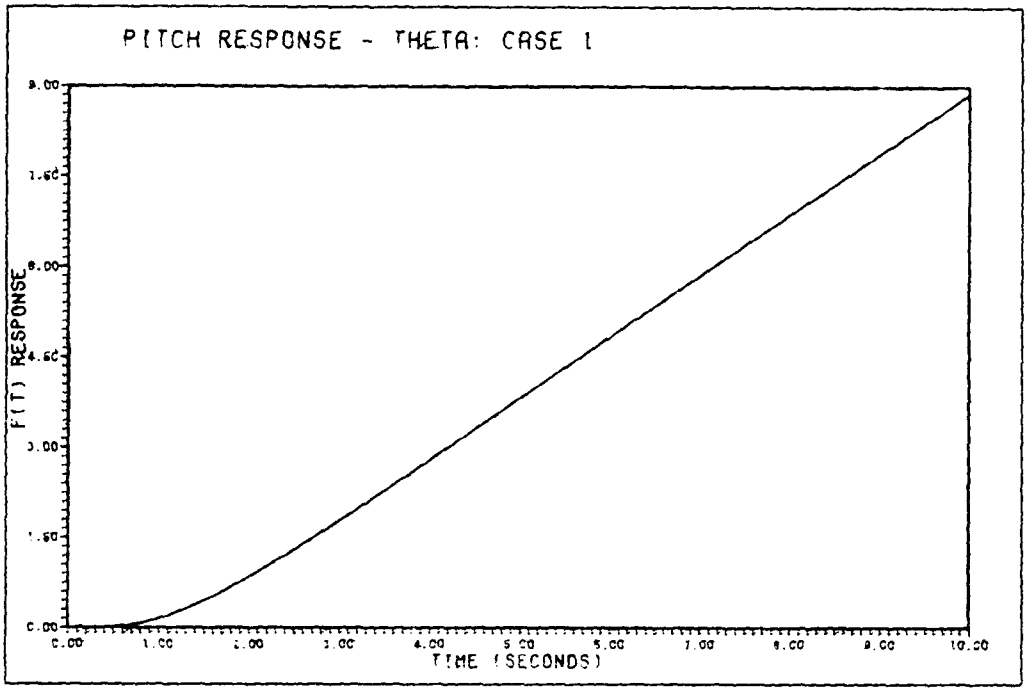

Fig. VI-8. System Response - Pitch Pointing Controller Design Pitch Response to a 1 deg/sec Step Command in Pitch Rate

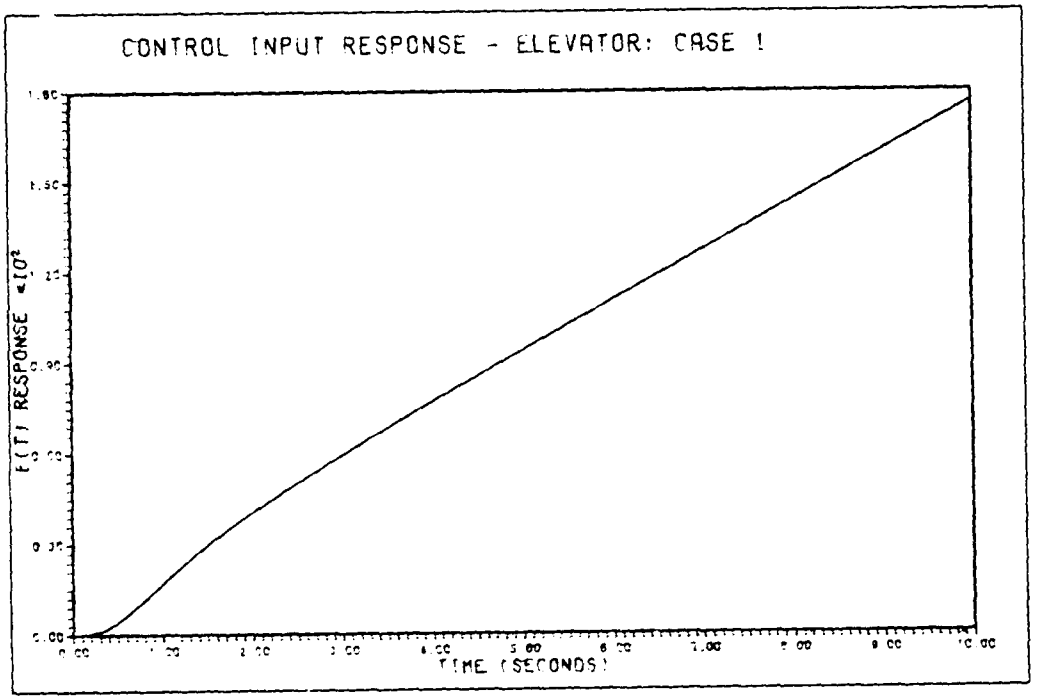

Fig. VI-9. System Response - Pitch Pointing Controller Design Elevator Command Response to a 1 deg/sec Step Command in Pitch Rate

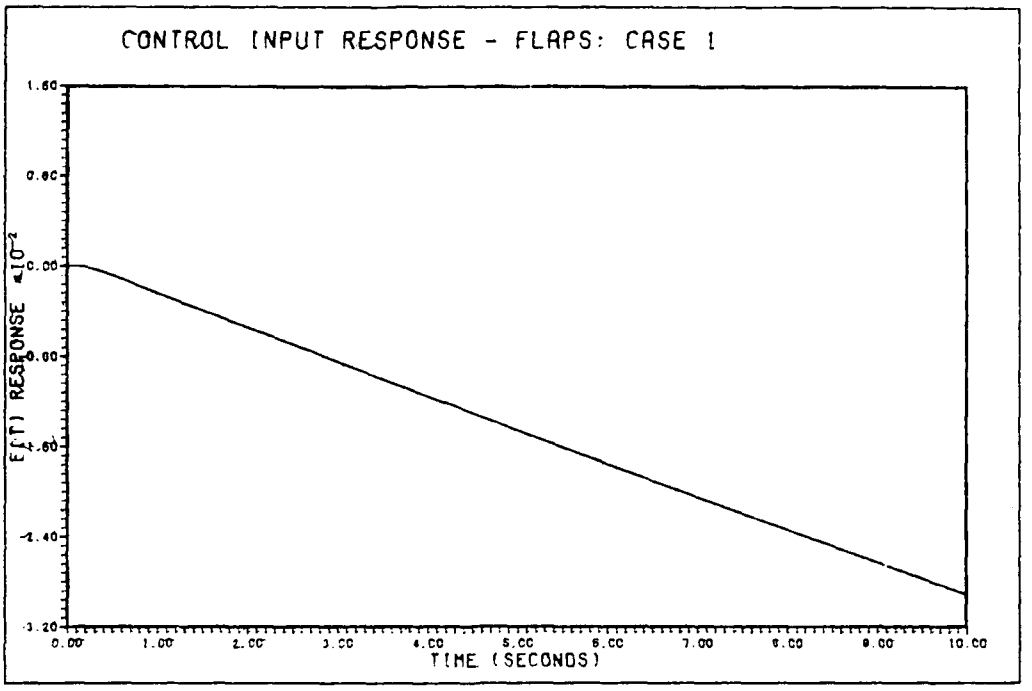

Fig. VI-10. System Response - Pitch Pointing Controller Design Flap Command Response to a 1 deg/sec Step Command in Pitch Rate

System Time Response for the Pitch Pointing Maneuver

Case 2: 0.9 Mach, 20,000 Feet

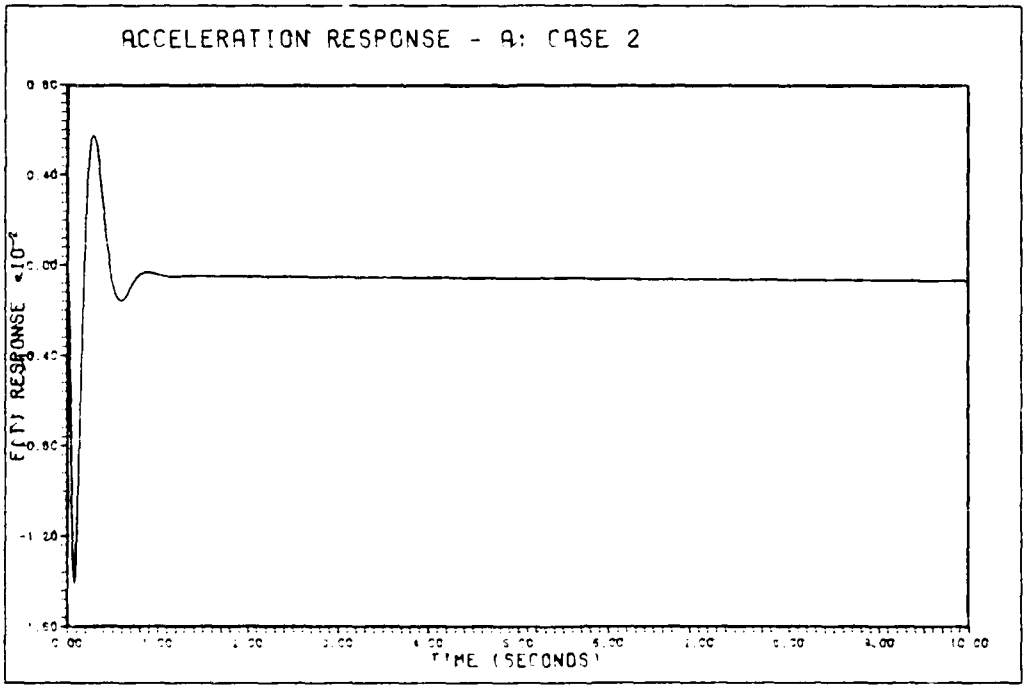

Fig. VI-11. System Response - Pitch Pointing Controller Design Acceleration Response to a 1 deg/sec Step Command in Pitch Rate

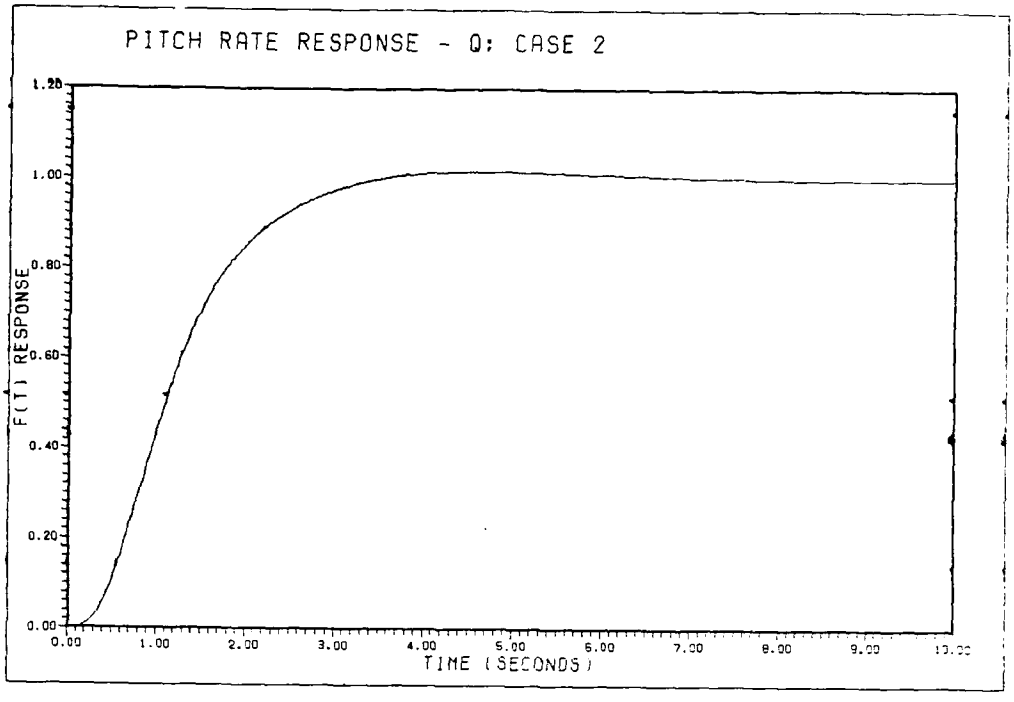

Fig. VI-12. System Response - Pitch Pointing Controller Design Pitch Rate Response to a 1 deg/sec Step Command in Pitch Rate

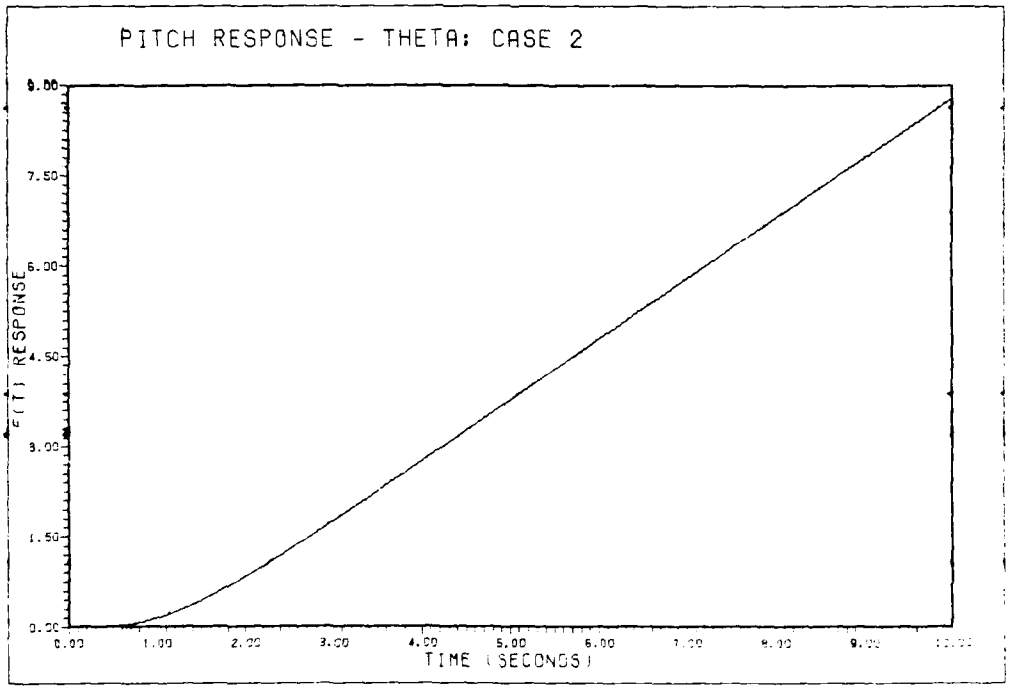

Fig. VI-13. System Response - Pitch Pointing Controller Design Pitch Response to a 1 deg/sec Step Command in Pitch Rate

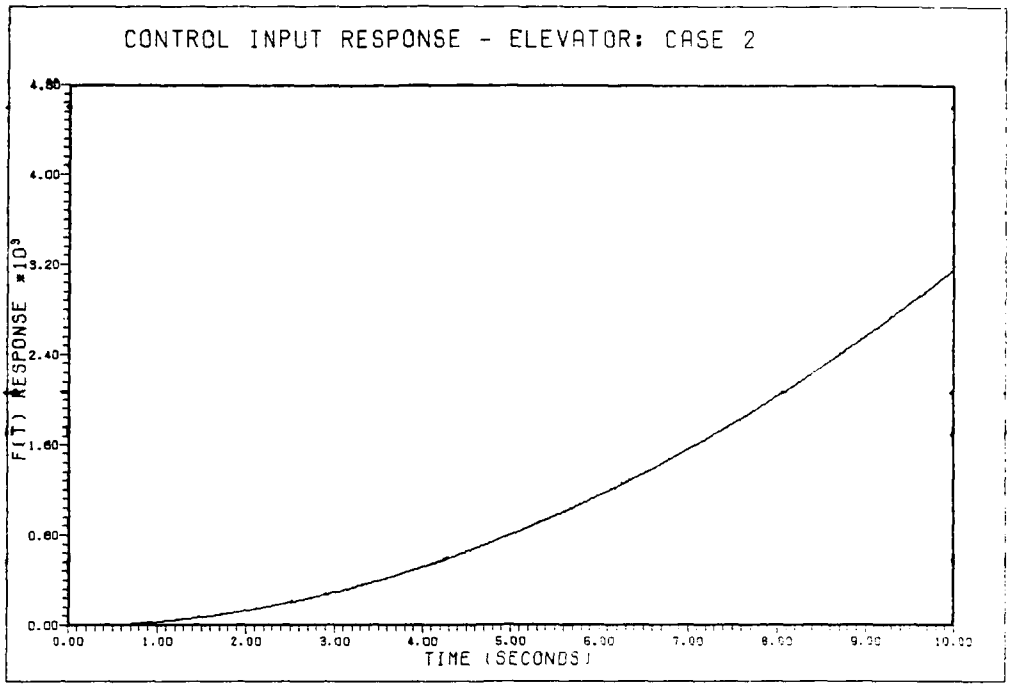

Fig. VI-14. System Response - Pitch Pointing Controller Design Elevator Command Response to a 1 deg/sec Step Command in Pitch Rate

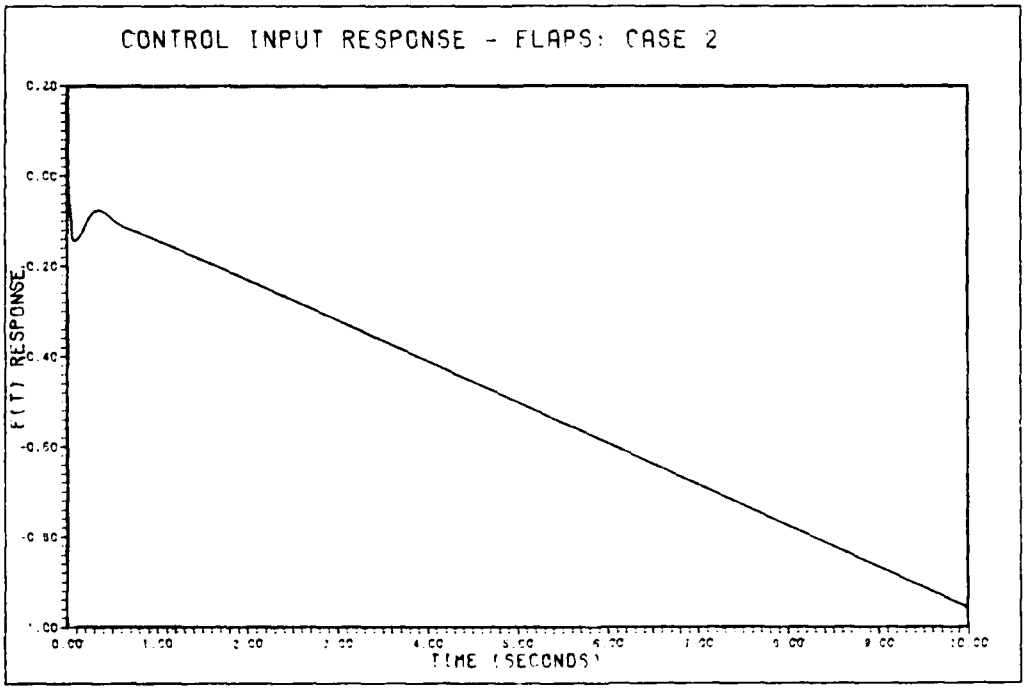

Fig. VI-15. System Response - Pitch Pointing Controller Design Flap Command Response to a 1 deg/sec Step Command in Pitch Rate

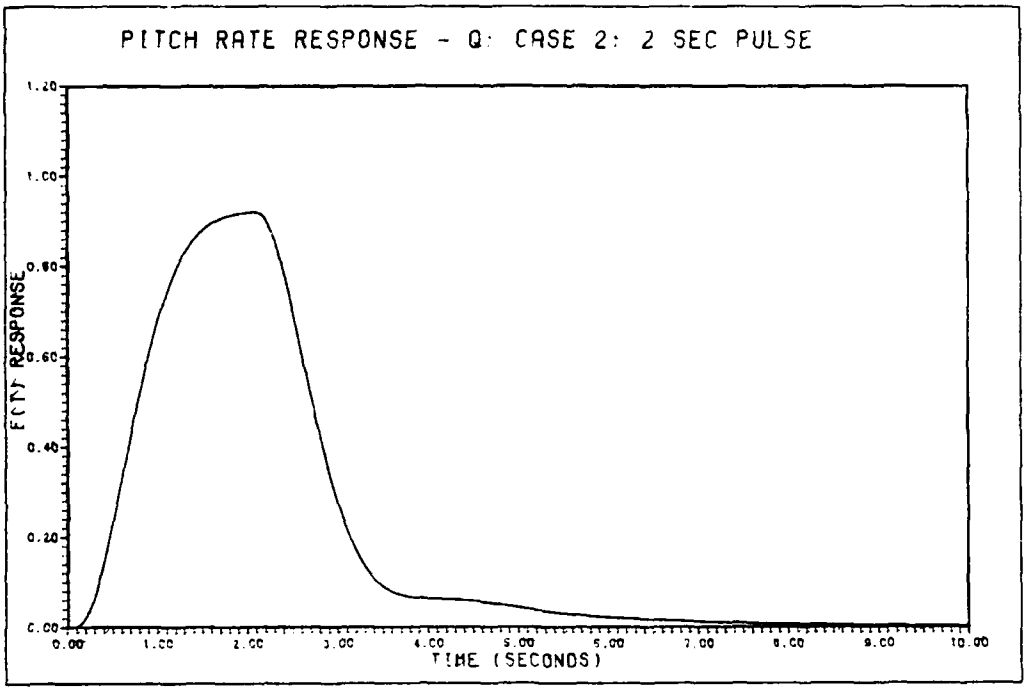

Fig. VI-16. System Response - Pitch Pointing Controller Design Pitch Rate Response to a 1 deg/sec Pulse Command in Pitch Rate, Pulse Length of 2 seconds

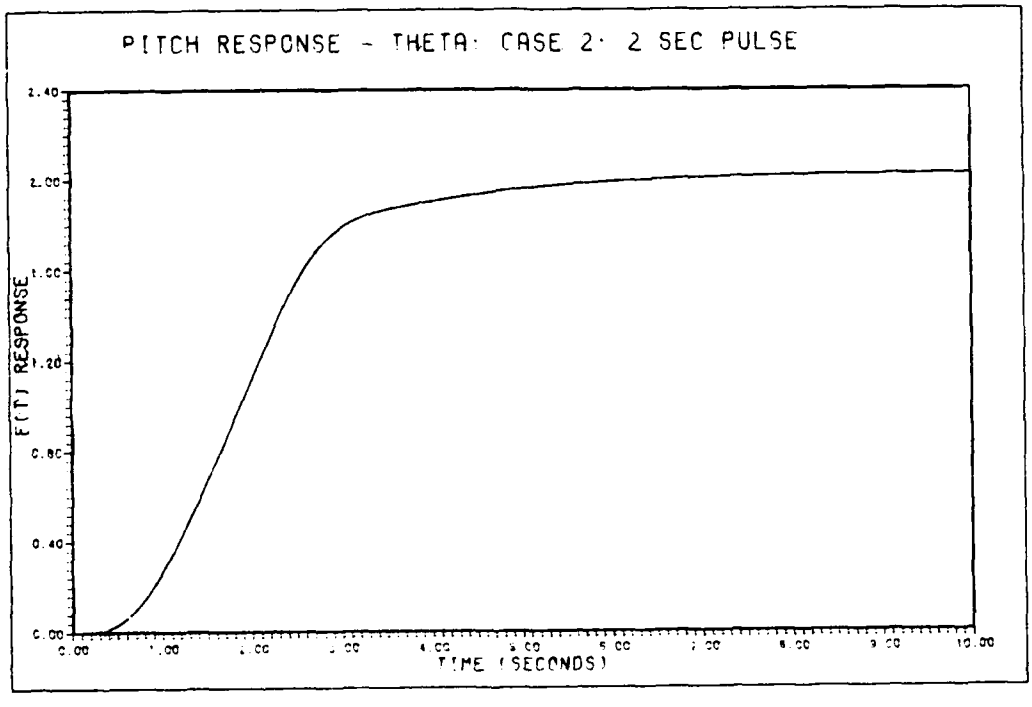

Fig. VI-17. System Response - Pitch Pointing Controller Design Pitch Response to a 1 deg/sec Pulse Command in Pitch Rate, Pulse Length of 2 seconds.

System Time Response for the Pitch Pointing Maneuver

Case 3: 1.6 Mach, 30,000 Feet

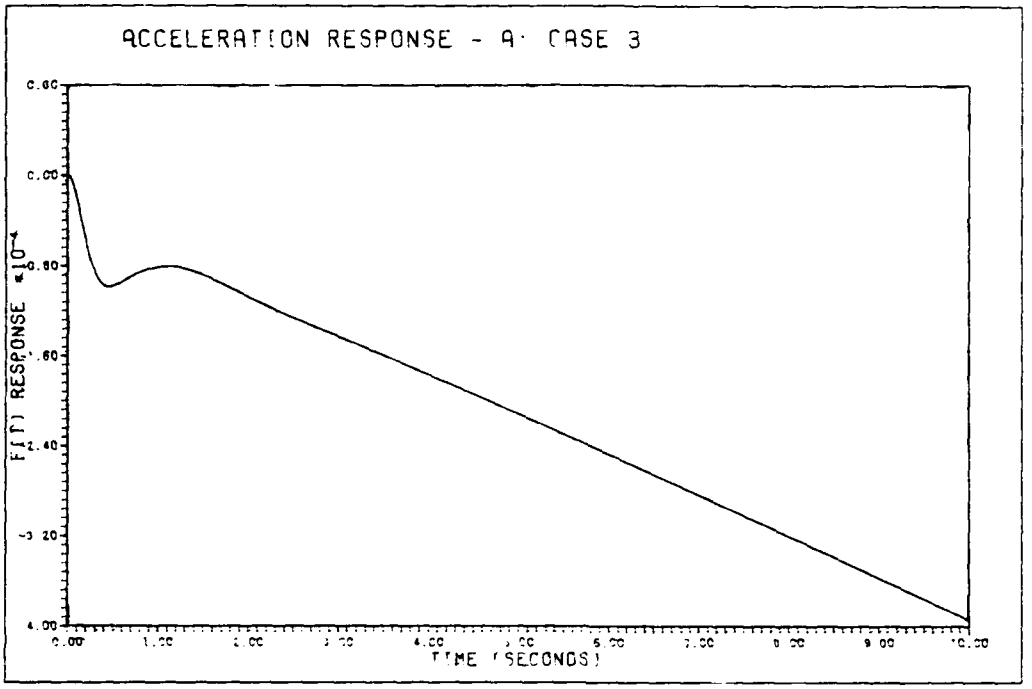

Fig. VI-18. System Response - Pitch Pointing Controller Design Acceleration Response to a 1 deg/sec Step Command in Pitch Rate

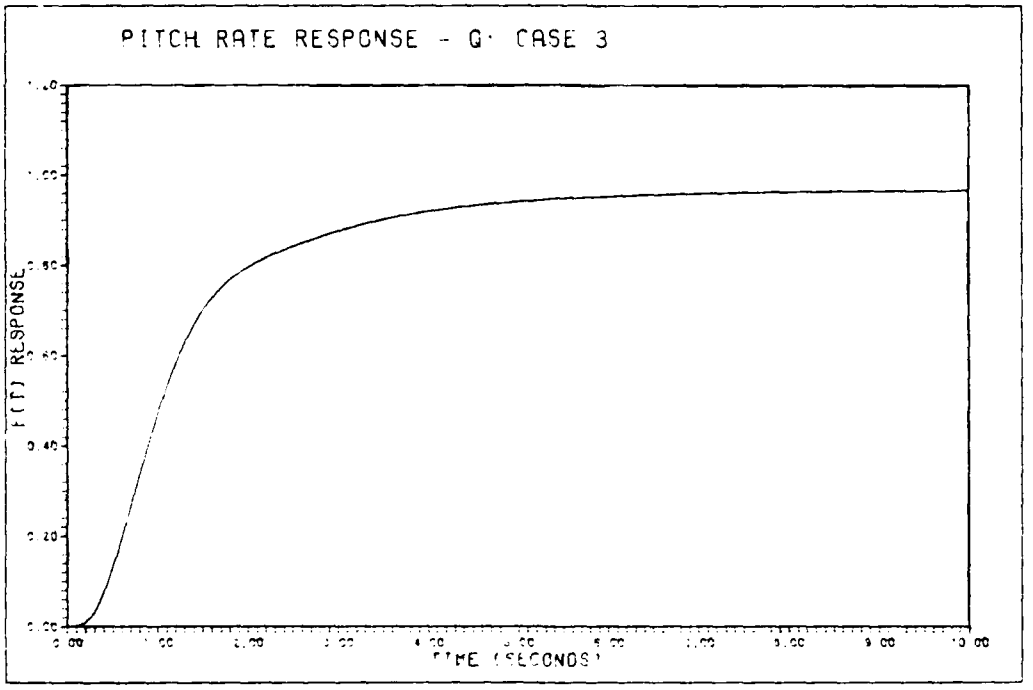

Fig. VI-19. System Response - Pitch Pointing Controller Design Pitch Rate Response to a 1 deg/sec Step Command in Pitch Rate

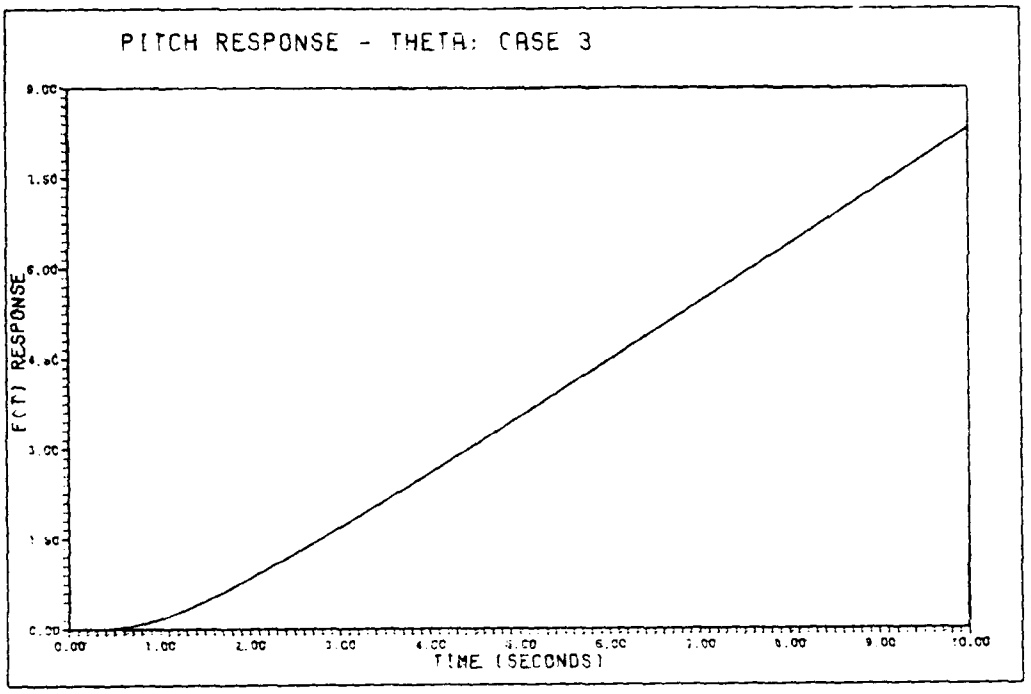

Fig. VI-20. System Response - Pitch Pointing Controller Design Pitch Response to a 1 deg/sec Step Command in Pitch Rate

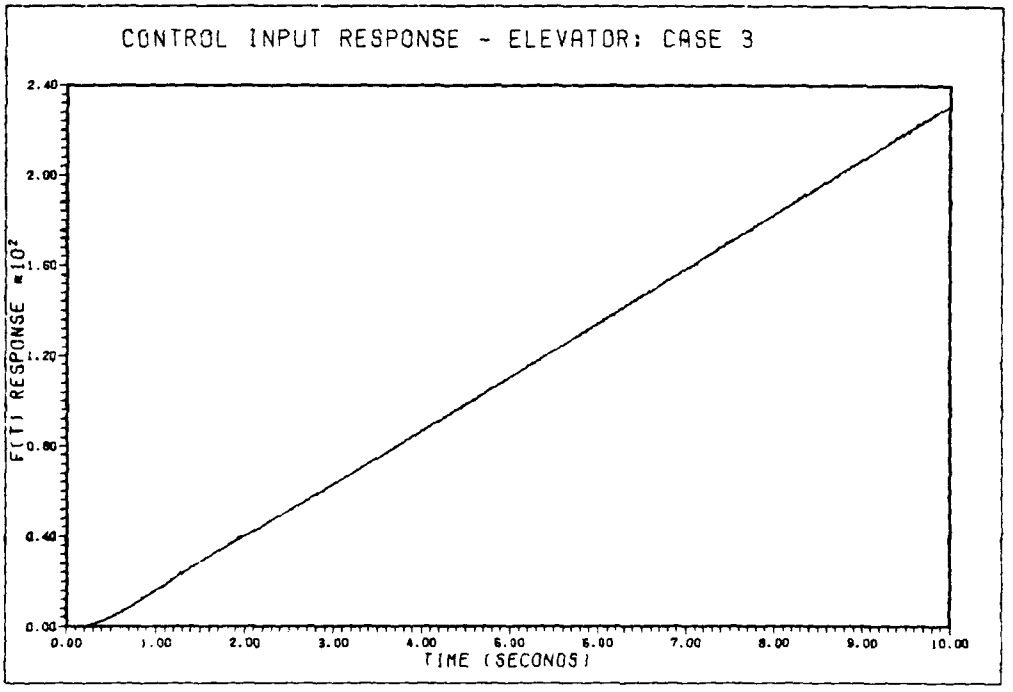

Fig. VI-21. System Response - Pitch Pointing Controller Design Elevator Command Response to a 1 deg/sec Step Command in Pitch Rate

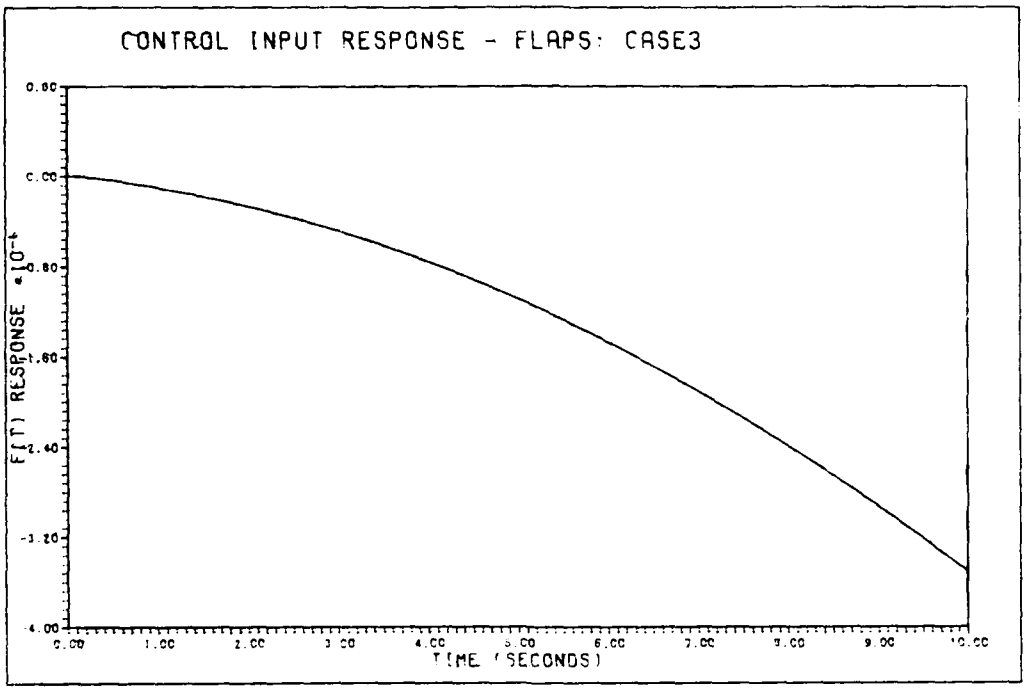

Fig. VI-22. System Response - Pitch Pointing Controller Design Flap Command Response to a 1 deg/sec Step Command in Pitch Rate

Discussion

The preceding figures are obtained using the same compensation for all three flight conditions. In all cases, control and stability are achieved. The acceleration response is maintained well below the acceleration time response performance specification of Figure V-6. In Cases 1 and 2, an initial acceleration transient is present which may appear to be undesirable, however the peak magnitude of the transient is well below the design specification and would be imperceptible to the pilot. Pitch rate response is smooth and well behaved in all cases. The pitch rate response results are somewhat overdamped, in proximity of the lower, a_{11}, pitch rate time response bound of Figure V-5. The use of a diagonal G compensator matrix is readily evident by observing the elevator and flap input command responses. Pitch rate commands dominate the elevator command input while flap command inputs are minimal. Elevator and flap command responses are smooth and well behaved. Surface rate limits are not exceeded, however elevator position limits are

exceeded between 1 and 2 seconds. Surface position limits were not directly incorporated in the preliminary design due to the limited scope of this effort.

Loop and compensator bandwidths are reasonable except for the acceleration loop compensator g_2. This bandwidth is large due to the large plant uncertainty at high frequencies. This uncertainty is evident by observing the magnitude difference between the maximum and minimum plant frequency responses as ω approaches infinity, see Figure F-4. Note at high frequency, over 20 dB of uncertainty exists between the maximum and minimum frequency responses (Cases 3 and 1 respectively). This large uncertainty manifests itself in the large UHF bound of the acceleration loop transmission problem, Figure V-9. Additionally, the $\omega = 2$ and $\omega = 4$ bounds dominate the shaping problem due to the stringent design specifications of b_{11}. A complex compensator having large bandwidth is required to overcome the plant uncertainty or risk not achieving the design specifications.

VII. Conclusions and Recommendations

Conclusions

The QFT design method provides a number of advantages over other design methods. A major benefit is the solution of a multiple input - multiple output control problem with plant uncertainty by solving an equivalent set of multiple input - single output control problems with plant uncertainty and disturbance inputs. Another benefit is the non-iterative nature of the design technique. The solution of each MISO loop is accomplished once, the solutions of which guarantee the solution of the MIMO system considered here. A single MIMO controller design is produced having robust stability and control margins over the range of flight conditions.

The design tradeoffs are readily apparent to the designer during the design procedure, particularly in terms of design complexity versus economy in bandwidth. As previously observed in the Discussion section of Chapter VI, the acceleration loop design was driven by large high frequency uncertainty in addition to stringent design specifications on the pitch rate response. Various tradeoffs are available but could not be explored here. For example, the design method inherently has some overdesign in the first loop. The result of the overdesign is observed in the acceleration responses of Chapter VI being well below the design specification. An alternative would be to design the pitch rate loop first, however this would require simultaneous solution of a disturbance rejection and command response problem, increasing the design effort required to obtain the control laws. Another alternative would be the use of scheduling to reduce the high frequency uncertainty of the plant. Referring again to Figure F-4, separate designs could be done by pairing Cases 2 and 3 while handling Case 1 separately. This would greatly reduce the high frequency uncertainty, from 20 dB to less than 10 dB, simplifying the shaping problem and reducing the acceleration loop compensator bandwidth. An acceleration loop compensator could be designed optimally placing the loop transmission frequency response on or just above each respective bound, however the extreme complexity of such a design is readily obvious.

Recommendations

This study provides a starting point for comparison of different control system design techniques. The design method used for this research is relatively new and contains distinct benefits for Air Force control system applications. Continued research and application of the design method is strongly recommended for the AFTI/F-16 vehicle. Particular areas worthy of further research include the use of off-diagonal **G** matrix compensator elements to reduce elevator deflection demand, incorporation of plant input amplitude and rate limits in the design process, and scheduling to reduce high frequency gain uncertainty. The design method permits a large region of plant uncertainty to be controlled by a single compensator design, thus larger groups of flight conditions should be considered in future design problems.

As this thesis represents a first application of the design method, a majority of the design effort required plotting of bounds and shaping the loop transmissions on the Nichols chart by hand. This greatly extended the time required to execute the design method and limited exploration of various design tradeoffs. Computer automation of bound calculation, Nichols chart plotting, and user interactive loop transmission shaping is recommended to fully explore the benefits of the design method. The program TOTAL would provide a starting point for a interactive user workstation.

Complex system models and compensator designs can result in very high order polynomials comprising the various transfer functions used in applying the technique. Polynomial root solving errors quickly arose when executing math operations on transfer functions using TOTAL. The root solving algorithms in TOTAL should be enhanced to reduce errors incurred with very high order polynomials.

BIBLIOGRAPHY

1. Ashworth, M. J. Feedback Design of Systems with Significant Uncertainty. Chinchester: Research Studies Press, 1982.

2. Barfield, A. Finley. Multivariable Control Laws for the AFTI/F-16. MS Thesis. Air Force Institute of Technology, Wright-Patterson AFB, Ohio, 1983.

3. Betzold, Robert W. Multiple Input - Multiple Output Flight Control Design with Highly Uncertain Parameters: Application to the C-135 Aircraft. MS Thesis. Air Force Institute of Technology, Wright-Patterson AFB, Ohio, 1983.

4. Blakelock, John J. Automatic Control of Aircraft and Missiles. New York: John Wiley and sons, Inc., 1965.

5. D'Azzo, John J. and Constantine H. Houpis. Linear Control System Analysis and Design, Conventional and Modern (Third Edition). New York: McGraw-Hill Book Company, 1988.

6. Etkin, Bernard. Dynamics of Atmospheric Flight. New York: John Wiley and Sons, Inc., 1972.

7. Horowitz, Isaac M. Synthesis of Feedback Systems. New York: Academic Press, 1963.

8. Horowitz, Isaac M. and Marcel Sidi. "Synthesis of Feedback Systems with Large Plant Ignorance for Prescribed Time-Domain Tolerances," International Journal of Control, 16 (2): 287-309 (1972).

9. Horowitz, Isaac. "Quantitative Synthesis of Uncertain Multiple Input-Output Feedback System," International Journal of Control, 30 (1): 81-106 (1979).

10. Horowitz, Isaac et al. Reserch in Advanced Flight Control Design. AFFDL-TR-79-3120. Department of Applied Mathematics, The Weizmann Institute of Science, Rehovot, Israel, January 1980.

11. Horowitz, Isaac, and Clayton Loecher. "Design of a 3x3 Multivariable Feedback System with Large Plant Uncertainty," International Journal of Control, 33 (4): 677-699 (1981).

12. Horowitz, Isaac. "Improved Design Technique for Uncertain Multiple-Input-Multiple-Output Feedback Systems, "International Journal of Control,36 (6): 977-988 (1982).

13. Horowitz, Isaac and T. Kopelman. Multivariable Flight Control Design with Uncertain Parameters. Department of Applied Mathematics, The Weizmann Institute of Science, Rehovot, Israel. Final Report, September 1982.

14. Horowitz, Isaac. "A Synthesis Theory for a Class of Saturating Systems," International Journal of Control, 38 (1): 169-187 (1983).

15. Walke, Jon G. Design of a Longitudinal Flight Control System Using the Singular "G" Method. MS Thesis. Air Force Institute of Technology, Wright-Patterson AFB, Ohio, 1983.

16. Houpis, C. H.: "Quantitative Feedback Theory (QFT): Technique for Designing Multivariable Control Systems," AFWAL-TR-86-3107, Air Force Wright Aeronautical Laboratories, Wright-Patterson AFB, Ohio, January 1987. (Available from Defense Technical Information Center, Cameron Station, Alexandria, VA 22314, document number AD-A176883.)

Appendix A

Loop Shaping Examples

Introduction

This appendix presents two examples of loop shaping. These examples are included to assist in understanding the concept of shaping a nominal loop transmission and the basic fundamentals of the single loop design process. The materials are reproduced with permission from Dr. Horowitz.

The first example is a numerical analysis of a loop shaping problem. The primary concepts required for shaping a nominal loop transmission are given.

The second design example demonstrates the main features of the single loop control problem. Template construction, nominal loop shaping, and solution for the compensators, G and F, are presented.

Example: Shaping of a nominal loop transmission $L_0(j\omega)$ to satisfy boundaries $B(\omega)$ on Nichols Chart.

Previous notes have described how tolerances on the closed-loop system frequency response are readily translated into bounds on a nominal loop transmission function $L_0(j\omega)$. In Fig. 1, for example, $L_0(j2)$ must be on or above the curve labelled B(2), etc. B_h is the "universal high-frequency boundary" applicable, in this example, to $\omega \geq \omega_h = 40$, i.e. $L_0(j\omega)$ (for $\omega \geq 40$) must be contained in the closed curve B_h in Fig. 1. Additional specification is $e_L = 4$, where e_L is excess of poles over zeros of $L_0(s)$. Also, L_0 is to be Type 1 (one pole at the origin). We proceed to describe a reasonable procedure for choosing a rational function $L_0(s)$ which satisfies the above specifications.

In our first step, we try to find the $B(\omega)$ which "dominates" $L_0(j\omega)$. E.g. suppose $L_{01}(j4) \approx 0db/\underline{-135°}$ (point A in Fig. 1). But at $\omega=1$, $|L_0(j)|$ needed is ≈27db. In order to decrease $|L_0|$ from 27db to about 0db in 2 octaves ($4/1=2^2$), the slope of $|L_0(j\omega)|$ would have to be, on the average, about -14db/octave, involving $\underline{/L_0} < -180°$. We assume "absolute" stability is required here for $L_0(j\omega)$ with a margin of 40°, not just at crossover ("crossover" is defined as the frequency at which $|L_0(j\omega)| = 1$). Hence B(1) dominates $L_0(j\omega)$, at least more than B(4). In the same way we see that B(1) dominates over all other $B(\omega)$ in Fig. 1.

The $B(\omega)$ for $\omega < 1$ are not shown in Fig. 1. We shall assume that for $\omega < 1$, a slope of -6 db/octave (with 27db at $\omega=1$, i.e. 33 db at $\omega=.5$, 39db at $\omega=.25$ etc.), suffices. We can tolerate ≈-140° for $\omega \geq 1$, so we choose a lag corner frequency (symbol lacf) at $\omega=1$ (i.e. pole at -1), and set $|L_0(j\omega)|$ (asymptotic) at 30 db (to allow for the -3db correction). Thus our L_0 is so far: $L_{01} = 31.6/s(s+1)$, whose phase $\underline{/L_{01}(j\omega)}$ is sketched in Fig. 2.

$\angle L_{01}(j\omega)$ violates the -140° bound at $\omega>1.2$, so a lead corner frequency (symbol lecf) is needed. Where should it be located? At $\omega=5$, $\angle L_{01}(j5)=-169°$ (see Fig. 2), so 29° lead is needed; but we know that later there will be a second lacf, so allow say additional 15° for it giving 15+29=45° lead required at $\omega=5$; which is achieved by a lecf at $\omega=5$ i.e. a zero at -5. The resulting $L_{02}(s)=\frac{31.6(1+\frac{s}{5})}{s(1+s)}$, whose phase $\angle L_{02}(j\omega)$ is sketched in Fig. 2.

In the Nichols Chart (N.C.) we are ($\simeq\omega=10$ or so) in the region where the maximum phase lag allowed is 135° (i.e. $\angle L_0(j\omega)$ must be $\gtrsim -135°$). Consider $\omega=10$, with present $\angle L_{02}(j\omega) = -112°$, so 135°-112°=23° more lag is allowed. But this lacf will be followed by a lecf, so allow say 10° for it, giving 23°+10°=33° more lag allowable. This locates the lacf at 15.4 (tan33°=.65, and 10/.65=15.4), so we set the lacf at $\omega=15$ (i.e. pole at -15), giving $L_{03}(s)=\frac{31.6(1+.2s)}{s(1+s)(1+\frac{s}{15})}$. $\angle L_{03}(j\omega)$ is sketched in Fig. 2.

Looking ahead at $\omega=40$, $|L_{03}(j40)| \simeq -20$db, so soon $L_0(j\omega)$ can make its asymptotic left turn under the B_h boundary. Our plan is to add two more lecfs, and finally two complex pole pairs, in order to have an excess e_L of poles over zeros of 4. We try one lecf at $\omega=40$, giving $L_{04}(s)=\frac{31.6(1+.2s)\ (1+\frac{s}{40})}{s(1+s)\ (1+\frac{s}{15})}$. $\angle L_{04}(j\omega)$ is sketched in Fig. 2.

We're ready now for the last lecf, in order to achieve (an asymptotic) horizontal segment for $|L_0(j\omega)|$, before the final -24db/octave slope. (We follow Bode in this respect, a good master to follow.) Where should this horizontal segment be located? The bottom of B_h (see Fig. 1) is at -22.5db. Allow 2db margin, 3db correction due to the last lecf, 1.5db for the effect of the lecf at $\omega=40$, giving a total of -(22.5+2+3+1.5)=-29db. We'll use a damping factor of $\zeta=.6$ for the 2 complex pole pairs, so no

correction need be allowed for them. Thus the final break for $|L_0(j\omega)|$ asymptotic is to be at -29db, which $|L_{04}(j\omega)|$ achieves at ω=60. Hence, the last lecf is at ω=60. The resulting phase due to L_{04} and the lecf at ω=60, is -66°. We could have -180° at this point, but we'll allow an additional 15° margin (a matter of taste; it depends on the problem -- presence of higher order modes, etc). This means 100° phase lag is permitted, 50° due to each complex pole pair (180-66-15≈100). For ζ=.6, this locates them at 100. Thus $L_0(s) = \dfrac{31.6(1+.2s)(1+\frac{s}{40})(1+\frac{s}{60})}{s(1+s)(1+\frac{s}{15})[1+\frac{(1.2)}{100}s+\frac{s^2}{10}4]^2}$.

Discussion

$L_0(j\omega)$ is sketched in Fig. 1. A well-designed, i.e. "economical" $L_0(j\omega)$ is close to its boundary $B(\omega)$ at each ω. The vertical line -140° is the dominating $B(\omega)$ for $\omega<5$ and the right side of B_h (line -135°) is the boundary effectively for $5\lesssim\omega\lesssim30$; so our $L_0(j\omega)$ is pretty good in this respect since it is pretty close to these boundaries. There is tradeoff between complexity of $L_0(s)$ (number of its poles and zeros) and its final cut-off frequency, now at ω=100. There is some phase to spare between $L_0(j\omega)$ and the boundaries. so use of more poles and zeros in $L_0(s)$ would permit this cut-off frequency to be reduced a bit below 100, but not by much. On the other hand, if we want to reduce the number of poles and zeros of $L_0(s)$, we must pay the price in a larger cut-off frequency. We could economize significantly, of course, by allowing more phase lag in the low frequency range. If -180° was permitted at ω=1, we could decrease $|L_0(j\omega)|$ at a rate of 12db/octave; so with $|L_0|$= 25db at ω=1, it would be 13db at ω=2 (instead of the present 18db). Even with no more saving, this 5db difference, would allow a cut-off frequency at about 70 instead of 100.

Also, Fig. 1 reveals (immediately, without any shaping of L_0 required) that reduction (i.e. easing) of the specifications at $\omega=1$ to about 21db (instead of ≈26db), would have the same effect as the above. One can check how badly the specifications are compromised by such easing. The design technique is thus highly "transparent" in revealing the trade-offs between performance tolerances, complexity of the compensation, stability margins, and the "cost of feedback" in bandwidth.

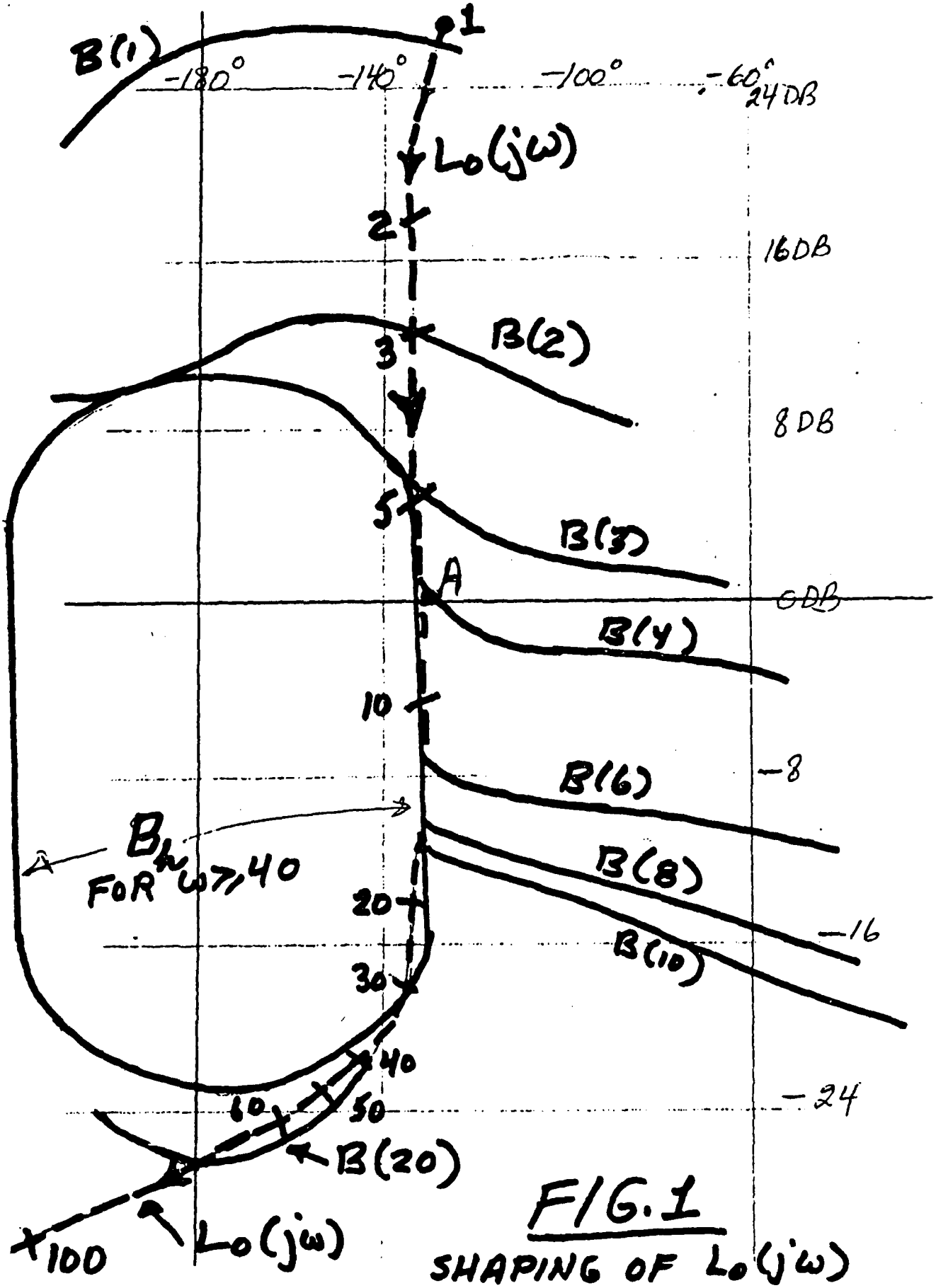

FIG. 1

SHAPING OF $L_o(j\omega)$ ON NICHOLS CHART.

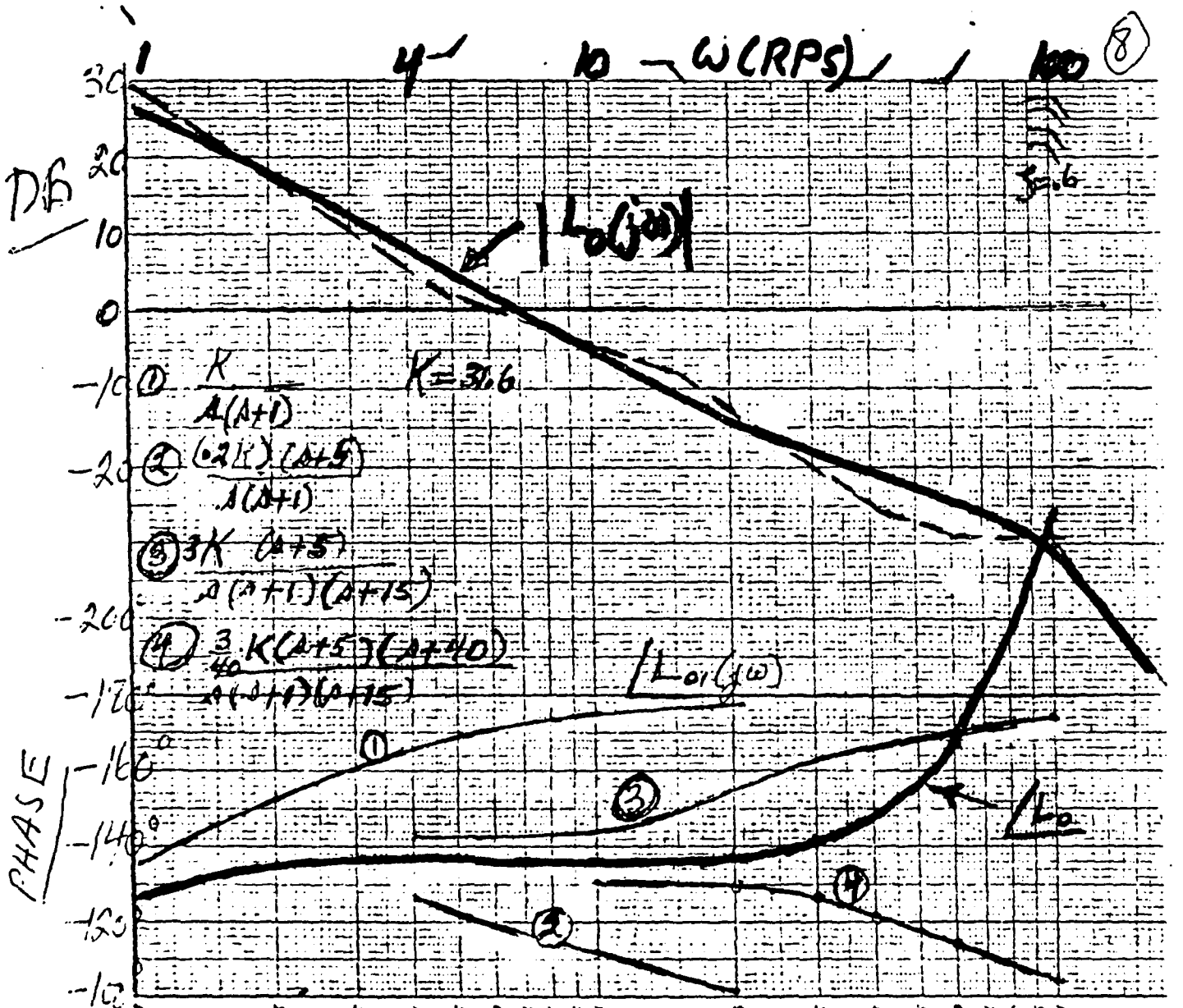

F16.2 SHAPING OF $L(j\omega)$ ON BODE PLOT.

DESIGN EXAMPLE: Uncertain Plant $P=\frac{k}{s(s+p)}$

k: [10,80], p: [-2,2].

Note: For part of range of p, plant is unstable.

Note: for $\omega=0$, plant template has infinite amplitude

Specifications on $|T(j\omega)|$. (see Fig. A)

ω	0	.5	1	2	5	10
MAX(DB)	0	1.3	1	-6	-17	-33
MIN(DB)	0	-2	-7	-19	-35	-65
$(\Delta\|T\|)$MAX	0	3.3	8	13	18	32

EXCESS e_L OF POLES OVER ZEROS OF L, IS 3.

ALSO $\left|\frac{L}{1+L}\right| \leq 3$DB, FOR ALL ω&P.

N.B. At high ω, $(\Delta|T|)$MAX MUST BE > $|\Delta P|$MAX. OK.

Step 1 Calculation and Construction of Plant Templates $\{P(j\omega)\}$=

The templates are shown in Fig. B_1. It suffices to calculate (at a fixed ω) several values of $1/j\omega(j\omega+p)$, i.e. at different p values. This gives the bottom curve of the template. Then extend vertically by 18db(80/10=8; 20log8=18).

Step 2 Use the procedure described in the notes (p.17 etc) to find bounds on $L_0(j\omega)$ in order to satisfy the specifications on $|T(j\omega)|$. A nominal plant must be chosen; p=2, k=1 was chosen as nominal and marked heavily in Fig. B_2. (It helps to have the templates on transparent paper or plastic.) Already at ω=1, the bound on $L_0(j)$, denoted by B(1) is determined by $|L/(1+L)| \leq 3$DB, rather than by the constraints on $|T(j\omega)|$. And this is so for $\omega>1$ also, which is not typical for stable plants but more likely for plants which can be open-loop unstable for part of the parameter range.

Shaping of $L_0(j\omega)$

The boundary at $\omega=2$ dominates, i.e. determines the level of $|L_0|$ at $\omega=2$ to be $\simeq$10db. The boundary at $\omega=5$ determines the phase there to be $\simeq$-85°or so. This necessitates a lead corner frequency at some $\omega<5$. This was chosen to be at 1 and lags introduced thereafter such that at $\omega=5$ the phase > -85°; they were chosen at 5 and 8 (see Figs. B_2,C). A lecf is then needed to be followed by a complex pole pair with $\zeta=0.6$. The corner below the high-frequency bound can be turned when $|L|$ is $\simeq$ -25db. If we try a lecf at 40, then phase requirements at $\omega=20$ force the final cut-off frequency to be well beyond the ω value at which $|L_0|$ =-25db. A lecf at $\omega=25$ gives compatibility of phase needs at $\omega=20$ and turning the corner when $|L_0|$ permits it. This gives 100 as the frequency at which the final complex pole pair can be inserted. This gives $L_0(s)=\dfrac{\hat{\kappa}(1+s)(1+\frac{s}{25})}{s(1+.2s)(1+\frac{s}{8})[1+\frac{1.2s}{100}+(\frac{s}{100})^2]}$

$=GP. = \dfrac{G(s)}{s(s+2)}$, giving G(s), -- see Figs. B_2, C.

Finding F(s)

The proper G guarantees that $\Delta|T|$ does not exceed those allowed. The next step is to find the range of $|L(j\omega)/(1+L(j\omega)|$. Place the template of the plant at $\omega=5$ (for example) on the point $L_0(j5)$ in the Nichols Chart, i.e. on 5db /-82° and it is seen that $|L/(1+L)|$ max$\simeq$ 2.4db, min -1.7db. But the specifications require $|T|=|FL/(1+L)|\varepsilon[-35, -17]$ db. Therefore, it is required that: $-33.3db<|F|\leq-19.4db$. In this way we obtain the bounds on$|F(j\omega)|$ shown in Fig. D. It is easy to find an F(s) which satisfies these bounds, e.g. $F(s) = \dfrac{1}{(s+1)(1+\frac{s}{1.5})(1+\frac{s}{10})}$.

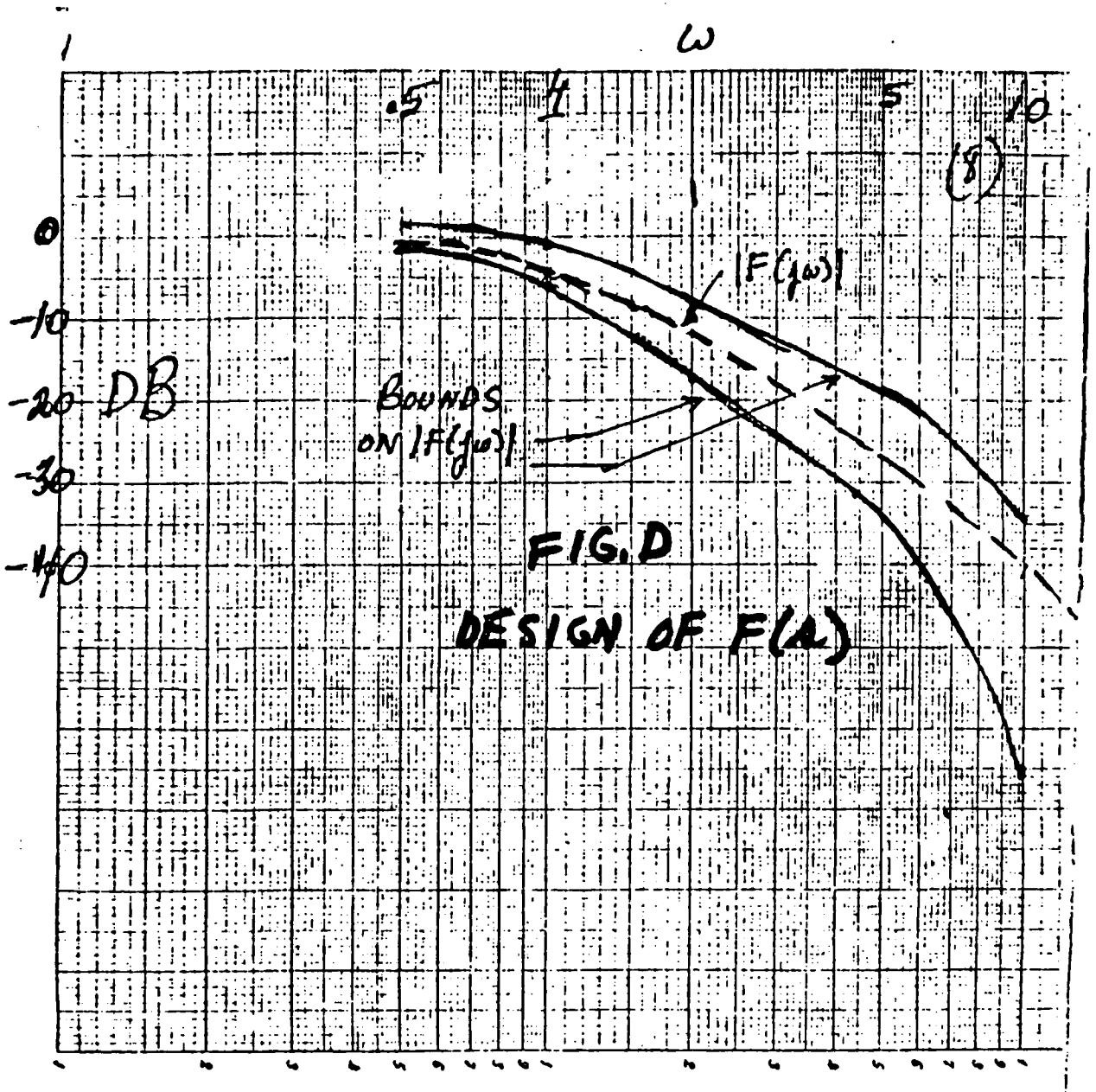

FIG. D

DESIGN OF F(s)

PLANT TEMPLATES- (NICHOLS CHART)

$P = \frac{k}{s(s+p)}$

FIG. B_1

k : 10 to 80

p : -2 to $+2$

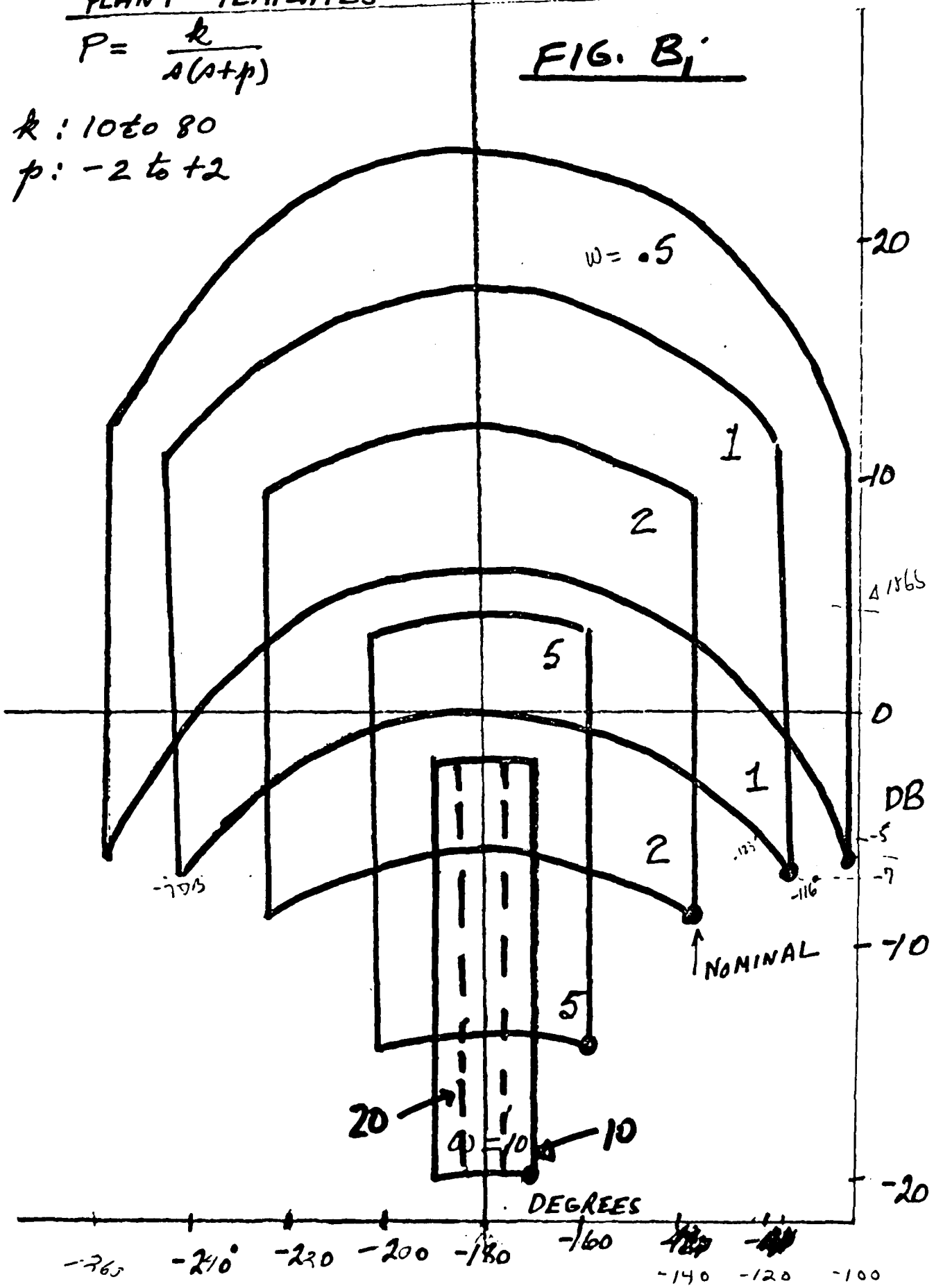

FIG. B.2

SHAPING OF $L_0(j\omega)$ TO SATISFY BOUNDS ON $L_0(j\omega)$

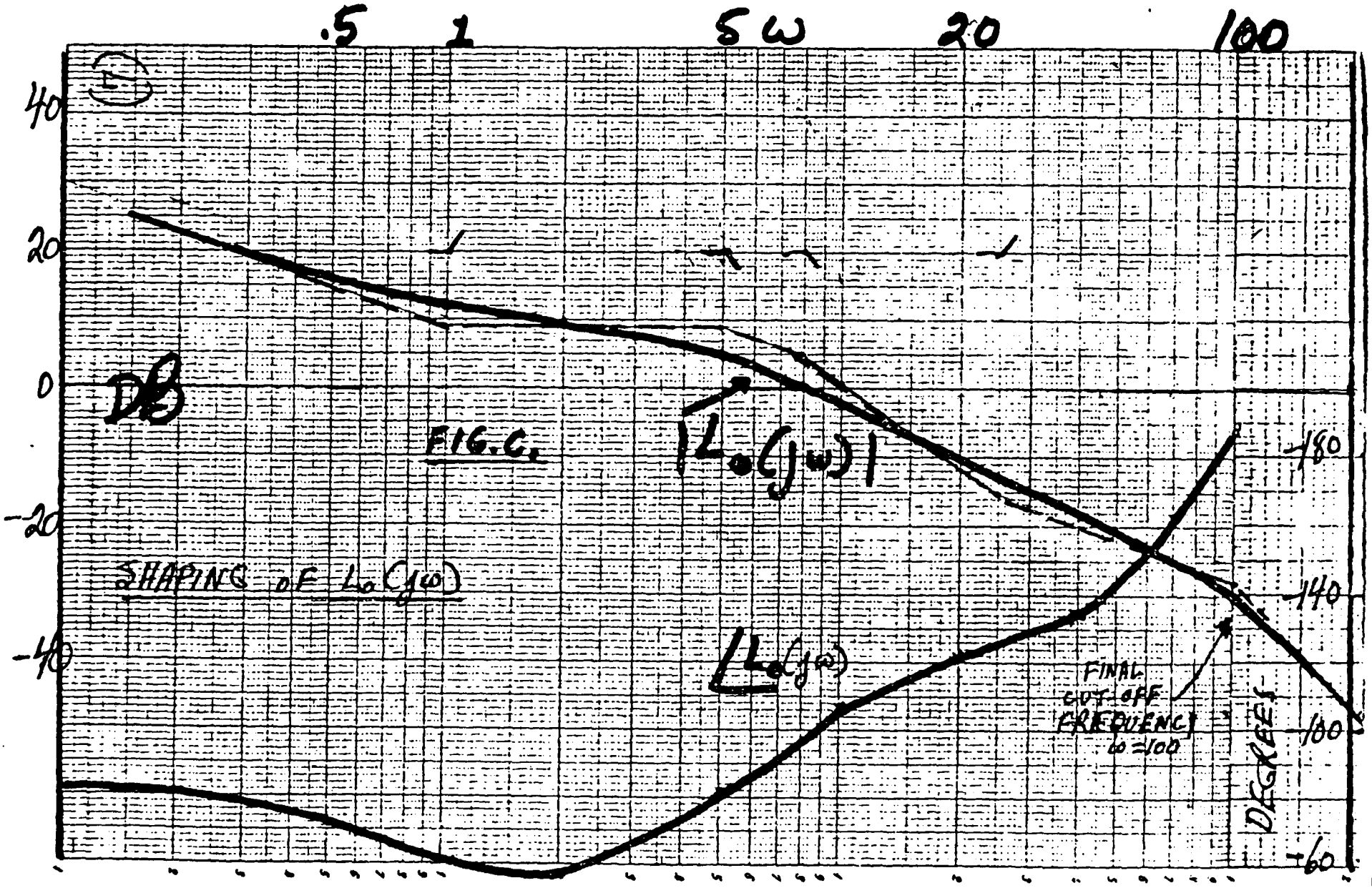
.5
1
5
ω
20
100
40
20
0
-20
-40
DB
-180
-140
-100
-60
DEGREES
FIG. C.
SHAPING OF $L_o(j\omega)$
$|L_o(j\omega)|$
$L_o(j\omega)$
FINAL CUT OFF FREQUENCY $\omega = 100$

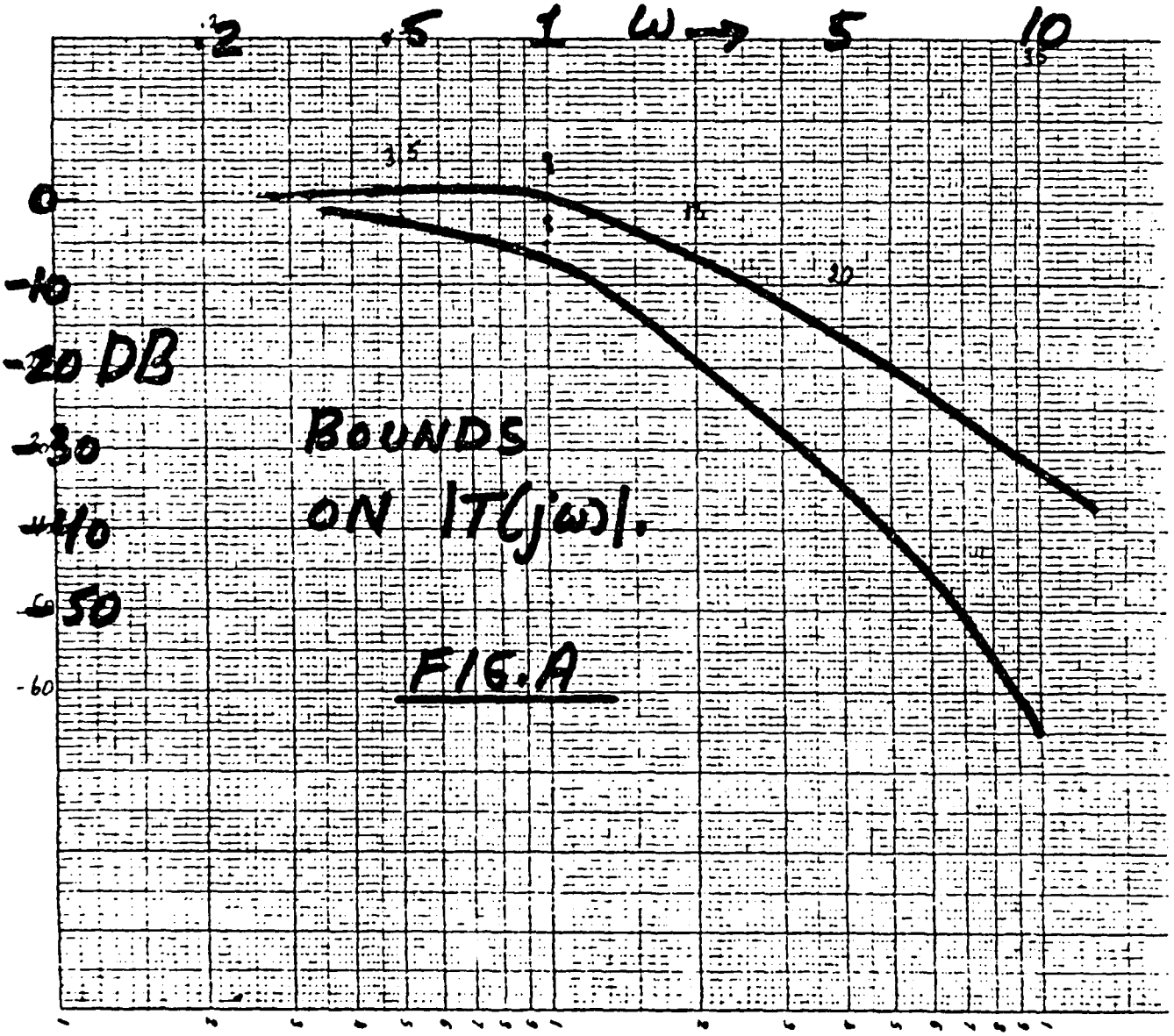

FIG. A

Appendix B

Longitudinal State Space Data

Introduction

The linear perturbation state space model describing the AFTI/F-16 was developed by A. Finley Barfield. The synthesis of the model and the aerodynamic data for the aircraft are provided in Chapter 2 and Appendices A and B of reference 2.

Definition of the State Space Model

The linear perturbation state space model used to describe the AFTI is of the form:

$$\dot{\mathbf{x}} = \mathbf{A}\mathbf{x} + \mathbf{B}\mathbf{u} \tag{B-1}$$

$$\mathbf{y} = \mathbf{C}\mathbf{x} \tag{B-2}$$

where the longitudinal state vector **x**, defined in Chapter IV, is given by:

$$\mathbf{x} = \begin{bmatrix} \alpha \\ \theta \\ u \\ A_{nps} + k_1\delta_e + k_2\delta_f \\ q \\ \delta_e \\ \delta_f \end{bmatrix} \tag{B-3}$$

and the output state vector **y** and the input state vector **u** are given by:

$$\mathbf{y} = \begin{bmatrix} A_{nps} \\ q \end{bmatrix} \qquad \mathbf{u} = \begin{bmatrix} \delta_{ecmd} \\ \delta_{fcmd} \end{bmatrix} \tag{B-4}$$

The constants k_1 and k_2 of **x** and the state space data for the matrices **A**, **B**, and **C**, are given on the following pages for each flight condition. Recall that the control inputs δ_{ecmd} and δ_{fcmd} refer to the actuator input signals in this and following appendices.

Table B-1. State Space Data for Case 1: 0.6 Mach; 30,000 Feet

A Matrix Data:

0.0	-4.418E-3	-1.035E-3	-2.779	9.925E-1	-6.615E-2	-1.117E-1
0.0	0.0	0.0	0.0	1.0	0.0	0.0
0.0	-5.601E-1	-9.114E-3	2.123	-8.495E-2	5.533E-2	-3.660E-2
0.0	-1.885E-3	-1.390E-4	-5.448E-1	1.869E-1	-2.640E-3	-2.064E-2
0.0	2.812E-4	-4.429E-2	1.334E+1	-3.196E-1	-5.862	-2.116E-1
0.0	0.0	0.0	0.0	0.0	-2.000E+1	0.0
0.0	0.0	0.0	0.0	0.0	0.0	-2.000E+1

B Matrix Data:

0.0	0.0
0.0	0.0
0.0	0.0
0.0	0.0
0.0	0.0
2.0E+1	0.0
0.0	2.0E+1

C Matrix Data:

0.0	0.0	0.0	1.0	0.0	-2.29207E-2	3.45517E-2
0.0	0.0	0.0	0.0	1.0	0.0	0.0

k_1 = 2.29207E-2

k_2 = -3.45547E-2

Table B-2. State Space Data for Case 2: 0.9 Mach; 20,000 Feet

A Matrix Data:

0.0	-1.123E-3	-1.596E-4	-1.896	9.886E-1	-1.492E-1	-2.449E-1
0.0	0.0	0.0	0.0	1.0	0.0	0.0
0.0	-5.617E-1	-1.258E-2	8.522E-1	-5.232E-1	3.492E-2	4.030E-2
0.0	-1.211E-3	-9.782E-5	-1.502	7.764E-1	-3.891E-2	-1.706E-1
0.0	3.213E-4	-1.068E-2	5.455	-7.595E-1	-2.406E+1	-6.473
0.0	0.0	0.0	0.0	0.0	-2.00E+1	0.0
0.0	0.0	0.0	0.0	0.0	0.0	-2.000E+1

B Mat. x Data:

0.0	0.0
0.0	0.0
0.0	0.0
0.0	0.0
0.0	0.0
2.0E+1	0.0
0.0	2.0E+1

C Matrix Data:

0.0	0.0	0.0	1.0	0.0	-1.064E-1	7.496E-2
0.0	0.0	0.0	0.0	1.0	0.0	0.0

k_1 = 1.064E-1

k_2 = -7.496E-2

Table B-3. State Space Data for Case 3: 1.6 Mach; 30,000 Feet

A Matrix Data:

0.0	-5.944E-4	6.413E-4	-1.672	9.973E-1	-1.153E-2	-7.509E-2
0.0	0.0	0.0	0.0	1.0	0.0	0.0
0.0	-5.617E-1	-3.054E-2	1.054	-8.126E-1	1.641E-1	-2.321E-1
0.0	-7.057E-4	5.240E-4	-1.297	7.455E-1	-1.125E-1	-6.093E-2
0.0	-1.087E-4	7.318E-2	-5.855E+1	-3.050E+1	-3.289E+1	-5.850
0.0	0.0	0.0	0.0	0.0	-2.000E+1	0.0
0.0	0.0	0.0	0.0	0.0	0.0	-2.000E+1

B Matrix Data:

0.0	0.0
0.0	0.0
0.0	0.0
0.0	0.0
0.0	0.0
2.0E+1	0.0
0.0	2.0E+1

C Matrix Data:

0.0	0.0	0.0	0.0	1.0	0.0	-1.49182E-1	2.0547E-2
0.0	0.0	0.0	0.0	0.0	1.0	0.0	0.0

$k_1 = 1.49182E-1$

$k_2 = -2.0547E-2$

Appendix C

Plant Tranfer Functions

Introduction

The plant transfer functions relating the output variables to the input variables are obtained from the state space model using Equation (III-7), repeated below.

$$\mathbf{P} = \mathbf{C}[s\mathbf{I} - \mathbf{A}]^{-1}\mathbf{B} \qquad \text{(C-1)}$$

The input/output transfer function relationships are written in matrix form as:

$$\mathbf{y} = \mathbf{P}\mathbf{u} \qquad \text{(C-2)}$$

In terms of the various matrix elements, this relationship is written as:

$$\begin{bmatrix} A_{nps} \\ q \end{bmatrix} = \begin{bmatrix} p_{11} & p_{12} \\ p_{21} & p_{22} \end{bmatrix} \begin{bmatrix} \delta_{ecmd} \\ \delta_{fcmd} \end{bmatrix} \qquad \text{(C-3)}$$

where:

$$p_{11} = \frac{[\ A_{nps}\ ]}{[\ \delta_{ecmd}\ ]} \qquad p_{12} = \frac{[\ A_{nps}\ ]}{[\ \delta_{fcmd}\ ]}$$

$$p_{21} = \frac{[\ q\ ]}{[\ \delta_{ecmd}\ ]} \qquad p_{22} = \frac{[\ q\ ]}{[\ \delta_{fcmd}\ ]} \qquad \text{(C-4)}$$

The plant transfer function matrix, **P**, is obtained for each flight condition using a computer program. The **P** matrices are tested to determine if the constraints on the two-by-two system are met. Recall from Chapter III, the two conditions are:

1. **P** must not be singular for any possible combination of plant parameters, i.e. $\mathbf{P}^{-1}$ must exist.
2. As $s \longrightarrow \infty$, $|p_{11}p_{22}| > |p_{12}p_{21}|$ for all possible plants.

The transfer functions and the results of the constraint tests are given on the following pages for the three flight conditions of this study.

Case 1: 0.6 Mach; 30,000 Feet

$$p_{11}(s) = \frac{-0.458414(s + 0.006431)(s - 0.006991)(s + 4946 \pm j6.7265)}{(s + 0.006473 \pm j0.07802)(s - 1.167)(s + 2.0276)(s + 20)}$$

$$p_{12}(s) = \frac{0.691034(s + 0.0006424 \pm j0.006178)(s + 2.0645)(s - 1.7871)}{(s + 0.006473 \pm j0.07802)(s - 1.167)(s + 2.0276)(s + 20)}$$

(C-5)

$$p_{21}(s) = \frac{-117.24(s)(s + 0.010028)(s + 0.5503)}{(s + 0.006473 \pm j0.07802)(s - 1.167)(s + 2.0276)(s + 20)}$$

$$p_{22}(s) = \frac{-4.232(s)(s + 0.001887)(s + 1.8456)}{(s + 0.006473 \pm j0.07802)(s - 1.167)(s + 2.0276)(s + 20)}$$

The results of testing **P** against the constraints for Case 1 are:

1. **P** is non-singular.
2. As $s \longrightarrow \infty$, $|p_{11}p_{22}| > |p_{12}p_{21}|$ becomes: $1.94 > 81.016$

Constraint 2 is not met for Case 1.

Case 2: 0.9 Mach; 20,000 Feet

$$p_{11}(s) = \frac{-2.128(s + 0.012228)(s - 0.001170)(s + 1.3144 \pm j13.07744)}{(s + 0.0075694 \pm j0.0540)(s - 0.96451)(s + 3.2234)(s + 20)}$$

$$p_{12}(s) = \frac{1.4992(s + 0.0122185)(s - 0.00113786)(s - 8.48425)(s + 8.4714)}{(s + 0.0075694 \pm j0.0540)(s - 0.96451)(s + 3.2234)(s + 20)}$$

(C-6)

$$p_{21}(s) = \frac{-481.2(s)(s + 0.012642)(s + 1.510776)}{(s + 0.0075694 \pm j0.0540)(s - 0.96451)(s + 3.2234)(s + 20)}$$

$$p_{22}(s) = \frac{-129.46(s)(s + 0.012548)(s + 1.64587)}{(s + 0.0075694 \pm j0.0540)(s - 0.96451)(s + 3.2234)(s + 20)}$$

The results of testing **P** against the constraints for Case 2 are:

1. **P** is non-singular.
2. As $s \longrightarrow \infty$, $|p_{11}p_{22}| > |p_{12}p_{21}|$ becomes: $275.5 > 721.4$

Constraint 2 is not met for Case 2.

Case 3: 1.6 Mach; 30,000 Feet

$$p_{11}(s) = \frac{-2.9836(s - 0.0005956)(s + 0.02983)(s + 1.1787 \pm j14.398)}{(s + 0.01517 \pm j0.02368)(s + 0.8011 \pm j6.5925)(s + 20)}$$

$$p_{12}(s) = \frac{0.61094(s - 0.00060805)(s + 0.033987)(s + 12.337)(s - 13.7033)}{(s + 0.01517 \pm j0.02368)(s + 0.8011 \pm j6.5925)(s + 20)}$$

(C-7)

$$p_{21}(s) = \frac{-657.8(s)(s + 0.029979)(s + 1.096926)}{(s + 0.01517 \pm j0.02368)(s + 0.8011 \pm j6.5925)(s + 20)}$$

$$p_{22}(s) = \frac{-117.0(s)(s + 0.034674)(s + 0.68595)}{(s + 0.01517 \pm j0.02368)(s + 0.8011 \pm j6.5925)(s + 20)}$$

The results of testing **P** against the constraints for Case 3 are:

1. **P** is non-singular.
2. As $s \longrightarrow \infty$, $|p_{11}p_{22}| > |p_{12}p_{21}|$ becomes: $349.1 > 401.9$

Constraint 2 is not met for Case 3.

Appendix D

Rearrange the Output Vector to Meet Constraints

Introduction

The constraints on the **P** matrix must be met in order to apply the Quantitative Synthesis Technique (see Chapter III). If the constraints are met, the MIMO systen can be broken into a set of equivalent MISO systems.

Rearrange the Output Vector

Constraint 2 was not met for all three flight conditions as shown in Appendix C. Chapter V described the method to rearrange the elements of the output vector, **y**, in order to meet Constraint 2. The modified relationship between the input and output variables is repeated below where **y = Pu**:

$$\begin{bmatrix} q \\ A_{nps} \end{bmatrix} = \begin{bmatrix} p_{11} & p_{12} \\ p_{21} & p_{22} \end{bmatrix} \begin{bmatrix} \delta_{ecmd} \\ \delta_{fcmd} \end{bmatrix} \tag{D-1}$$

The output vector, **y**, is redefined as:

$$\mathbf{y} = \begin{bmatrix} q \\ A_{nps} \end{bmatrix} \tag{D-2}$$

and the **P** matrix elements are given by:

$$p_{11} = \frac{[\ q\ ]}{[\ \delta_{ecmd}\ ]} \qquad p_{12} = \frac{[\ q\ ]}{[\ \delta_{fcmd}\ ]}$$

$$p_{21} = \frac{[\ A_{nps}\ ]}{[\ \delta_{ecmd}\ ]} \qquad p_{22} = \frac{[\ A_{nps}\ ]}{[\ \delta_{fcmd}\ ]} \tag{D-3}$$

As described in Chapter V, the affect of rearranging the output vector on the **P** matrix elements, $p_{ij,}$ is easily observed by simply changing the subscripts of the p_{ij} elements from

the old set to the new set as shown in Table V-1 and repeated in Table D-1 below for convenience.

Table D-1. Plant Transfer Function Subscript Change

Subscript Value		
OLD	——›	NEW
11		21
12		22
21		11
22		12

The transfer functions obtained after performing the transformations on the output vector are given on the following pages for each flight condition. The constraints on the **P** matrix are checked again for the revised set of transfer functions.

Case 1: 0.6 Mach; 30,000 Feet

$$p_{11}(s) = \frac{-117.24(s)(s + 0.010028)(s + 0.5503)}{(s + 0.006473 \pm j0.07802)(s - 1.167)(s + 2.0276)(s + 20)}$$

$$p_{12}(s) = \frac{-4.232(s)(s + 0.00187)(s + 1.8456)}{(s + 0.006473 \pm j0.07802)(s - 1.167)(s + 2.0276)(s + 20)} \qquad \text{(D-4)}$$

$$p_{21}(s) = \frac{-0.458414(s + 0.006431)(s - 0.006991)(s + 0.4946 \pm j6.7265)}{(s + 0.006473 \pm j0.07802)(s - 1.167)(s + 2.0276)(s + 20)}$$

$$p_{22}(s) = \frac{0.691034(s + 0.006424 \pm j0.006178)(s + 2.0645)(s - 1.7871)}{(s + 0.006473 \pm j0.07802)(s - 1.167)(s + 2.0276)(s + 20)}$$

The results of testing **P** against the constraints for Case 1 are:

1. **P** is non-singular.
2. As $s \longrightarrow \infty$, $|p_{11}p_{22}| > |p_{12}p_{21}|$ becomes: $81.0 > 1.94$

Both constraints are met for Case 1.

Case 2: 0.9 Mach; 20,000 Feet

$$p_{11}(s) = \frac{-481.2(s)(s + 0.012642)(s + 1.510776)}{(s + 0.0075694 \pm j0.0540)(s - 0.96451)(s + 3.2234)(s + 20)}$$

$$p_{12}(s) = \frac{-129.46(s)(s + 0.012548)(s + 1.64587)}{(s + 0.0075694 \pm j0.0540)(s - 0.96451)(s + 3.2234)(s + 20)}$$

$$p_{21}(s) = \frac{-2.128(s + 0.012228)(s - 0.001170)(s + 1.3144 \pm j13.07744)}{(s + 0.0075694 \pm j0.0540)(s - 0.96451)(s + 3.2234)(s + 20)} \quad \text{(D-5)}$$

$$p_{22}(s) = \frac{1.4992(s + 0.0122185)(s - 0.00113786)(s - 8.48425)(s + 8.4714)}{(s + 0.0075694 \pm j0.0540)(s - 0.96451)(s + 3.2234)(s + 20)}$$

The results of testing **P** against the constraints for Case 2 are:

1. **P** is non-singular.
2. As $s \longrightarrow \infty$, $|p_{11}p_{22}| > |p_{12}p_{21}|$ becomes: $721.4 > 275.5$

Both constraints are met for Case 2.

Case 3: 1.6 Mach; 30,000 Feet

$$p_{11}(s) = \frac{-657.8(s)(s + 0.029979)(s + 1.096926)}{(s + 0.01517 \pm j0.02368)(s + 0.8011 \pm j6.5925)(s + 20)}$$

$$p_{12}(s) = \frac{-117.0(s)(s + 0.034674)(s + 0.68595)}{(s + 0.01517 \pm j0.02368)(s + 0.8011 \pm j6.5925)(s + 20)}$$

$$p_{21}(s) = \frac{-2.9836(s - 0.0005956)(s + 0.02983)(s + 1.1787 \pm j14.398)}{(s + 0.01517 \pm j0.02368)(s + 0.8011 \pm j6.5925)(s + 20)} \quad \text{(D-6)}$$

$$p_{22}(s) = \frac{0.61094(s - 0.00060805)(s + 0.033987)(s + 12.337)(s - 13.7033)}{(s + 0.01517 \pm j0.02368)(s + 0.8011 \pm j6.5925)(s + 20)}$$

The results of testing **P** against the constraints for Case 3 are:

1. **P** is non-singular.
2. As $s \rightarrow \infty$, $|p_{11}p_{22}| > |p_{12}p_{21}|$ becomes: $401.9 > 349.1$

Both constraints are met for Case 3.

Appendix E

Derivation of the Q Matrix

Introduction

The MIMO system can be broken into an equivalent set of MISO systems as stated in Chapter III with a corresponding proof and derivation in reference 9. The equivalent MISO set is obtained from the reciprocal of the elements on the inverse plant matrix.

The Q Matrix

The equivalent MISO set of transfer functions describing the MIMO system are obtained form the P-1 matrix. This set, in matrix form, is defined as:

$$\mathbf{Q} = \begin{bmatrix} q_{11} & q_{12} \\ q_{21} & q_{22} \end{bmatrix} \tag{E-1}$$

where:

$$q_{ijk} = \frac{\det [\mathbf{P}]}{\mathrm{Adj}[p_{ij}]}, \quad k = \text{flight condition} \tag{E-2}$$

Note the elements of **Q** are the reciprocals of the $\mathbf{P}^{-1}$ matrix.

A computer program is used to obtain the q_{ij}'s for each flight condition. The sets of q_{ij}'s are listed below.

Case 1: 0.6 Mach; 30,000 Feet

$$q_{111}(s) = \frac{0.707581(s + 0.00486676 \pm j0.006373737)}{(s + 0.010028)(s + 0.550313)(s + 20)}$$

$$q_{121}(s) = \frac{-180.96487(s)(s + 0.00486676 \pm j0.006373737)}{(s - 0.0069911)(s + 0.006431)(s + 0.49463 \pm j6.72646)(s + 20)} \tag{E-3}$$

$$q_{211}(s) = \frac{-19.602276(s + 0.00486676 \pm j0.006373737)}{(s + 0.00188663)(s + 1.845599)(s + 20)}$$

$$q_{221}(s) = \frac{-120.047393(s)(s + 0.00486676 \pm j0.006373737)}{(s - 0.00064239 \pm j0.0061777)(s - 1.7871)(s + 2.06449)(s + 20)} \quad \text{(E-3)}$$

Case 2: 0.9 Mach; 20,000 Feet

$$q_{112}(s) = \frac{2.07171(s + 0.0027369)(s + 0.0121827)}{(s + 0.0126422)(s + 1.510776)(s + 20)}$$

$$q_{122}(s) = \frac{-468.47082(s)(s + 0.0027369)(s + 0.0121827)}{(s - 0.00117)(s + 0.012228)(s + 1.31436 \pm j13.077)(s + 20)}$$

$$q_{212}(s) = \frac{-7.700494(s + 0.0027369)(s + 0.0121827)}{(s + 0.0125478)(s + 1.64587)(s + 20)} \quad \text{(E-4)}$$

$$q_{222}(s) = \frac{-664.9586(s)(s + 0.0027369)(s + 0.0121827)}{(s - 0.0011379)(s + 0.012219)(s - 8.48425)(s + 8.4714)(s + 20)}$$

Case 3: 1.6 Mach; 30,000 Feet

$$q_{113}(s) = \frac{0.941623(s + 0.000736492)(s + 0.02836)}{(s + 0.029979)(s + 1.09693)(s + 20)}$$

$$q_{123}(s) = \frac{-207.59833(s)(s + 0.000736492)(s + 0.02836)}{(s - 0.0005956)(s + 0.02983)(s + 1.1787 \pm j14.3981)(s + 20)}$$

$$q_{213}(s) = \frac{-5.294(s + 0.000736492)(s + 0.02836)}{(s + 0.034674)(s + 0.685947)(s + 20)} \quad \text{(E-5)}$$

$$q_{223}(s) = \frac{-1507.2923(s)(s + 0.000736492)(s + 0.02836)}{(s - 0.00060805)(s + 0.033987)(s - 13.7033)(s + 12.3371)(s + 20)}$$

Appendix F

Nominal Transfer Functions

Introduction

Loop transmission shaping is based on using a nominal q(s) transfer function. Once the loop transmission is shaped, the corresponding compensator element is obtained by dividing the loop transmission by the nominal q(s) transfer function $q_{ij0}(s)$. In this study, nominal $q_{ij0}(s)$ functions are chosen which have similar frequency response magnitude characteristics as the actual $q_{ij}(s)$ functions over the range of flight conditions. The nominal transfer functions are not required to have this property but are chosen in this manner for convenience.

The transfer functions are denoted using the notation: $q_{ijk}(s)$, where the (ij) subscripts define the element of the **Q** matrix being referred to and the (k) subscript defines the case or flight condition in question. The (k) subscripts are specified by:

k = 0 Nominal q_{ij} transfer function

k = 1 Case 1: 0.6 Mach, 30,000 feet Flight Condition

k = 2 Case 2: 0.9 Mach, 20,000 feet Flight Condition

k = 3 Case 3: 1.6 Mach, 30,000 feet Flight Condition

The $q_{ij}(s)$ transfer functions for the three flight conditions are given in Appendix E. The nominal $q_{ij0}(s)$ transfer functions chosen are shown in Equation (F-1). A Log-magnitude plot for each (ij) set of four q_{ijk}'s is provided.

Nominal $q_{ij0}(s)$ Transfer Functions:

$$q_{110}(s) = \frac{0.72(s + 0.0007)}{(s + 0.8)(s + 20)} \qquad q_{120}(s) = \frac{-122.0(s)(s + 0.0007)}{(s - 0.0006)(s + 1 \pm j11)(s + 20)}$$

(F-1)

$$q_{210}(s) = \frac{-4.7(s + 0.003)}{(s + 1)(s + 20)} \qquad q_{220}(s) = \frac{-158.0(s)(s + 0.001)(s + 0.02)}{(s - 0.0009)(s + 0.025)(s + 4)(s - 4.1)(s + 20)}$$

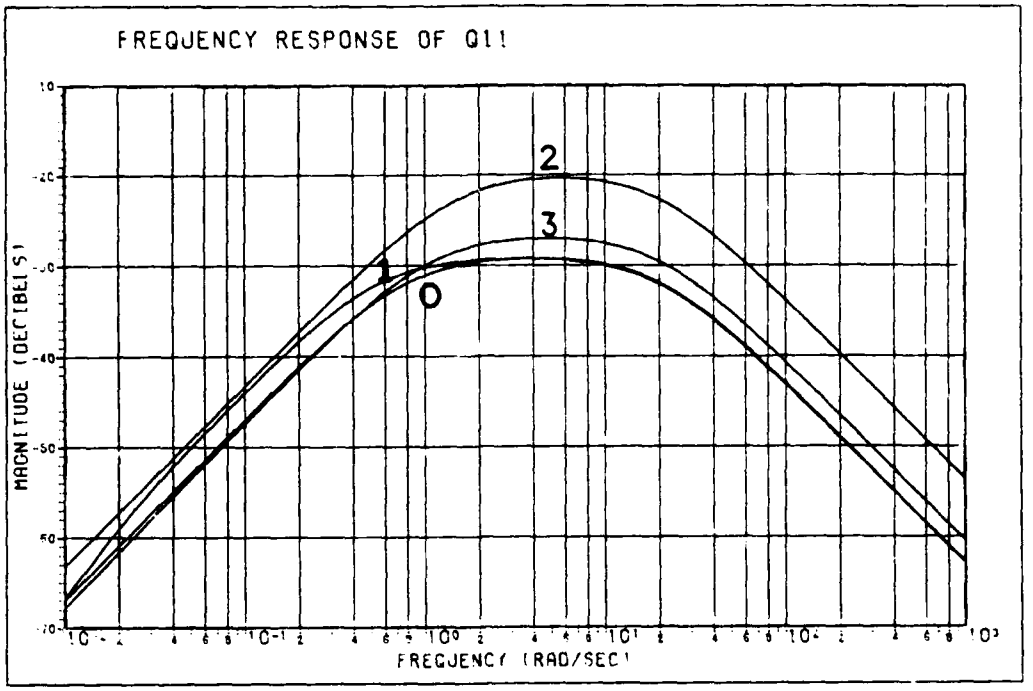

Fig. F-1. Log Magnitude Plot of $q_{11k}(j\omega)$ for k = 0, 1, 2, 3.

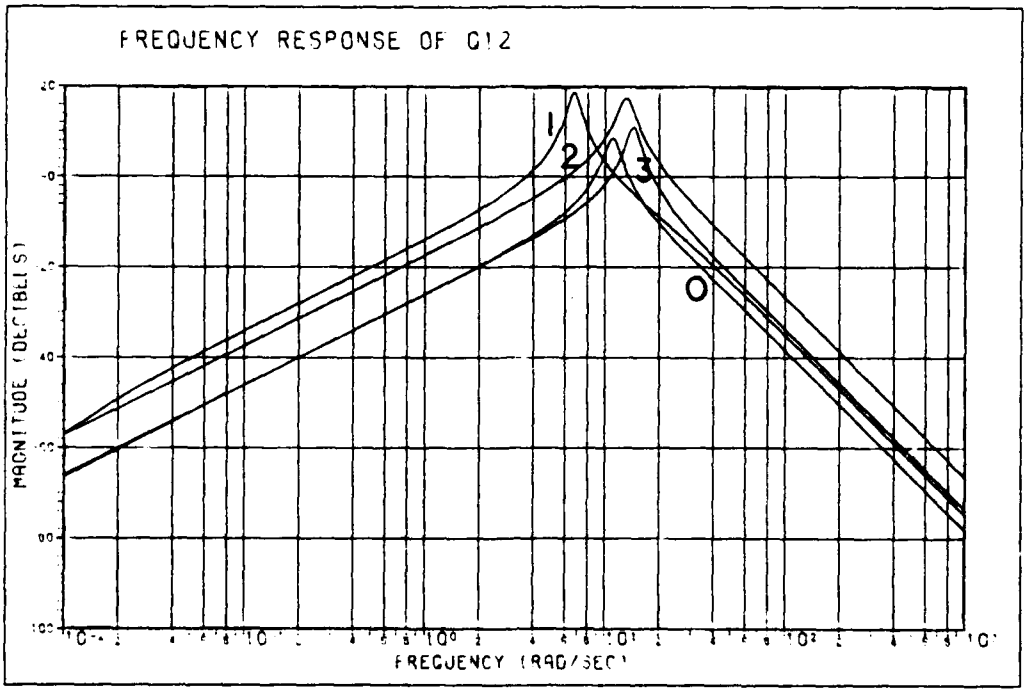

Fig. F-2. Log Magnitude Plot of $q_{12k}(j\omega)$ for k = 0, 1, 2, 3.

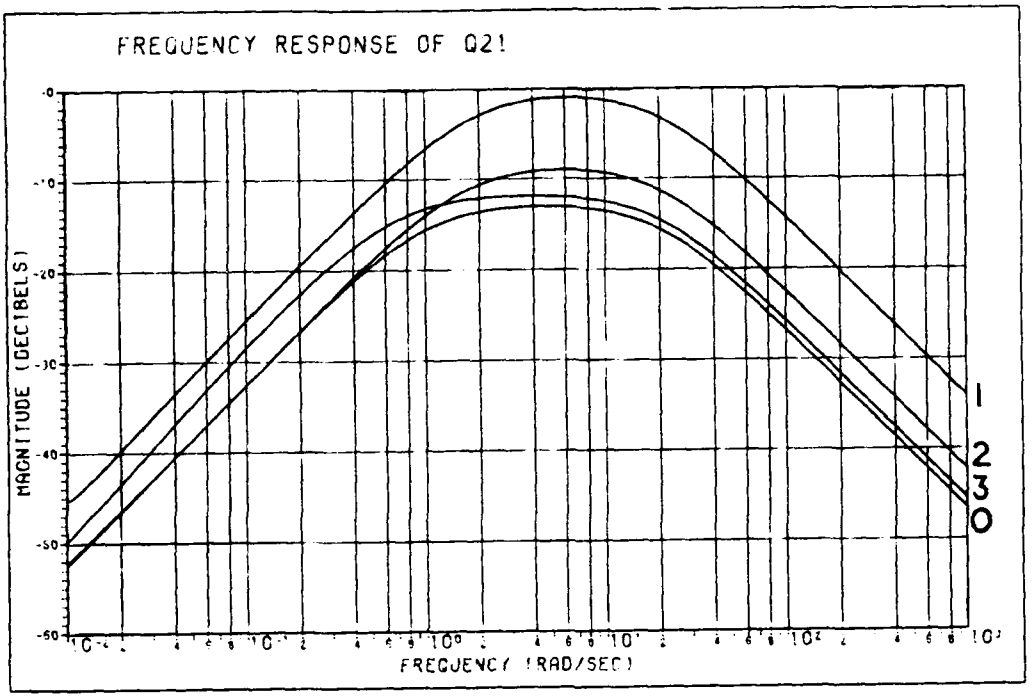

Fig. F-3. Log Magnitude Plot of $q_{21k}(j\omega)$ for k = 0, 1, 2, 3.

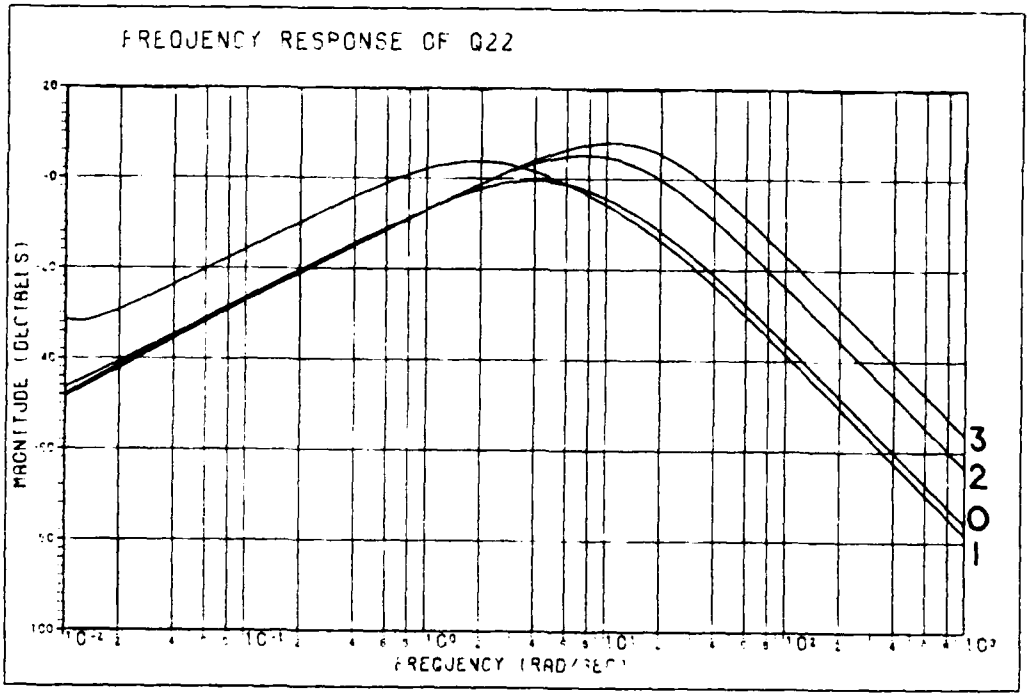

Fig. F-4. Log Magnitude Plot of $q_{22k}(j\omega)$ for k = 0, 1, 2, 3.

Appendix G

Effective Pitch Rate Loop Transfer Functions

Introduction

The improved QFT design technique (Ref 12) requires calculating an effective q equation for the final loop (two-by-two case). Recall from Equations (V-44), (V-38), and (V-39) of Chapter 5, the effective q transfer function, q*, is a function of the first (acceleration) loop design and the q_{ij} elements of the Q matrix. Equations (V-44), (V-38), and (V-39) are repeated below for convenience. In this study, q_{11}* is required for the final (pitch rate) loop design. Note the subscript (k) refers to the case or flight condition considered as defined in Appendix F.

$$q_{11k}(s)^* = \frac{q_{11k}(s)}{1 + \dfrac{-\gamma_k(s)}{1 + l_{2k}(s)}} \tag{G-1}$$

where:

$$l_{2k}(s) = g_2(s)q_{22k}(s) \tag{G-2}$$

and

$$\gamma_k(s) = \frac{q_{11k}(s)q_{22k}(s)}{q_{12k}(s)q_{21k}(s)} \tag{G-3}$$

The software program, TOTAL, is used to perform a series of transfer function manipulations to derive the $q_{11k}(s)$* transfer functions. The complexity of the derivation is reduced by simplifying the $\gamma_k(s)$ components prior to using TOTAL as follows. First, each $q_{ijk}(s)$ term is rewritten in the form:

$$q_{ijk}(s) = \frac{K_{ijk}N_{ijk}}{D_{ijk}} \tag{G-4}$$

where K_{ijk} is the transfer function constant, N_{ijk} is the numerator root term and D_{ijk} is the

denominator root term. Equation (G-3) then becomes:

$$\gamma_k(s) = \frac{\dfrac{K_{11k}N_{11k}\,K_{22k}N_{22k}}{D_{11k}\,D_{22k}}}{\dfrac{K_{12k}N_{12k}\,K_{21k}N_{21k}}{D_{12k}\,D_{21k}}} \qquad \text{(G-5)}$$

Investigating the roots of the numerator terms (see Appendix E), the following equality is observed for all flight conditions: $(s)N_{11k} = N_{22k} = N_{12k} = (s)N_{21k}$. Inserting the equality into Equation (G-5), then $\gamma_k(s)$ becomes:

$$\gamma_k(s) = \frac{\dfrac{K_{11k}N_{11k}\,K_{22k}(s)N_{11k}}{D_{11k}\,D_{22k}}}{\dfrac{K_{12k}(s)N_{11k}\,K_{21k}N_{11k}}{D_{12k}\,D_{21k}}} \qquad \text{(G-6)}$$

Cancelling the common numerator roots, $\gamma_k(s)$ is written as:

$$\gamma_k(s) = \frac{K_{11k}K_{22k}D_{12k}D_{21k}}{K_{12k}K_{21k}D_{11k}D_{22k}} \qquad \text{(G-7)}$$

Having defined $\gamma_k(s)$ as shown in Equation (G-7) greatly reduces the order of the transfer functions manipulated in TOTAL. Prior cancellation of common roots also reduces root solving errors resulting from the TOTAL root solution algorithms when operating on large order transfer functions. The effective $q_{11k}(s)^*$ transfer functions derived for each flight condition are given below as well as a Log-magnitude plot of the frequency response for the transfer functions.

Effective $q_{11k}(s)^*$ Transfer Functions

$$q_{111}(s)^* = \frac{0.691(s + 0.004936 \pm j0.006363)}{(s + 0.009915)(s + 0.551)(s + 20)} \qquad \text{(G-8)}$$

$$q_{112}(s)^* = \frac{1.499(s + 0.002898)(s + 3.692)(s + 4.582)(s + 47.57 \pm j79)}{(s + 1.511)(s + 4.017 \pm j\,0.1583)(s + 39.11 \pm j\,63.55)(s + 20)}$$

$$q_{113}(s)^* = \frac{0.4109(s + 0.000802)(s + 3.673)(s + 4.657)(s + 102.6 \pm j141)}{(s + 1.094)(s + 3.928 \pm j0.4551)(s + 20)(s + 47.14)(s + 79.15)}$$

$$q_{110}(s)^* = \frac{0.6008(s+0.0007)(s+3.995)(s+4.0)(s+15.755\pm j21.995)(s+35.736)}{(s+0.8015)(s+3.856\pm j0.4836)(s+11.9893\pm j\ 20.2778)(s+20)(s+42.021)}$$

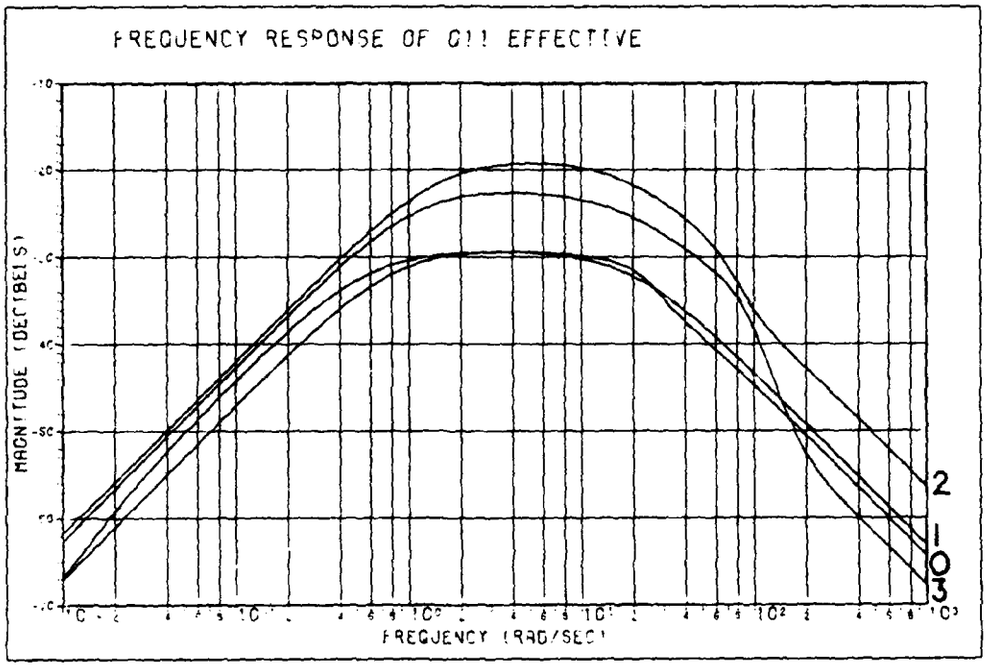

Fig. G-1. Effective $q_{11k}(s)^*$ Frequency Response

Appendix H

Maximum Acceleration Loop Transmission Bounds

Introduction

This appendix describes the numerical procedure used to obtain the maximum acceleration loop transmission bounds $B_{20}(j\omega_i)$ at each design frequency, $\omega = \omega_i$, listed in Table V-2. These bounds are the maximum design constraints used to shape the nominal loop transmission $l_{20}(j\omega)$ on the Nichols chart. Recall from Chapter V, plant templates are impractical to plot and use on the Nichols chart at most of the acceleration loop design frequencies. Therefore, the procedure described in Chapter V is used to obtain point values for $Lm[B_{20}(j\omega_i)]Ang[B_{20}(j\omega_i)]$ which can be plotted on the Nichols chart. An example of the procedure is given for $\omega_i = 8$. A math spreadsheet program is used to calculate the values for $Lm[B_{20}(j\omega_i)]$ and $Ang[B_{20}(j\omega_i)]$. The procedure below is performed for all acceleration loop design frequencies given in Table V-2. The frequency response of the various transfer functions used below are obtained using the Computer Aided Design program, TOTAL.

Numerical Bound Calculation Procedure

Equation (H-1) (Equation (V-29)) establishes the constraint on $[1 + l_{2k}(j\omega)]$.

$$|1 + g_2(j\omega)q_{22k}(j\omega)| \geq \frac{|b_{11}(j\omega)|\,|q_{22k}(j\omega)|}{|b_{21}(j\omega)|\,|q_{21k}(j\omega)|} \qquad \text{(H-1)}$$

where the acceleration loop transmission is given by:

$$l_{2k}(j\omega) = g_2(j\omega)q_{22k}(j\omega) \qquad \text{(H-2)}$$

First, the quotient on the right side of Equation (H-1) is evaluated at a design frequency, $\omega = \omega_i$, for one of the flight conditions. The result is a Log-magnitude value expressed in dB. Using the curved grid on the inverted Nichols chart, the magnitude curve corresponding to the resulting quotient is located. Taking points along the curve at small

increments, the magnitude and angle values for the bound $B_{2k}(j\omega_i)$ on $l_{2k}(j\omega)$ are read from the rectangular grid on the inverted chart. This is accomplished for all design frequencies of Table V-2 at each flight condition k. The resulting constraint on the acceleration loop transmission for a given flight condition is given by Equation (H-3).

$$l_{2k}(j\omega) \geq B_{2k}(j\omega_i) \tag{H-3}$$

For example, at $\omega_i = 8$, the constraint derived from Equation (H-1) is -5 dB for Case 1. The bound $B_{21}(j8)$ is calculated using the -5 dB curved magnitude grid of the inverted Nichols chart. Taking points along the curve at small intervals, the Log-magnitude and angle values are read from the rectangular $l_2(j\omega)$ grid (see Table H-1, Columns 1 and 2). Thus, the bound $B_{21}(j8)$ on $l_{21}(j8)$ is obtained for Case 1 via correspondence between [L] and [1 + L] on the Nichols chart. Columns 1 and 2 of Tables H-2 and H-3 give the Log-magnitude and angle values of the bounds $B_{22}(j8)$ and $B_{23}(j8)$ for Cases 2 and 3.

Recall however, the maximum constraint over the range of flight conditions is needed to obtain the bounds on the nominal loop transmission $l_{20}(j\omega)$. Using the relationship of Equation (H-2) and the known equivalent plant $q_{22k}(j\omega)$ (Appendix E), the constraint on the loop transmission can be converted to a constraint on the compensator $g_{2k}(j\omega_i)$.

$$g_{2k}(j\omega_i) \geq \frac{B_{2k}(j\omega_i)}{q_{22k}(j\omega_i)} = B_{g2k}(j\omega_i) \tag{H-4}$$

The frequency response of $q_{221}(j8)$ (q_{22} Case 1 at $\omega_i = 8$) is given in Columns 3 and 4 of Table H-1. By dividing each $B_{21}(j8)$ Log-magnitude and angle value by $Lm[q_{221}(j8)]$ $Ang[q_{221}(j8)]$, the bound $B_{g21}(j\omega_i)$ on $g_{21}(j8)$ is found for Case 1. Since the Log-magnitude values are expressed in dB and the angles in degrees, the quotient of Equation (H-4) becomes a simple subtraction, i.e. $Lm[B_{g2k}(j\omega_i)] = Lm[B_{2k}(j\omega_i)] - Lm[q_{22k}(j\omega_i)]$ and the $Ang[B_{g2k}(j\omega_i)] = Ang[B_{2k}(j\omega_i)] - Ang[q_{22k}(j\omega_i)]$. This procedure readily lends itself to the use of a math spreadsheet program. Columns 5 and 6 of Tables H-1, H-2 and H-3 show the resulting $B_{g2k}(j8)$ Log-magnitude and angle values for the three flight conditions at the design frequency, $\omega_i = 8$.

Next, the maximum constraint on $g_{2k}(j\omega_i)$ determined. By investigating the Log-magnitude values of the three $B_{g2k}(j\omega_i)$ bounds (Column 5 of Tables H-1, H-2 and H-3) at a given angle, the maximum Log-magnitude value is selected for that angle value. This selection process is repeated at each angle considered. The set of maximum Log-magnitude values selected for the set of angle values is the maximum bound $B_{g20}(j\omega_i)$ on $g_2(j\omega_i)$. For the example at $\omega_i = 8$, the $B_{g20}(j8)$ values obtained are given in Columns 1 and 2 of Table H-4.

The maximum constraint $B_{g20}(j\omega_i)$ on $g_2(j\omega_i)$ is converted to the maximum constraint $B_{20}(j\omega_i)$ on the nominal loop transmission $l_{20}(j\omega)$ by multiplying $q_{220}(j\omega_i)$ through Equation (H-3). In equation form:

$$g_2(j\omega_i)q_{220}(j\omega_i) \geq B_{20}(j\omega_i) = B_{g20}(j\omega_i)q_{220}(j\omega_i) \qquad \text{(H-5)}$$

When expressed in terms of the nominal loop transmission, Equation (H-5) becomes:

$$l_{20}(j\omega) \geq B_{20}(j\omega_i) \qquad \text{(H-6)}$$

The bound $B_{20}(j\omega_i)$ places the greatest demand on the nominal loop transmission $l_{20}(j\omega)$ at a given design frequency, $\omega = \omega_i$. Again, obtaining $B_{20}(j\omega_i)$ from Equation (H-5) is a point by point process involving simple addition, i.e.: $Lm[B_{20}(j\omega_i)] = Lm[B_{g20}(j\omega_i)] + Lm[q_{220}(j\omega_i)]$ and $Ang[B_{20}(j\omega_i)] = Ang[B_{g20}(j\omega_i)] + Ang[q_{220}(j\omega_i)]$. This process is demonstrated for $\omega_i = 8$ in Table H-4 using the spreadsheet program. The Log-magnitude and angle values of $B_{20}(j\omega_i)$ (Columns 5 and 6 of Table H-4 for $\omega_i = 8$) define points to be plotted on the rectangular grid of the Nichols chart. Connecting the points establishes the bounds $B_{20}(j\omega_i)$ for shaping the nominal loop transmission $l_{20}(j\omega)$ on the Nichols chart (Figure V-9).

Math Spreadsheet Parameters and Results

Tables H-1, H-2 and H-3 are the calculations of the $B_{g2k}(j8)$ bounds, where (k) defines the flight condition: Case 1, 2 or 3. In each table, Columns 1 and 2 are the Log-magnitude and angle values of the bound $B_{2k}(j8)$ read from the Nichols chart.

Columns 5 and 6 are the resulting Log-magnitude and angle values of $B_{g2k}(j8)$ found by evaluating Equation (H-4) for each data point in columns 1 and 2.

Table H-4 is the calculation of the maximum bound $B_{20}(j8)$ on the nominal loop transmission $l_{20}(j\omega)$ at the design frequency, $\omega_i = 8$. In Table H-4, Columns 1 and 2 list the $B_{g20}(j8)$ Log-magnitude and angle values. Columns 3 and 4 are the Log-magnitude and angle values of the nominal q, $q_{220}(j8)$. Columns 5 and 6 are the resulting Log-magnitude and the angle values of the maximum bound $B_{20}(j8)$ found by evaluating Equation (H-5) at $\omega_i = 8$ for each data point in Columns 1 and 2.

Table H-1. Spreadsheet Calculation of Acceleration Loop Bound, $B_{g21}(j8)$.

(Note: All values below are for Case 1, $\omega_i = 8$)

Lm[$B_{21}(j8)$]	Ang[$B_{21}(j8)$]	Lm[$q_{221}(j8)$]	Ang[$q_{221}(j8)$]	Lm[$B_{g21}(j8)$]	Ang[$B_{g21}(j8)$]
-7.25	-180	-3.60	-290	-3.65	110
-7.20	-185			-3.60	105
-6.90	-190			-3.30	100
-6.60	-195			-3.00	95
-6.20	-200			-2.60	90
-5.40	-205			-1.80	85
-4.25	-210			-0.65	80
-1.50	-214			2.10	76
0.80	-210			4.40	80
2.00	-205			5.60	85
2.75	-200			6.35	90
3.25	-195			6.85	95
3.60	-190			7.20	100
3.75	-185			7.35	105
3.80	-180			7.40	110
3.75	-175			7.35	115
3.60	-170			7.20	120
3.25	-165			6.85	125
2.75	-160			6.35	130
2.00	-155			5.60	135
0.80	-150			4.40	140
-1.50	-146			2.10	144
-4.25	-150			-0.65	140
-5.40	-155			-1.80	135
-6.20	-160			-2.60	130
-6.60	-165			-3.00	125
-6.90	-170			-3.30	120
-7.20	-175			-3.60	115
-7.25	-180			-3.65	110

Table H-2. Spreadsheet Calculation of Acceleration Loop Bound, $B_{g22}(j8)$.

(Note: All values below are for Case 2, $\omega_i = 8$)

Lm[$B_{22}(j8)$]	Ang[$B_{22}(j8)$]	Lm[$q_{222}(j8)$]	Ang[$q_{222}(j8)$]	Lm[$B_{g22}(j8)$]	Ang[$B_{g22}(j8)$]
1.60	-360	5.20	-292	-3.60	-68
1.75	-350			-3.45	-58
2.00	-340			-3.20	-48
2.25	-330			-2.95	-38
2.70	-320			-2.50	-28
3.10	-310			-2.10	-18
3.25	-300			-1.95	-8
4.40	-290			-0.80	2
5.10	-280			-0.10	12
5.90	-270			0.70	22
6.60	-260			1.40	32
7.30	-250			2.10	42
8.00	-240			2.80	52
8.60	-230			3.40	62
9.10	-220			3.90	72
9.50	-210			4.30	82
9.80	-200			4.60	92
10.00	-190			4.80	102
10.10	-180			4.90	112
10.00	-170			4.80	122
9.80	-160			4.60	132
9.50	-150			4.30	142
9.10	-140			3.90	152
8.60	-130			3.40	162
8.00	-120			2.80	172
7.30	-110			2.10	182
6.60	-100			1.40	192
5.90	-90			0.70	202
5.10	-80			-0.10	212
4.40	-70			-0.80	222
3.25	-60			-1.95	232
3.10	-50			-2.10	242
2.70	-40			-2.50	252
2.25	-30			-2.95	262
2.00	-20			-3.20	272
1.75	-10			-3.45	282
1.60	0			-3.60	292

Table H-3. Spreadsheet Calculation of Acceleration Loop Bound, $B_{g23}(j8)$.

(Note: All values below are for Case 3, $\omega_i = 8$)

$Lm[B_{23}(j8)]$	$Ang[B_{23}(j8)]$	$Lm[q_{223}(j8)]$	$Ang[q_{223}(j8)]$	$Lm[B_{g23}(j8)]$	$Ang[B_{g23}(j8)]$
10.00	-360	7.60	-294	2.40	-66
10.10	-350			2.50	-56
10.20	-340			2.60	-46
10.25	-330			2.65	-36
10.50	-320			2.90	-26
10.80	-310			3.20	-16
11.10	-300			3.50	-6
11.40	-290			3.80	4
11.70	-280			4.10	14
12.00	-270			4.40	24
12.30	-260			4.70	34
12.75	-250			5.15	44
13.10	-240			5.50	54
13.40	-230			5.80	64
13.70	-220			6.10	74
13.90	-210			6.30	84
14.10	-200			6.50	94
14.20	-190			6.60	104
14.25	-180			6.65	114
14.20	-170			6.60	124
14.10	-160			6.50	134
13.90	-150			6.30	144
13.70	-140			6.10	154
13.40	-130			5.80	164
13.10	-120			5.50	174
12.75	-110			5.15	184
12.30	-100			4.70	194
12.00	-90			4.40	204
11.70	-80			4.10	214
11.40	-70			3.80	224
11.10	-60			3.50	234
10.80	-50			3.20	244
10.50	-40			2.90	254
10.25	-30			2.65	264
10.20	-20			2.60	274
10.10	-10			2.50	284
10.00	0			2.40	294

Table H-4. Spreadsheet Calculation of Maximum Acceleration Loop Bound, $B_{20}(j8)$.

(Note: All values below are for the Nominal Case, $\omega_i = 8$)

$Lm[B_{g20}(j8)]$	$Ang[B_{g20}(j8)]$	$Lm[q_{220}(j8)]$	$Ang[q_{220}(j8)]$	$Lm[B_{20}(j8)]$	$Ang[B_{20}(j8)]$
2.40	-66	-2.70	-292	-0.30	-358
2.50	-56			-0.20	-348
2.60	-46			-0.10	-338
2.65	-36			-0.05	-328
2.90	-26			0.20	-318
3.20	-16			0.50	-308
3.50	-6			0.80	-298
3.80	4			1.10	-288
4.10	14			1.40	-278
4.40	24			1.70	-268
4.70	34			2.00	-258
5.15	44			2.45	-248
5.50	54			2.80	-238
5.80	64			3.10	-228
6.10	74			3.40	-218
6.30	84			3.60	-208
6.85	95			4.15	-197
7.20	100			4.50	-192
7.35	105			4.65	-187
7.40	110			4.70	-182
7.35	115			4.65	-177
7.20	120			4.50	-172
6.85	125			4.15	-167
6.50	134			3.80	-158
6.30	144			3.60	-148
6.10	154			3.40	-138
5.80	164			3.10	-128
5.50	174			2.80	-118
5.15	184			2.45	-108
4.70	194			2.00	-98
4.40	204			1.70	-88
4.10	214			1.40	-78
3.80	224			1.10	-68
3.50	234			0.80	-58
3.20	244			0.50	-48
2.90	254			0.20	-38
2.65	264			-0.05	-28
2.60	274			-1.10	-18
2.50	284			-0.20	-8
2.40	294			-0.30	2

Appendix J

Derivation of the MIMO System Closed-Loop Transfer Functions

Introduction

The closed-loop system transfer functions are needed to obtain the system response at each flight condition, thus permitting verification that the control laws obtained adequately provide system performance within the desired response specifications. The system transfer functions derived below are found by applying Mason's Gain Rule to the MIMO system of Figure V-2.

Derivations

First, the closed-loop transfer function t_{11} is found for the pitch rate output y_1 due to the command input r_1. Applying Mason's Rule to Figure V-2, then:

$$t_{11} = \frac{y_1}{r_1} = \frac{f_{11}g_1p_{11}\,(1 + g_2p_{22}) - f_{11}g_1p_{21}g_2p_{12}}{1 - (-g_1p_{11} + -g_2p_{22} + g_1p_{21}g_2p_{12}) + g_1p_{11}g_2p_{22}} \qquad \text{(J-1)}$$

$$t_{11} = \frac{f_{11}g_1p_{11} + f_{11}g_1p_{11}\,g_2p_{22} - f_{11}g_1p_{21}g_2p_{12}}{1 + g_1p_{11} + g_2p_{22} - g_1g_2p_{21}p_{12} + g_1g_2p_{11}p_{22}} \qquad \text{(J-2)}$$

$$t_{11} = \frac{f_{11}g_1(p_{11} + g_2(p_{11}p_{22} - p_{21}p_{12}))}{1 + g_1p_{11} + g_2p_{22} + g_1g_2(p_{11}p_{22} - p_{21}p_{12})} \qquad \text{(J-3)}$$

Let $\Delta = \det[\mathbf{P}] = p_{11}p_{22} - p_{21}p_{12}$, then from Equation (V-12);

$$p_{11} = \Delta/q_{22}\,; \quad p_{12} = -\Delta/q_{12}\,; \quad p_{21} = -\Delta/q_{21}\,; \quad p_{22} = \Delta/q_{22}\,; \qquad \text{(J-4)}$$

Inserting Equation (J-4) into (J-3), t_{11} becomes:

$$t_{11} = \frac{f_{11}g_1(\Delta/q_{22} + g_2\Delta)}{1 + g_1\Delta/q_{22} + g_2\Delta/q_{11} + g_1g_2\Delta} \qquad \text{(J-5)}$$

$$t_{11} = \frac{f_{11}g_1(1/q_{22} + g_2)}{1/\Delta + g_1/q_{22} + g_2/q_{11} + g_1g_2} \qquad \text{(J-6)}$$

$$t_{11} = \frac{f_{11}g_1(q_{11} + g_2q_{11}q_{22})}{q_{11}q_{22}/\Delta + g_1q_{11} + g_2q_{22} + g_1g_2q_{11}q_{22}} \qquad \text{(J-7)}$$

Δ is rewritten in terms of q_{ij} by inserting Equation (J-4) into det[**P**]:

$$\Delta = \Delta^2/q_{22}q_{11} - \Delta^2/q_{12}q_{21} \text{ or } \Delta = q_{22}q_{11}q_{12}q_{21} / (q_{12}q_{21} - q_{22}q_{11}) \quad \text{(J-8)}$$

Inserting Equation (J-8) into Equation (J-7), then:

$$t_{11} = \frac{f_{11}g_1(q_{11} + g_2q_{11}q_{22})}{\dfrac{(q_{12}q_{21} - q_{22}q_{11})}{q_{12}q_{21}} + g_1q_{11} + g_2q_{22} + g_1g_2q_{11}q_{22}} \quad \text{(J-9)}$$

$$t_{11} = \frac{f_{11}g_1(q_{11} + g_2q_{11}q_{22})}{1 - q_{22}q_{11}/q_{12}q_{21} + g_1q_{11} + g_2q_{22} + g_1g_2q_{11}q_{22}} \quad \text{(J-10)}$$

Inserting Equation (V-39) into Equation (J-10) and regrouping terms, then:

$$t_{11} = \frac{f_{11}g_1q_{11}(1+ g_2q_{22})}{(1 + g_1q_{11})(1 + g_2q_{22}) - \gamma} \quad \text{(J-11)}$$

Note Equation (J-11) is the same as Equation (V-37) when written in terms of the loop transmissions l_1 and l_2 of Equation (V-38). The various transfer function components of Equation (J-11) were input to TOTAL and the pitch rate responses of Chapter VI were obtained for each flight condition. The pitch response was obtained simply by taking the integral of the pitch rate, i.e. $\theta(s) = (1/s)t_{11}(s)$ using TOTAL.

Second, the closed-loop transfer function t_{21} is found for the acceleration output y_2 due to the command input r_1. Applying Mason's Rule to Figure V-2, then:

$$t_{21} = \frac{y_2}{r_1} = \frac{f_{11}g_1p_{21}}{1 - (-g_1p_{11} + -g_2p_{22} + g_1p_{21}g_2p_{12}) + g_1p_{11}g_2p_{22}} \quad \text{(J-12)}$$

$$t_{21} = \frac{f_{11}g_1p_{21}}{1 + g_1p_{11} + g_2p_{22} - g_1g_2p_{21}p_{12} + g_1g_2p_{11}p_{22}} \quad \text{(J-13)}$$

Rewriting Equation (J-13) in terms of q_{ij}, then;

$$t_{21} = \frac{-f_{11}g_1(1/q_{21})}{1/\Delta + g_1/q_{22} + g_2/q_{11} + g_1g_2} \quad \text{(J-14)}$$

$$t_{21} = \frac{-f_{11}g_1(q_{11}q_{22}/q_{21})}{q_{11}q_{22}/\Delta + g_1q_{11} + g_2q_{22} + g_1g_2q_{11}q_{22}} \quad \text{(J-15)}$$

$$t_{21} = \frac{-f_{11}g_1(q_{11}q_{22}/q_{21})}{(1 + g_1q_{11})(1 + g_2q_{22}) - \gamma} \tag{J-16}$$

$$t_{21} = \frac{f_{11}g_1q_{12}}{\dfrac{1 + (1 + g_1q_{11})(1 + g_2q_{22})}{-\gamma}} \tag{J-17}$$

The transfer function components of Equation (J-17) were input into TOTAL and the acceleration response plots of Chapter VI were obtained for each flight condition.

Finally, the plant input responses were obtained using TOTAL on the following relationships. Recall that u_1 is the elevator command input and u_2 is the flap command input.

$$u_1 = f_{11}g_1r_1 - g_1y_1 = f_{11}g_1r_1 - g_1t_{11}r_1 = g_1(f_{11} - t_{11})r_1 \tag{J-18}$$

or,

$$\frac{u_1}{r_1} = g_1(f_{11} - t_{11}) \tag{J-19}$$

and

$$u_2 = -g_2y_2 = -g_2t_{21}r_1 \tag{J-20}$$

or,

$$\frac{u_2}{r_1} = -g_2t_{21} \tag{J-21}$$

The transfer functions defined by Equations (J-19) and (J-21) were processed in TOTAL and the commanded plant input responses of Chapter VI were obtained. Note the closed-loop transfer functions contain very large order polynomials in the numerator and denominator. The complexity of these transfer functions increases proportionally to the complexity of the plant and compensator transfer functions.

Vita

Brian J. Pawlowski [redacted] A native of Neenah, Wisconsin, he graduated from the University of Wisconsin - Madison in May, 1982 with a Bachelor of Science Degree in Electrical Engineering. Graduating with honors, he was designated a Distinguished Graduate by Air Force ROTC and received a regular commission in the Air Force. He is pursuing a graduate degree in Electrical Engineering from the Air Force Institute of Technology, Wright-Patterson Air Force Base, Ohio. He is currently serving on active duty with Detachment 2, Air Force Operational Test and Evaluation Center, Eglin Air Force Base, Florida. He is serving as the Assistant for Analysis, Advanced Medium Range Air-to-Air Missile (AMRAAM) Initial Operational Test & Evaluation (IOT&E) Test Team.

UNCLASSIFIED

SECURITY CLASSIFICATION OF THIS PAGE

REPORT DOCUMENTATION PAGE

Form Approved OMB No. 0704-0188

1a. REPORT SECURITY CLASSIFICATION UNCLASSIFIED	1b. RESTRICTIVE MARKINGS
2a. SECURITY CLASSIFICATION AUTHORITY	3. DISTRIBUTION/AVAILABILITY OF REPORT Approved for public release; distribution unlimited.
2b. DECLASSIFICATION/DOWNGRADING SCHEDULE	
4. PERFORMING ORGANIZATION REPORT NUMBER(S) AFIT/GE/ENG/89M-1	5. MONITORING ORGANIZATION REPORT NUMBER(S)
6a. NAME OF PERFORMING ORGANIZATION School of Engineering 6b. OFFICE SYMBOL (If applicable) AFIT/ENG	7a. NAME OF MONITORING ORGANIZATION
6c. ADDRESS (City, State, and ZIP Code) Air Force Institute of Technology Wright-Patterson AFB, OH 45433	7b. ADDRESS (City, State, and ZIP Code)
8a. NAME OF FUNDING/SPONSORING ORGANIZATION Flight Control Applications Group 8b. OFFICE SYMBOL (If applicable) WRDC/FIGX	9. PROCUREMENT INSTRUMENT IDENTIFICATION NUMBER
8c. ADDRESS (City, State, and ZIP Code) WRDC/FIGX Wright-Patterson AFB, OH 45433	10. SOURCE OF FUNDING NUMBERS PROGRAM ELEMENT NO. / PROJECT NO. / TASK NO. / WORK UNIT ACCESSION NO.

11. TITLE (Include Security Classification)

Multivariable Flight Control Design with Parameter Uncertainty for the AFTI/F-16

12. PERSONAL AUTHOR(S)

Brian J. Pawlowski, Capt, USAF

13a. TYPE OF REPORT	13b. TIME COVERED	14. DATE OF REPORT (Year, Month, Day)	15. PAGE COUNT
MS Thesis	FROM _____ TO _____	1989 March	140

16. SUPPLEMENTARY NOTATION

17. COSATI CODES			18. SUBJECT TERMS (Continue on reverse if necessary and identify by block number)
FIELD	GROUP	SUB-GROUP	Quantitative Feedback Theory; AFTI/F-16; CCV; Multivariable Flight Control Design; Pitch Pointing Controller; Plant Uncertainty; Frequency Domain
01	03		

19. ABSTRACT (Continue on reverse if necessary and identify by block number)

Thesis Chairman: Constantine H. Houpis
Professor of Electrical Engineering

Abstract:
Quantitative Feedback Theory (QFT) techniques are used in the design of a multivariable control law for the AFTI/F-16. The techniques were developed by Professor Isaac Horowitz, University of California, Davis, California. The flight control problem involves a multiple input-multiple output (MIMO) plant requiring regulation and control in the presence of parameter uncertainty and disturbances. Based on frequency response fundamentals, the technique uses feedback to achieve closed-loop system response within performance tolerances despite plant uncertainty. The range of uncertainty and the output performance specifications are quantitative parameters in the design process. The MIMO control problem is restructured into a set of two input-single output (multiple input-single output (MISO)) problems where one input is a command input to the system

20. DISTRIBUTION/AVAILABILITY OF ABSTRACT	21. ABSTRACT SECURITY CLASSIFICATION
☒ UNCLASSIFIED/UNLIMITED ☐ SAME AS RPT. ☐ DTIC USERS	UNCLASSIFIED
22a. NAME OF RESPONSIBLE INDIVIDUAL Dr. Constantine H. Houpis	22b. TELEPHONE (Include Area Code) 513-255-2024 22c. OFFICE SYMBOL AFIT/ENG

DD Form 1473, JUN 86 *Previous editions are obsolete.*

SECURITY CLASSIFICATION OF THIS PAGE

UNCLASSIFIED

19. and the other is a disturbance input to be attenuated. The control laws for the MISO problems taken together form the solution of the MIMO problem.

To obtain a point of comparison between various design techniques, the identical aircraft model previously developed by Mr. A. Finley Barfield is used in this study. The state space form of the model is converted to the transfer function relationships between the plant input and output variables. A single design is performed over the range of flight conditions investigated.

The approach along with evaluations of the final control laws is presented. Recommendations for further study and discussion of the results obtained are provided.